RICE UNIVERSITY

Carbon Nanotubes Filled Polymer Composites: A Comprehensive Study on Improving Dispersion, Network Formation and Electrical Conductivity.

by

Divya Kannan Chakravarthi

A THESIS SUBMITTED
IN PARTIAL FULFILLMENT OF THE
REQUIREMENTS FOR THE DEGREE

Doctor of Philosophy

Approved Thesis Committee:

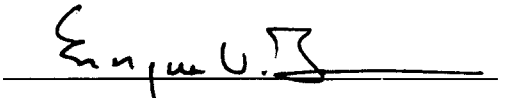

Enrique.V.Barrera, Professor, Chair
Mechanical Engineering and Materials Science

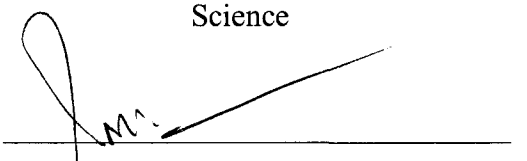

Pulickel. M. Ajayan, Benjamin M. and Mary Greenwood Anderson Professor in Engineering, Materials Science and, Nanotechnology

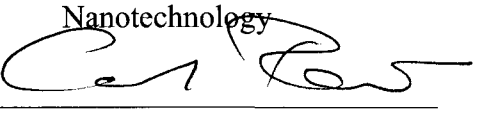

Carl Rau, Professor, Physics and Astronomy

HOUSTON, TX
JUNE 2010

ABSTRACT

Carbon Nanotubes filled Polymer Composites: A comprehensive study on improving dispersion, network formation and electrical conductivity.

By

Divya Kannan Chakravarthi

In this dissertation, we determine how the dispersion, network formation and alignment of carbon nanotubes in polymer nanocomposites affect the electrical properties of two different polymer composite systems: high temperature bismaleimide (BMI) and polyethylene. The knowledge gained from this study will facilitate optimization of the above mentioned parameters, which would further enhance the electrical properties of polymer nanocomposites.

BMI carbon fiber composites filled with nickel-coated single walled carbon nanotubes (Ni-SWNTs) were processed using high temperature vacuum assisted resin transfer molding (VARTM) to study the effect of lightning strike mitigation. Coating the SWNTs with nickel resulted in enhanced dispersions confirmed by atomic force microscopy (AFM) and dynamic light scattering (DLS). An improved interface between the carbon fiber and Ni-SWNTs resulted in better surface coverage on the carbon plies. These hybrid composites were tested for Zone 2A lightning strike mitigation. The electrical resistivity of the composite system was reduced by ten orders of magnitude with the addition of 4 weight percent Ni-SWNTs (calculated with respect to the weight of a single carbon ply). The Ni-SWNTs - filled composites showed a reduced amount of damage to simulated lightning strike compared to their unfilled counterparts indicated by the minimal carbon fiber pull out.

Methods to reduce the electrical resistivity of 10 weight percent SWNTs – medium density polyethylene (MDPE) composites were studied. The composites processed by hot coagulation method were subjected to low DC electric fields (10 V) at polymer melt temperatures to study the effect of viscosity, nanotube welding, dispersion and, resultant changes in electrical resistivity. The electrical resistivity of the composites was reduced by two orders of magnitude compared to 10 wt% CNT-MDPE baseline. For effective alignment of SWNTs, a new process called Electric field Vacuum Spray was devised to overcome viscosity within the dispersed nanotube polymer system, and produce conductive MDPE-SWNT thin films. Polarized Raman spectroscopy and scanning electron microscopy (SEM) analysis on the samples showed an improvement in SWNT – SWNT contacts and alignment in the polymer matrix. The resistivity of the samples processed by this new method was two order magnitudes lower than the samples processed by hot coagulation method subjected to electric field.

ACKNOWLEDGEMENT

My sincere thanks to my advisor, Dr. Enrique Barrera for giving me an opportunity to pursue my doctoral study in his group and his guidance, support and motivation. I am grateful to Dr. Khabashesku and Dr. Ranji Vaidyanathan for availing me of their knowledge in the lightning strike project and for all their help and encouragement throughout my graduate studies.

Thank you to my committee members Dr. Ajayan and Dr. Rau for readily agreeing to be on my committee and your valuable suggestions on my research. My sincere thanks to Dr. Loos and Dr. Brotzen for all the help rendered during my graduate study and most importantly passing on the importance of science through your courses and your dedication. Thanks to MEMS department staff: Maria, Alicia, Gary, Linda, Lisa, Sherry and Leah for your kind love and support.

I am grateful to the Barrera group: Claudia, Marvin, Ahmad, Padraig, Yao, Daneesh, Grace, Laura, Hubert, Jennifer, Suman, Luke, Andres for your relentless support and most of all your friendship. I have thoroughly enjoyed my time here and have such wonderful memories that I would cherish forever. Thank you my precious friends at Rice and in Houston: Claudia, Merlyn, Nethra, Hari, Ahmad, Sarah, Urmi, Trina, Shraddha, Rizia and, Cary. You've been my family away from home. Thank you Nanoridge team: Mike, Lori, Dean, Josh and Kyle, for all your help and input on my research and constant encouragement. I would like to thank my advisor at the Indian Institute of Science Dr. Seshan who always inspired me with his scientific and personal ethics.

My eternal love and gratitude to the most important people in my life: Rajeev, mom, dad, Nandu, Chelli and my parents in law for always being there for me and believing in me. You are my world and I dedicate this thesis to you!

I know how lucky I am to have gotten this opportunity and have all of you in my life. This work wouldn't have been possible without you all.

Table of Contents

CHAPTER 1: Introduction 1

CHAPTER 2: Background on Polymer Nanocomposites and Carbon Nanotubes 4

2.1 Polymer Nanocomposites 4

2.2 Background on Carbon Nanotubes and their Electrical Properties 5

2.3 Processing of Polymer Nanotube Composites and their Electrical Properties 8

CHAPTER 3: High Temperature Bismaleimide/Carbon Fiber Composites Filled with Nickel Coated Single Walled Carbon Nanotubes for Lightning Strike Protection. 11

3.1 Introduction 11

3.2 Experimental 14

3.2.1 Pretreatments and electroless plating of SWNTs with nickel 14

3.2.2.1. Dispersion of SWNTs 16

3.2.2.2. Dispersion of Ni-SWNTs 16

3.2.3. Surface coverage of purified and Ni-SWNTs on the carbon plies. 17

3.2.4. Composite Processing and characterization. 18

3.2.5. Lightning Strike Simulation Testing and Failure Analysis 19

3.3. Results and Discussion. 21

3.3.1 Characterization of purified SWNTs and Ni-SWNTs. 21

3.3.2. Dispersion Studies. 23

3.3.2.1 Dispersion of purified SWNTs 25

3.3.2.2 Dispersion of Ni-SWNTs 27

3.3.2.3 Raman Analysis of the Ni-SWNTs suspensions 33

3.3.3 Surface coverage of purified SWNTs and Ni-SWNTs on the surface of carbon plies 34

3.3.3.1 Surface coverage of Ni- SWNTs on carbon plies. 35

3.3.3.2. Surface coverage of purified SWNTs on carbon plies 39

3.4. BMI/carbon fiber/Ni-SWNT composites. 40

3.4.1. Resistivity of BMI/Carbon fiber/ Nanotube composites. 46

3.5. Lightning Strike Testing and Characterization of Composites. 47

3.5.1 Raman Spectroscopy analysis of the samples. 51
3.5.2 Characterization of damage using SEM 53
3.5.3 Analysis of the presence of nickel after each processing step 56
3.6. Conclusions. 59
CHAPTER 4: Achieving High Electrical Conductivities in Polyethylene – Carbon Nanotube Composite Systems. 60
4.1. Introduction 60
4.2 Background on improving the electrical conductivity in polymer composites 61
4.2.1 Effect of dispersion and process optimization 61
4.2.2. Effect of nanotube type and electric field. 65
4.2.3. Effect of magnetic field on the alignment of CNTs 73
4.2.4. In-situ polymerization and melt spinning techniques for alignment in thin films. 74
4.2.5. Theoretical studies on nanotube conductivity in the polymer composites. 76
4.3. Experimental Methods and Materials. 78
4.3.1. Materials 78
4.3.2. Processing of polyethylene / SWNT composites and electric field studies. 78
4.3.3. Characterization of PE / SWNT composites. 81
4.4 Results and discussion 83
4.4.1 Composites processed by hot coagulation method and subjected to electric field. 83
4.4.2 Composites processed by Electric Field Vacuum Spray process and their characterization. 92
4.4.2.1 Dispersion of SWNTs 92
4.4.2.2 Processing of composites. 94
4.4.2.3 Electrical Resistivity of the polyethylene / SWNT composites. 97
4.4.2.4 Characterization of alignment and network formation of SWNTs in MDPE composites 103
4.5. Conclusions 110
CHAPTER 5: Conclusions 112
Achieving high electrical conductivities in polyethylene – carbon nanotube composite systems 115

REFERENCES 116

APPENDIX-1 126

List of Figures

Figure 2.1. Various forms of carbon. (This photo was downloaded from http://cohesion.rice.edu/naturalsciences/smalley/emplibrary/allotropes.jpg) 5

Figure 2.2. Effect of thickness of the insulating layer and the nanotube diameter on the tunneling resistance (adapted from Li et al). 9

Figure 3.1. Boeing 787 lightning strike protection system (downloaded from Bloomberg News, NASA). 12

Figure 3.2. Schematic of electroless plating procedure used to deposit nickel on the outer surface of carbon nanotube 15

Figure 3.3. Schematic of the spray set up used to study the surface coverage of Ni-SWNTs and purified SWNTs on the carbon fiber (adapted from Kim *et al* [38]). 18

Figure 3.4. (a)Modified VARTM method for BMI-carbon composite fabrication. (b)Oven temperature cycle used for BMI/Carbon fiber composite fabrication. 19

Figure 3.5. Simulated lighting strike testing set up at Lightning Technologies Inc. 20

Figure 3.6. TGA of purified SWNTs (amount of metal content 0.7467%) 21

Figure 3.7. Raman spectrum of purified SWNTs. 22

Figure 3.8. SEM images of A) Ni-SWNTs, B) purified SWNTs 22

Figure 3.9. Various types of functionalization of SWNTs a) non – covalent functionalization b) defect functionalization c) functionalization through π stacking d) sidewall covalent functionalization and e) endohedral functionalization by filling the SWNTs [42]. 24

Figure 3.10. Dispersion of purified SWNTs in A) DMF indicating large amounts of agglomeration B) NMP indicating a uniform network along with some agglomeration and no sedimentation. 25

Figure 3. 11. Diameter and length of SWNTs in NMP suspensions after decanting at 15000 rpm for 30 minutes. 26

Figure 3.12. Nickel particles on the sidewall of the SWNTs obtained by electroless plating. 27

Figure 3.13. Structure of Oleylamine 28

Figure 3.14. Dispersions of Ni-SWNTs in various solvents after 14 days (no visible sedimentation was observed: A) Ni-SWNTs dispersed in THF / Oleylamine B) Ni-SWNTs in toluene / Oleylamine C) Ni-SWNTs in ethylenediamine. 28

Figure 3.15. Decanted Ni-SWNTs-THF suspensions indicating agglomeration..... 29

Figure 3.16. Decanted Ni-SWNTs in oleylamine and THF showing a reduction in the diameter of the agglomerates by addition of surfactant A) 0.2 mg/ml B) 0.35 mg/ml..... 30

Figure 3. 17. Decanted Ni-SWNTs-Toluene suspensions indicating agglomeration A) 0.2mg/ml B) 0.35mg/ml..... 30

Figure 3.18. Decanted Ni-SWNTs in oleylamine and toluene showing a reduction in the diameter of the agglomerates by addition of surfactant A) 0.2 mg/ml B) 0.35 mg/ml..... 31

Figure 3.19. Decanted Ni-SWNTs in ethylenediamine showing a reduction in the diameter of the agglomerates by addition of surfactant A) 0.2 mg/ml B) 0.35 mg/ml..... 31

Figure 3.20. Cross sectional height analysis of dispersion of Ni-SWNTs: a and b) 0.2 mg/ml and 0.35mg/ml in toluene with oleylamine, c and d) 0.2 mg/ml and 0.35mg/ml in THF with oleylamine, e and f) 0.2 mg/ml and 0.35mg/ml in ethylenediamine..... 32

Figure 3.21. Raman spectra of Ni-SWNTs and Ni-SWNT suspensions 34

Figure 3.22. Surface coverage of Ni-SWNTs on the carbon fiber (a) dispersed in toluene-oleylamine suspensions (b) dispersed in THF-oleylamine suspensions (c) dispersed in ethylenediamine. 36

Figure 3.23. 1 wt% Ni-SWNTs suspended in ethylenediamine sprayed onto carbon plies showing a non uniform and discontinuous surface coverage. 37

Figure 3.24. Partial surface coverage of 2 wt% Ni-SWNTs dispersed in ethylenediamine. 37

Figure 3.25. Ni-SWNTs in ethylenediamine (4 wt %) showing a continuous surface coverage on the carbon plies..... 38

Figure 3.26. Higher magnification image of the carbon plies showing a uniform coverage of Ni-SWNTs. 38

Figure 3.27. Surface coverage of purified SWNTs dispersed in NMP on carbon plies (a) 1wt% SWNTs (2) 2wt% SWNTs (3) 4wt% SWNTs..... 39

Figure 3.28. Mechanical properties of BMI / Carbon fiber laminates (adapted from Zhang et al[59])..... 41

Figure 3.29. Mechanical and electrical properties of the MWNT / BMI composite as a function of the stretch ratio of the MWNT sheets (adapted from Cheng *et al*). 42

Figure 3.30. BMI/Carbon fiber/Ni-SWNT composite sample showing resin peel off indicated by the rectangle box. 43

Figure 3.31.a) network of Ni-SWNTs in the BMI composite, b) adhesion of Ni-SWNTs to the BMI resin, c) Diameter and length of the Ni-SWNTs that bridges the cracks in the BMI matrix 44

Figure 3.32. Ni-SWNTs BMI interaction in the composites showing a polymer coating of the Ni-SWNTs. 45

Figure 3.33. Schematic of the test probe used for simulated zone 2A lightning strike (adapted from Fielding et al [28]). 47

Figure 3.34. Photographs of BMI composite samples hit by simulated lightning showing a) minimal damage to the top layer of the Ni-SWNTs filled composite b) carbon fiber pull out in the baseline composite damaging the top layer. 48

Figure 3.35. Electrical conductivity, depth of damage and area of damage of composites with various reinforcements (adapted from Fielding et al and modified to add our data to the figure for comparison purposes). 49

Figure 3.36. Electrical conductivity of NiCCF composites filled with various nanomaterials and their depth and area of damage due to simulated zone 2A lightning strike (adapted from Fielding et al). 50

Figure 3.37. Raman spectra of the samples showing a shift in G peak after each processing. 53

Figure 3.38. Regions away from the central region of the lightning strike showing no damage. 54

Figure 3.39. Effect of strike on the BMI resin showing charring and pulverizing of the resin and pulling of nanotubes. 55

Figure 3.40. BMI residue after TGA showing complete degradation of the resin similar to the lightning strike sample. 55

Figure 3.41. Carbon fiber and SWNT rich regions of the composite after exposure to simulated lightning strike 56

Figure 3.42. XPS spectrum of pure nickel showing the signature peak for Ni $2p_{3/2}$. 57

Figure 3.43. Presence of nickel indicated by the Ni $2p_{3/2}$ in a) Ni-SWNTs b) Ni-SWNT BMI carbon fiber composites c) Ni-SWNTs sprayed on carbon fiber. 58

Figure 4.1. Optical absorbance spectra of (a) IPCNTs (◆) (b) VGCNTs (▲,■) showing the maximum energy required for exfoliation. (adapted from Grossiord et al). 61

Figure 4.2. Conductivity of the PS composites filled with a) VGCNTs (▲) (b) IPCNTs (◆). (adapted from Grossiord et al). 62

Figure 4.3. Electrical conductivity of PPE functionalized SWNTs in A) polystyrene matrix B) polycarbonate matrix. 63

Figure 4.4. Electrical conductivity of PMMA composites filled with A) Pristine SWNTs B) $SOCl_2$ doped SWNTs [75]. 64

Figure 4.5. Maximum conductivities achieved in polymer composites using various types of fillers (Bauhofer *at al*). 66

Figure 4.6. Effect of electric field on the composite conductivity for various concentrations of MWNTs (adapted from Bauhofer *et al*). 67

Figure 4.7. Optical micrographs of 0.01 MWNTs in bulk composites (a) DC field 100 V/cm (b) AC field (adapted from Martin *et al*). 68

Figure 4.8. Electrical conductivity of the composites at different frequencies and configurations of electric field (adapted from Zhu *et al*) 69

Figure 4.9. Alignment of (a) pristine MWNTs (b) oxidized MWNTs in an AC electric field showing a more uniform alignment of the latter. (Adapted from Ma et al). 70

Figure 4.10. Polarized Raman spectra of pristine MWNTs composites (left) and oxidized MWNTs composites (rights). The electrical conductivity of various composites is also shown (adapted from Ma *et al*). 71

Figure 4.11. Electrical conductivity of SWNT / PMMA composites as a function of (a) concentration (b) alignment of SWNTs indicated by the FWHM. (adapted from Du et al). 72

Figure 4.12. Inplane alignment of SWNT films using a high magnetic field (adapted from Walters *et al*). 73

Figure 4.13. Electrical conductivity of MWNT-PANI composite films as a function of temperature (adapted from Feng *et al*) 75

Figure 4.14. Electric field set up used for hot coagulated polyethylene / carbon nanotube composites 79

Figure 4.15. Schematic of the electric field vacuum spray set up used to process polyethylene/carbon nanotube composites. 81

Figure 4.16. Effect of sonication time of SWNTs on the resistance of MDPE-SWNT composites 83

Figure 4.17. TEM image of the CG-SWNT/DCB suspensions before and after decanting showing the removal of catalyst and heavily bundled SWNTs after the centrifugation process..... 84

Figure 4.18. Mechanism of alignment of SWNTs when subjected to an electric field (adapted from Du *et al*)..... 86

Figure 4.19. Current voltage statistics for 10 wt% CG SWNT / MDPE composites after each conditioning run showing an improvement in the current carrying capability of the composite..... 88

Figure 4.20. Electric resistivity of SWNT / MDPE composites (A) subjected to electric field at 145°C (B) subjected to electric field at 145°C and cooled to room temperature. 88

Figure 4.21. MDPE / HiPco composites (A) processed by hot coagulation method before the application of electric field. (B, C and, D) after the application of electric field showing an improved network and contact between the nanotubes..... 89

Figure 4.22. Samples subjected to current greater than 2 amperes showing polymer degradation (indicated by the area enclosed in white)..... 90

Figure 4.23. Raman mapping for SWNTs / MDPE composites (A) processed by hot coagulation method before subjecting to electric field. (B) samples subject to electric field and cooled to room temperature (C) samples subjected to high currents..... 91

Figure 4.24. SWNT / NMP suspensions after decanting at 10000 rpm showing the presence of: (A) bundles (B) bundled and individually dispersed SWNTs..... 93

Figure 4.25. DLS analysis on the SWNT suspensions showing bundle diameters ranging from 4 to 13 nm and length from 385 – 700 nm..... 94

Figure 4.26. The difference in network formation when the samples were subjected to electric field (A) batch layer processing (B) diffuse layer processing..... 95

Figure 4.27. Raman map of G peak intensities of the samples processed by (A) pouring the SWNT suspension (B) spraying..... 96

Figure 4.28. Raman spectra of purified SWNTs and SWNT/ MDPE composites. 97

Figure 4.29. Resistivity of HiPco/MDPE composites as a function of the SWNT concentration..... 99

Figure 4.30. Effect of electric field on the resistivity of HiPco / PE SWNTs. 101

Figure 4.31. Effect of nanotube curl ratio on the conductivity of nanotube composites (adapted from Li et al). 102

Figure 4.32. Aligned and non aligned bucky paper. 103

Figure 4.33. Net alignment of nanotubes in PE/SWNT composites showing some waviness and curling. 104

Figure 4.34. Aligned SWNTs coated with polyethylene. 105

Figure 4.35. Raman spectra of 10wt%/MDPE composites orientated at 0 and 90 degrees showing the reduction in the intensity of all the Raman modes. 106

Figure 4.36. Reduction in the tangential "G" mode intensity of the composites aligned parallel and perpendicular to the direction of laser beam by almost a factor of 5. 106

Figure 4.37. Reduction in the intensity of the radial breathing modes for 10 wt% SWNT/MDPE composites in the aligned and perpendicular directions 107

Figure 4.38. Reduction in G peak intensities for the 10 wt% SWNT – HiPco composite films. 108

Figure 4.39. Plot of ln (σ) vs. $p^{-1/3}$ for SWNT/MDPE composites. 110

Figure A1.1. SEM images of CG-SWNTs showing heavy agglomerations. 126

Figure A1.2. SEM images of purified HiPco SWNTs. 126

Figure A1.3. Raman spectrum of CG-SWNTs. 127

Figure A1.4. Raman spectrum of purified HiPco-SWNTs. 127

Figure A1.5. DSC thermogram of neat MDPE. 128

Figure A1.6. DSC thermogram 10 wt%-MDPE composites processed by hot coagulation method 128

Figure A1.7. DSC thermogram of composites processed by hot coagulation method subjected to low DC field. 129

Figure A1.8. DSC thermogram of composites processed by electric field vacuum spray process 129

Figure A1.9. DSC thermograms of the various samples processed using the hot coagulation method subjected to electrical and current conditioning. 130

Figure A1.10. Effect of the variables on the electrical resistivity of the composite (if P_r the probability is less than F, the variable has an effect). 131

Figure A1.11. Effect of interaction between the parameters on the electrical resistance. 132

List of Tables

Table 2.1. Physical properties of carbon nanotubes (All values are for SWNTs unless specified; the references are shown in the table). 6

Table 3.1. Nanomaterials considered for lightning strike protection.....13

Table 3.2. Composition and operating conditions of electroless nickel coating bath..... 16

Table 3.3. Resistance and Resistivity of the composites measured using cylindrical and four point probe..... 46

Table 3.4. Position of the G peak in the Raman spectra of the samples, showing the effect of coating, processing of composites and simulated lightning strike on the tangential G mode of the SWNTs..... 52

Table 4.1. Basic matrix used for the analysis of variance study (ANOVA).....82

Table 4.2. Optimizing the temperature of the samples prior to application of the electric field. 85

Table 4.3. Influence of processing and electric field on the resistivity of the SWNT/PE composites..... 98

Table 4.4. Comparison of anisotropy in resistivity and Raman G modes for 10wt% SWNT-MDPE composites subjected to 75 V/cm DC field..... 109

CHAPTER 1: Introduction

Carbon nanotubes (CNTs) have attracted considerable attention for a wide variety of applications since their discovery two decades ago. Their remarkable electrical, mechanical and thermal properties combined with their large aspect ratios make them the most sought after nanofillers for multifunctional polymer composites' research.[1] Despite extensive research in this field, their full potential has not been harnessed in providing superior properties to the composite. A number of factors such as purity of CNTs, their dispersion in the polymer matrix, interfacial bonding and alignment have an impact on these superior properties.[2]

One of the most important challenges posed, is the dispersion of CNTs in the polymer matrix. Nanotubes tend to form agglomerates and bundles due to substantial Van der Waal's attraction between them. This diminishes their mechanical and electrical properties along with reduction in aspect ratios. Functionalization, high shear mixing, ultra-sonication and surfactant wrapping are some of the methods that aid in enhancing the dispersion of nanotubes. When electrical properties of the composite are under consideration, functionalization and surfactant wrapping disrupt the sidewall sp^2 hybridization resulting in reduced electrical conductivity of the nanotubes. Hence a trade off between good dispersion and non-functionalization has to be made. Since nanotubes conduct along their length, alignment is another important factor that needs to be considered in improving the electrical properties. A good network formation using high aspect ratio SWNTs along with modest alignment is essential.

In spite of the above mentioned challenges in processing highly conductive composites for large scale purposes, their potential as the best reinforcing agents continues to be a

dominant motivation for further research in this area. As new applications for CNTs emerge, it becomes necessary to understand the basic behavior of these nano-scaled particles.

The motivation for this dissertation is to explore how the dispersion of carbon nanotubes, network formation in the polymer matrix, their alignment and surface coverage can be optimized to combat the challenge of reducing the electrical resistivity of polymer composites.

The organization of this thesis is as follows: The fundamental properties of carbon nanotubes and the effect of various parameters on their electrical properties are discussed in Chapter 2 along with a brief discussion on polymer nanocomposites.

Chapter 3 presents an elaborate study on processing of Bismaleimide (BMI) - carbon fiber composites filled with nickel coated single walled carbon nanotubes (Ni-SWNTs) which were used for lightning strike mitigation testing. The dispersion of purified and Ni-SWNTs, surface coverage on carbon plies, processing and characterization of these hybrid composites along with lightning strike testing results are detailed in this chapter.

Optical microscopy and atomic force microscopy (AFM) in conjunction with dynamic light scattering (DLS) were used to characterize the dispersions. The combined use of these three techniques provides a good view on the state of dispersion of the SWNTs and their aspect ratios in the solvent. Scanning electron microscopy and Raman spectroscopy were used to analyze the surface coverage and the distribution of SWNTs in the polymer matrix. Electrical resistivity measurements were made using both cylindrical and four point probe. The composites subjected to lightning strike were characterized using SEM and Raman. Inductively coupled plasma (ICP) analysis and X-ray photoelectron

spectroscopy (XPS) were used to study the presence of nickel before and after simulated lightning strike.

In Chapter 4, different methods to improve the electrical conductivity of polyethylene are demonstrated. Polyethylene/SWNT composites were processed by hot coagulation method developed by Du et al [3]. The composites were subjected to electric fields at high temperatures to determine the effect of viscosity, nanotube welding and alignment on their electrical resistivity. High viscosity of the polymer hindered the CNT rotations and translations and hence, very little improvement in the electrical conductivity was obtained. A new method "electric field vacuum spray process" to produce conductive MDPE-SWNT thin films was established. The path to creating a conductive system is presented demonstrating how it came to execution. The nanocomposite system processed by this method improves the CNT-CNT contacts and alignment which enhance the electrical conductivity of the composite.

Chapter 5 presents the overall conclusion of this dissertation along with suggestions for future work which can extend this effort in a number of directions. Appendix 1 contains the characterization of Southwest CG-SWNTs and HiPco SWNTs used in the polyethylene study along with the results for analysis of variance (ANOVA).

CHAPTER 2: Background on Polymer Nanocomposites and Carbon Nanotubes

2.1 Polymer Nanocomposites

A material that consists of two or more physically or chemically different components separated by an interface can be termed as a composite [4]. Composites are characterized by having unique final properties which are not exhibited by any of the constituents when they are by themselves. The two main constituents of composite materials are the matrix and the reinforcement. Based on the type of matrix they are classified into metal matrix composites, polymer matrix composites and ceramic matrix composites.

Polymer nanocomposites are a class of materials where at least one of the dimensions of the filler material is of the order of a nanometer. The unique combination of the nanomaterial's characteristics, such as size, electrical, thermal and mechanical properties, low concentrations necessary to change the composite properties coupled with advanced characterization techniques has made them one of the most sought after materials for a variety of applications [5].

The dramatic change in their physical properties due to reduction in dimensions to nanoscale is what makes them unique. Some of the most common nanomaterials are silica nanoparticles, carbon black, carbon nanotubes, nanofibers etc. One of the main advantages of nanomaterials is their large surface area. The surface area per unit volume is inversely proportional to the diameter [6]. Since most of the physical and chemical interactions are governed by the surface properties, surface area plays a major role in the determining the ultimate properties of a composite material. Surface area and quantum effects are two main factors that distinguish the nanomaterials from other materials [7].

Since the focus of this thesis is using carbon nanotubes as fillers the following sections present properties of carbon nanotubes, polymer composite processing and a brief overview of their electrical properties.

2.2 Background on Carbon Nanotubes and their Electrical Properties

Carbon atoms produce a variety of allotropes, such as diamond, fullerene cages, graphite, and nanotubes as shown in Figure 2.1. Since their discovery in 1991 by Ijima *et al*, [8] they have attracted the attention of researchers worldwide due to their unique size, shape, and remarkable physical properties [9]. A single walled carbon nanotube is essentially a layer of graphene rolled up into a seamless cylinder capped by half fullerene. It can be viewed as an elongated fullerene with hemispherical cap at each end.

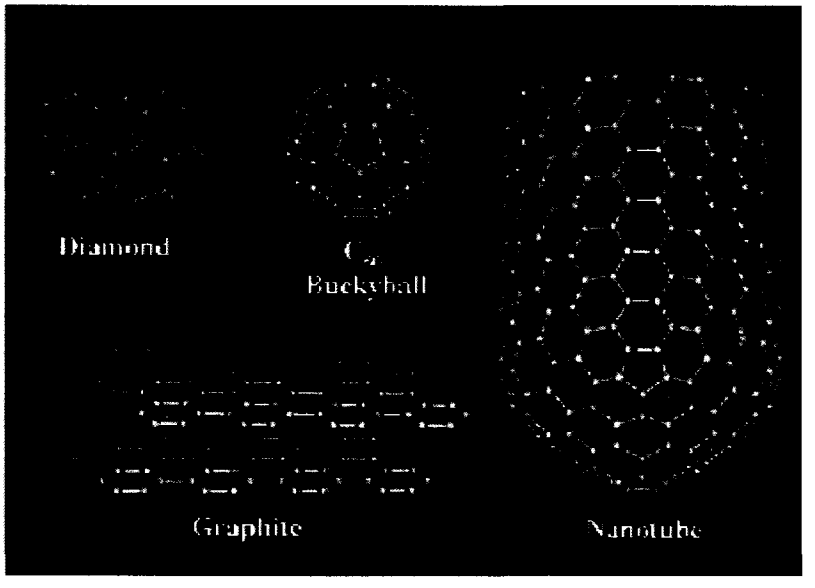

Figure 2.1. Various forms of carbon. (This photo was downloaded from http://cohesion.rice.edu/naturalsciences/smalley/emplibrary/allotropes.jpg)

The different kinds of nanotubes that have been produced are multi walled (MWNTs), single walled (SWNTs) and double-walled (DWNTs). Multi-wall carbon nanotubes are the coaxial assembly of cylinders of SWNTs within one another. MWNTs and SWNTs have similar properties, however, SWNTs are considered to have superior mechanical, electrical and, thermal properties. They are classified into chiral, armchair and zigzag nanotubes based on their chirality and diameters. It is this chirality or the twist that affects the electrical properties, lattice structure, density and other properties. Carbon nanotubes can be metallic or semiconducting based on their chiral vector [10]. The physical properties of carbon nanotubes are shown in Table 2.1. They can be produced by (1) arc discharge [11] (2) chemical vapor deposition [12] (3) laser ablation methods [13].

Table 2.1. Physical properties of carbon nanotubes (All values are for SWNTs unless specified; the references are shown in the table).

Average diameter of SWNTs [14]	~ 1.2 – 1.4 nm
Electrical Resistivity [15]	~ 10^{-4} Ω.cm
Maximum current density [16]	~ $4*10^{9}$ A/cm^{3}
Thermal conductivity [17,18]	~ 2000 - 6000 W/m-K
Young's Modulus (SWNT) [19,20]	~ 1 TPa
Young's Modulus (MWNT)	~ 1.28 TPa
Maximum Tensile Strength [21]	~ 128 GPa
Density	~ 1.33 – 1.40 g/cm^{3}

Carbon nanotubes find their applications in the field of electronics, multifunctional polymer composites, sensors, hydrogen storage, space research and pharmaceuticals. However, to harness their full potential one must overcome the large Van der Waal's attraction (0.5 eV/nm) [22] to separate them into smaller bundles or individual tubes. Some of the common methods to separate them are use of functionalization [23,24,25,26,27,28,29] to

make them more reactive, surfactant wrapping [30,31,32], sonication [33,34] or high shear mixing. Pertinent to this dissertation, the effect of nanotube processing into composites on the electrical conduction is important.

The conduction in a nanotube is quantized and it acts as a ballistic conductor. Frank *et al* [35] were one among the first group of researchers to study the conduction in MWNTs. In their study, they replaced the tip of a scanning probe microscope with a nanotube fiber which was used to establish a gentle contact with a liquid metal (mercury). They explain that the electron transport is ballistic when the length of the conductor is shorter than the electron mean free path and no energy is dissipated in the conductor. Any collision leads to increase in resistance of the materials. Shiraishi *et al* [36] studied the conduction mechanisms of non-aligned SWNTs. They observed that by changing the thickness of the SWNT mats, the conduction mechanism was varied and they attributed this to both the quantity and the quality of the metallic SWNTs included in the mats and also the contact tunneling. Wei *et al* [37] studied the effect of nanotube reliability and failure under high current carrying densities. They observed no change in the resistance for temperatures up to 250°C and time scales up to 2 weeks suggesting that they can be good candidates for electronic applications. The intrinsic conductivity of CNTs and the contact resistance are the most important factors for developing highly conductive composite materials. The contact resistance between the metallic – metallic and semiconducting – semiconducting CNTs can be close to 100 – 400 kΩ and that of metallic – semiconducting is higher by almost two orders of magnitude.[38] Theoretical calculations show that the contact resistance between CNTs can vary from 100 kΩ – 3.4 kΩ.[39] Having a polymer insulating

layer further increases the contact resistance (~ 10^{13} ohms [40]) by preventing tunneling if the polymer thickness is high.[41]

2.3 Processing of Polymer Nanotube Composites and their Electrical Properties

The first polymer nanocomposites using carbon nanotubes as filler were reported in 1994 by Ajayan *et al* [42]. The properties of polymer nanotube composites depend on the carbon nanotube type, quality, amount of impurities present, their aspect ratios, dispersion and nanotube orientation in the matrix.[43] The focus of most fabrication methods have been on improving the dispersion of nanotubes because improved dispersions in the polymer matrices has been found to improve properties. Some of the commonly used methods to process the composites are solution blending, melt blending and in-situ polymerization. In case of fiber reinforced composites resin transfer molding (RTM) and vacuum assisted resin transfer molding (VARTM) are used.

Addition of small amounts of CNTs reduces the electrical resistivity of an insulating polymer when a network is formed [44]. Dispersion and alignment of carbon nanotubes coupled with the polymer nanotube contacts play an important role in governing the electrical conductivity of the composite.

Li *et al* [45] studied the effect of nanotube-nanotube contact resistance on the electrical conductivity of carbon nanotube–based nanocomposites. They answered the most fundamental questions on tunneling resistance and investigated its effect on electrical conductivity in CNT-based composite films. The following are the considerations used by them to model the system.

(1) It is a multilayer CNT based composite.

(2) The nanotubes are randomly distributed.

(3) The intertube spacing ranged from 0 to maximum possible thickness of the insulating layer that allows for tunneling.

(4) The thickness of the composite layer is assumed to be twice the tube diameter plus the largest intertube spacing.

Their results showed that tunneling resistance increases rapidly with increase in insulating thickness layer as seen in Figure 2.2. Also, diameters of the CNTs have a moderate effect on the nanotubes. An increase in diameter resulted in a decrease in tunneling resistance.

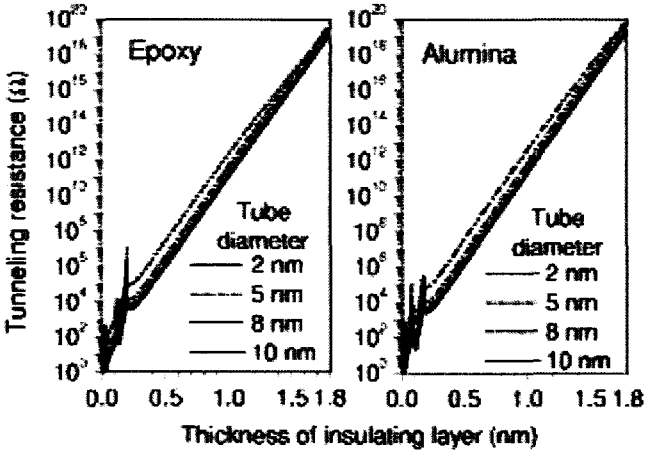

Figure 2.2. Effect of thickness of the insulating layer and the nanotube diameter on the tunneling resistance (adapted from Li et al).

The electrical conductivity of the composite strongly depends on the contact resistance. It sharply drops with increase in contact resistance. Their findings emphasize that the contact resistance plays a dominant role in determining the properties of polymer / ceramic composites as compared to the intrinsic resistance of CNT in CNT mats. The maximum allowable thickness of the insulating layer can be 1.8 nm for tunneling. In the

following chapters we investigate and demonstrate the effect of using SWNTs and tuning their processing capabilities to develop conductive polymer composites.

Ajayan *et al* [42] were among the first group to observe the alignment of carbon nanotubes polymer composites. Since CNTs conduct along their sidewall, by aligning them in a polymer composite the electrical resistivity in the direct of the alignment can be lowered. They obtained alignment of CNTs in a polymer composite by cutting thin slices it. A detailed discussion on the dispersion and alignment is presented in chapters 3 and 4.

CHAPTER 3: High Temperature Bismaleimide/Carbon Fiber Composites Filled with Nickel Coated Single Walled Carbon Nanotubes for Lightning Strike Protection.

3.1 Introduction

Multifunctional carbon fiber composites are imperative for next generation lightweight aircraft structures. However, lightning strike protection is a lacking feature in many modern carbon fiber high temperature polymer systems due to their high electrical resistivity. Every airplane on an average is struck by lightning at least once a year, hence, lightning strike protection is one of the most important considerations taken into account in building new aircrafts. When lightning strikes the unprotected structure, extremely high amounts of current ranging from 10 K to 100 K amperes seeks the path of least resistance. The two main goals of lightning strike protection are: to provide a continuous conductive path so the lightning remains on the exterior of the surface and secondly, electromagnetic interference (EMI) shielding to prevent the damage of onboard electronics.[46]

Figure 3.1 shows a schematic for the protection of the Boeing 787 dreamliner which is a new generation aircraft that incorporates the use of composites for fuel efficiency.[47] Materials used to overcome the issue of high resistivity in lightweight composites include incorporation of metal meshes, [48] carbon nanofibers, [49] metal foils, and various nanomaterials. Nanostructural materials like carbon nanotubes show tremendous promise for structural applications due to their excellent electrical, mechanical and thermal properties combined with their lightweight.[50,11,51] Wei *et al* [37] discuss the possibility of

using carbon nanotubes as lightning arrestors due to their outstanding electrical conductivity and sharpness of their tips.

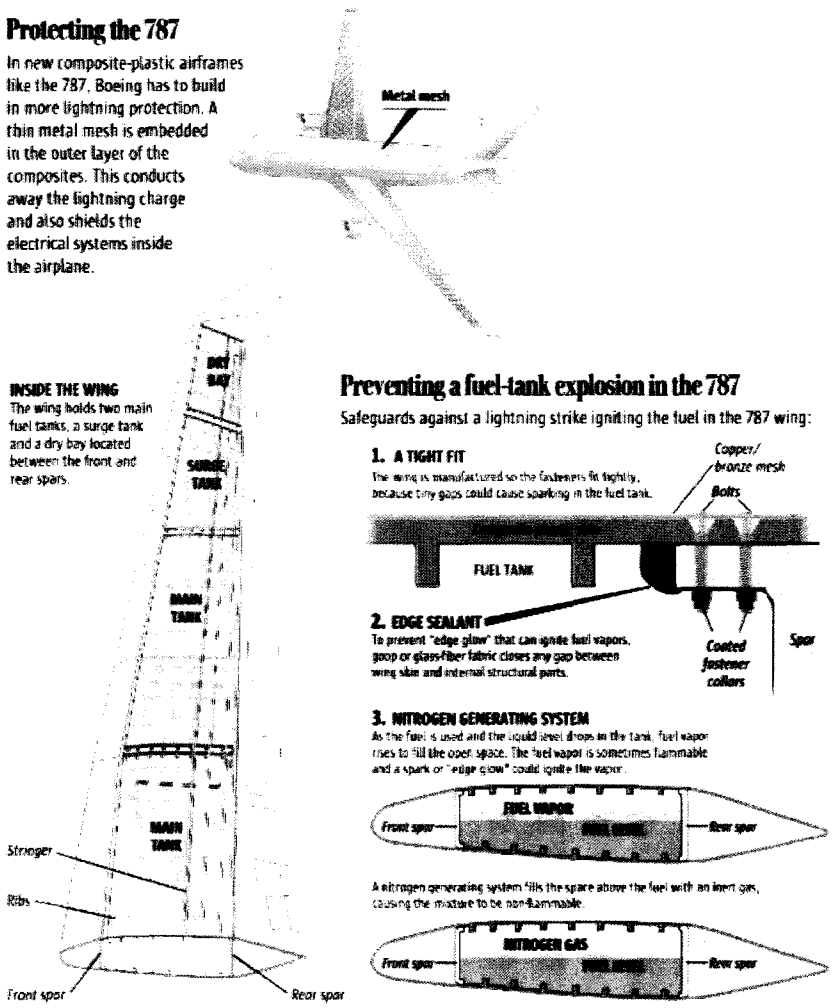

Figure 3.1. Boeing 787 lightning strike protection system (downloaded from Bloomberg News, NASA).

Gou *et al* [52] studied the lightning strike damage in epoxy composites reinforced with porous, non woven, flexible papers of carbon nanofiber and nickel nanostrands. They observed that the electrical conductivity of the carbon nanofiber – nickel nanostrand

paper played an important role in providing safe conductive paths for lightning strike dissipation. Gibson and Fielding [48] investigated the use of copper and nickel coated carbon nanofibers with bucky papers as reinforcements for lightning strike protection. They showed that these reinforcements tremendously increase the electrical conductivity of the epoxy composites as compared to their uncoated carbon fiber-epoxy counterparts. Also, they observed that the use of specially aligned bucky paper reduced the fiber damage caused by simulated lightning strike by 47%. Nanomaterials that are promising candidates for improving the electrical properties of polymer composites are shown in Table 3.1.

Table 3.1. Nanomaterials considered for lightning strike protection.

Materials	**Property Advances**
Carbon nanotubes	Very high aspect ratios, Excellent thermal, electrical properties and mechanical strength.
Bucky planes [53]	Bucky paper weighs only 15% as much as copper, only thin sheets are required. Aligned bucky papers can distribute current all through the aircraft so it can dissipate. Good for electro-magnetic interference shielding.
Graphene sheets [54]	Low costs, easy to process, low weight and exceptional electrical properties combined with good mechanical strength.
Vapour grown carbon fibres [55]	Tailored electrical and mechanical properties, better heat distortion temperatures and increased electromagnetic interference shielding.
Nickel nanostrands [56]	They are very similar to carbon nanofibers and multiwall carbon nanotubes and also provide the additional electromagnetic, chemical, catalytical, and metallurgical properties of nickel.

The exclusive effect of nanomaterials and the failure analysis at the central region of the lightning strike is essential to understand the efficiency of these new materials in preventing lightning strike damage.

3.2 Experimental

Pristine SWNT material (lot PO289, average SWNT diameter ~ 0.7 nm – 1.2 nm, length ~ 1 micron) grown by HiPco process was obtained from Carbon Nanotechnology, Inc. (at present, Unidym) and before further use, was purified using the process described by Chiang *et al.* [57,58] The purified SWNTs were coated with nickel using an electroless plating method adapted from Ang *et al.*[59] Carbon plies (2D, plain weave, 6K tow, carbon fiber fabrics) used as reinforcement and Bismaleimide (BMI, CYCOM® 5250-4 RTM) resin used as a matrix were purchased from Fabric Development, Inc. and Cytec Engineered Materials, respectively.

3.2.1 Pretreatments and electroless plating of SWNTs with nickel

SWNTs (1 mg/ml) were sonicated in 2-propanol (IPA) for 10 minutes to disentangle the bundles. Further, they were centrifuged and the well isolated SWNTs were collected for coating with nickel.

A schematic of electroless plating procedure is shown Figure 3.2. Electroless plating can be divided into three steps: sensitization, activation and plating. In the sensitization step, dispersed SWNTs were sonicated in 0.1M $SnCl_2$/0.1M HCl solution for 30 minutes. Then, the Sn^{2+} sensitized SWNTs were stirred in an activating solution of 0.0014M $PdCl_2$ / 0.25M HCl for 30 minutes and washed with de-ionized water before introduction into an electroless plating bath. Composition of plating solution and the reaction conditions

are given in Table 3.2. The pH and the temperature of the plating bath were maintained at 8 and 25°C respectively.

After the plating process, plated SWNTs were washed with de-ionized water followed by a methanol wash. The morphology and size of the nickel-coated SWNTs was analyzed by scanning electron microscopy (SEM) and transmission electron microscopy (TEM).

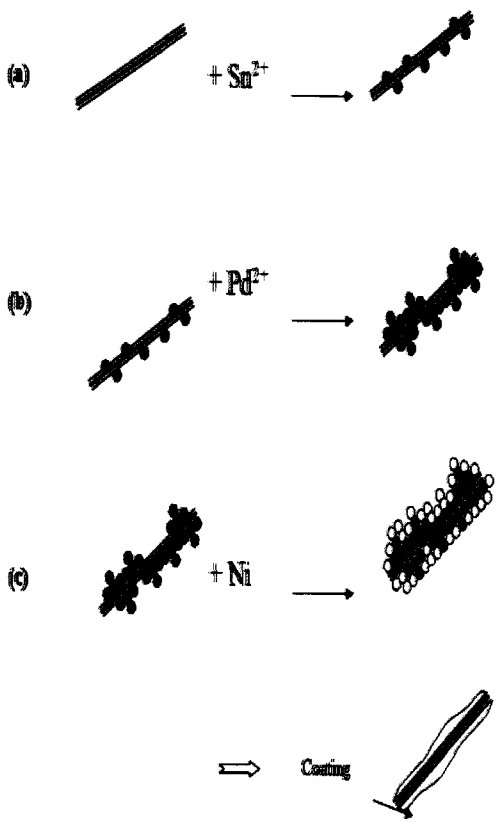

Figure 3.2. Schematic of electroless plating procedure used to deposit nickel on the outer surface of carbon nanotube

Table 3.2. Composition and operating conditions of electroless nickel coating bath

Compound	Concentration (mol/l)
$NiCl_2 \cdot 6H_2O$	0.25
$NiSO_4 \cdot 6H_2O$	0.09
$Na_2C_6H_5O_7 \cdot 1.5H_2O$	0.054
$NaH_2PO_2 \cdot 2H_2O$	0.84
NH_4Cl	1.87
$Pb(NO_3)_2$	$7.5*10^{-3}$

3.2.2.1. Dispersion of SWNTs

Dispersions of purified SWNTs (1mg/ml) were prepared in dimethyl formamide (DMF), ethanol, tetrahydrofuran, toluene and NMP. All the suspensions were sonicated for 60 minutes using a tip sonicator (Cole Parmer ultrasonic homogenizer) and, for 30 minutes in a bath sonicator (Branson 5200 ultrasonic cleaner). Further, the effect of decanting on the bundle diameters was studied using dynamic light scattering (DLS).

3.2.2.2. Dispersion of Ni-SWNTs.

Dispersions of 0.2, 0.35, and 0.5 mg of Ni-SWNTs in 1 ml of three different solvents were studied. The solvents used were ethylenediamine, tetrahydrofuran (with oleylamine) and toluene (with oleylamine). The amount of oleylamine surfactant added was, 0.5 ml for every 15 ml of the solvent. Ni-SWNT suspensions were sonicated for 60 minutes using a tip sonicator and, for 30 minutes in a bath sonicator. After sonication, the

suspensions were divided into 1.5 ml aliquots and centrifuged at 13000 rpm for 30 minutes. The supernatant obtained was used for dispersion studies. This step removed large agglomerates and can be used for any number of Ni-SWNT treatment processes.

Atomic force microscopy (Digital Instrument Nanoscope IIIA Atomic Force Microscope, AFM) was used to analyze the effectiveness of the solvent in dispersing Ni-SWNTs. For AFM measurements, silicon chips functionalized with APTS ((3-Aminopropyl triethoxysilane) were used as substrates. Samples were made by depositing a drop of the dispersion on the substrate and drying them overnight under vacuum. To get an approximate measure of the aspect ratios DLS was used to analyze the suspensions.

3.2.3. Surface coverage of purified and Ni-SWNTs on the carbon plies.

To study the surface coverage, 1, 2 and 4 wt % (with respect to the weight of the carbon fiber) Ni-SWNTs and purified SWNTs were sprayed onto 10 cm x 10 cm fabric using a Paasche VL-SET airbrush. Surface coverage was analyzed using Scanning Electron Microscopy (FEI Quanta 400 ESEM). A schematic of the spray set up is shown in Figure 3.3.

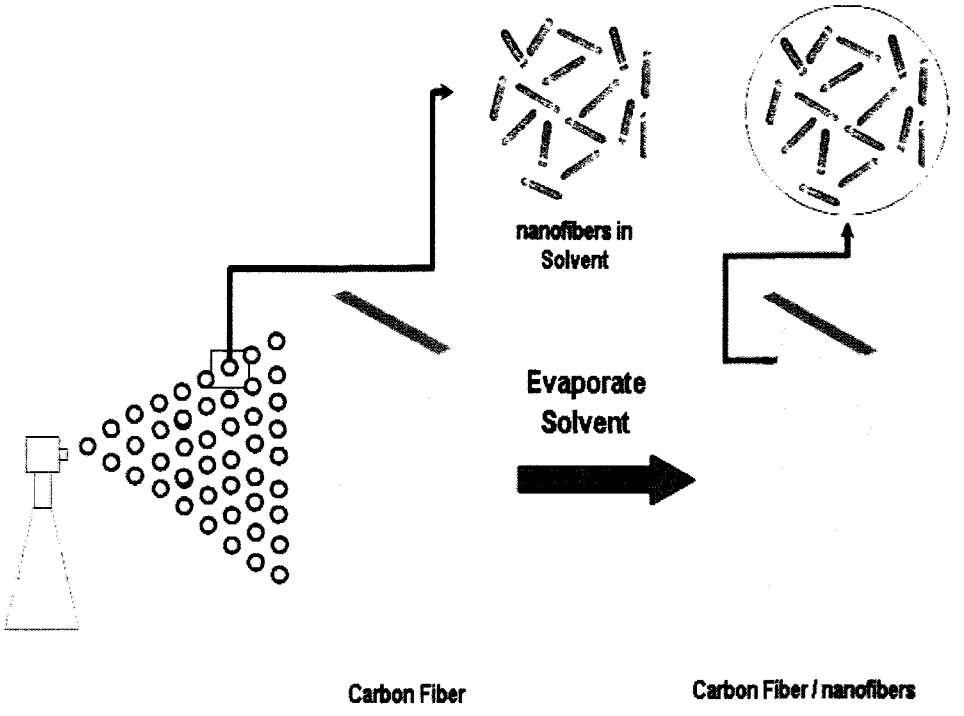

Figure 3.3. Schematic of the spray set up used to study the surface coverage of Ni-SWNTs and purified SWNTs on the carbon fiber (adapted from Kim *et al* [60]).

3.2.4. Composite Processing and characterization.

Composites were processed using a high temperature vacuum assisted resin transfer molding (VARTM) process (Figure 3.4A). An appropriate amount of BMI (210 grams for 8 layers of 14" x 14" carbon plies) that is frozen in a large block was pulverized with mallet. Figure 3.4 shows the lay up of the high temperature BMI infusion process. When heated to 107°C (225°F), BMI liquefies and saturates the carbon fiber preform. Due to the gas permeable membrane, the air is evacuated and the resin stays in leaving a void free part. BMI cures when heated above the melt stage. Figure 3.4B shows the oven temperature cycle used in the processing.

Surface electrical resistivity of the composites was measured using a Monroe 262A Surface Resistance Meter (at the NASA Johnson Space Center by Padraig Moloney) and four point probe. Composites processed with 1, 2 and 4 wt% Ni-SWNTs were used in this study. The weight percent was calculated with respect to the weight of 17.8 cm x 17.8 cm size carbon ply sample which weighed 12.75 grams. Raman spectroscopy analysis (Renishaw Micro Raman system) operating with a 780 nm AlGaAs diode laser source was used to study the attachment of nickel to the sidewall of the SWNTs and the effect of composite processing on the Ni-SWNTs.

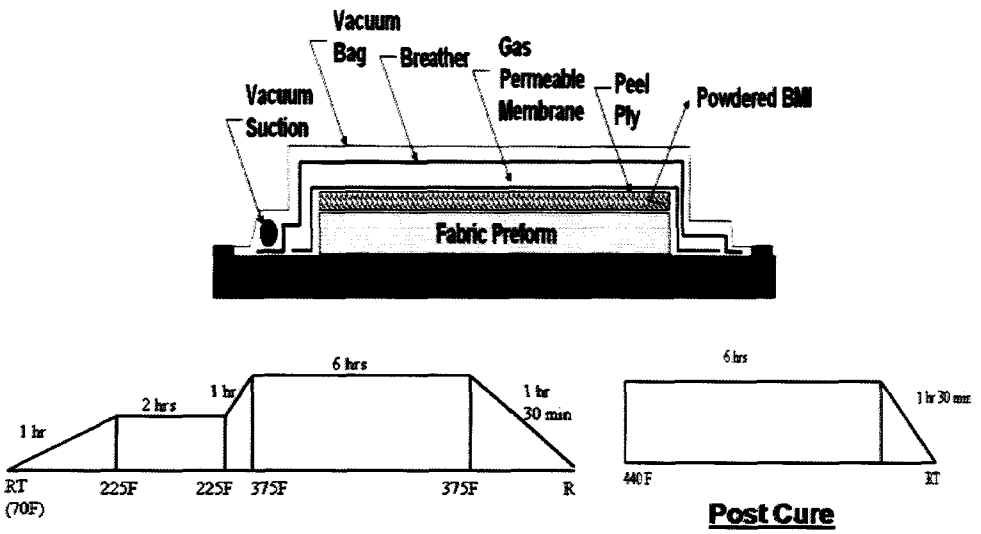

Figure 3.4. (a) Modified VARTM method for BMI-carbon composite fabrication.

(b) Oven temperature cycle used for BMI/Carbon fiber composite fabrication.

3.2.5. Lightning Strike Simulation Testing and Failure Analysis

4 wt% Ni-SWNTs/Carbon fiber/BMI composites were subjected to simulated lightning strike experiments at Lightning Technologies, Inc. in Pittsfield, Massachusetts. The

composite panels were coated with a paint, which provides a reasonably good dielectric finishing coating. When lightning approaches this finish, the lightning channel tends to concentrate at the weakest point in the dielectric, resulting in a high concentration of energy being applied. The panels were tested based on MIL STD 1757A (Zone 2A lightning strike), with the current being 100 KA (component D), 3.8 KA (component B), and 0.558 KA (component C) [48]. A photograph of the actual test set up is shown in Figure 3.5. Failure analysis of simulated lightning strike tested samples involved studies of the effects of high currents on the resin, fiber and Ni-SWNTs. Most of the characterization involved SEM analysis of different areas of the samples. EDS, XPS and ICP (inductively coupled plasma) techniques were also used to analyze the presence of Ni-SWNTs before and after lightning strike, and any structural changes that may have occurred due to very high temperature and current.

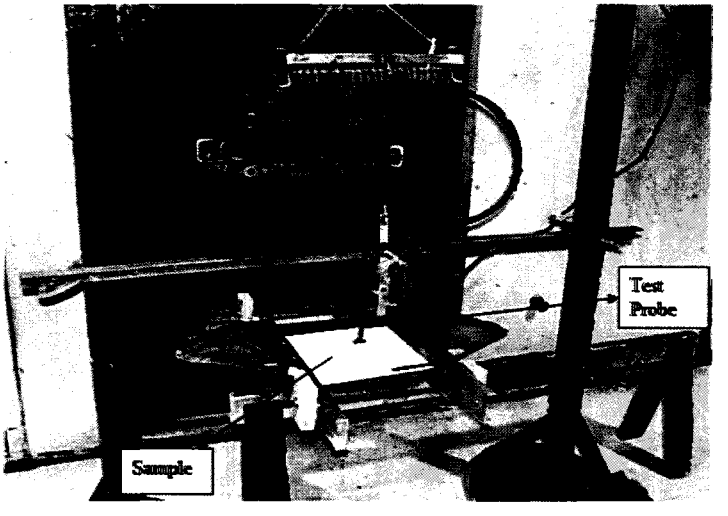

Figure 3.5. Simulated lighting strike testing set up at Lightning Technologies Inc.

3.3. Results and Discussion.

3.3.1 Characterization of purified SWNTs and Ni-SWNTs.

Thermo gravimetric analysis (TGA) was performed to determine the amount of metal content in the tubes after purification. From Figure 3.6 the amount of metal impurity after purification was determined to be 0.7467%.

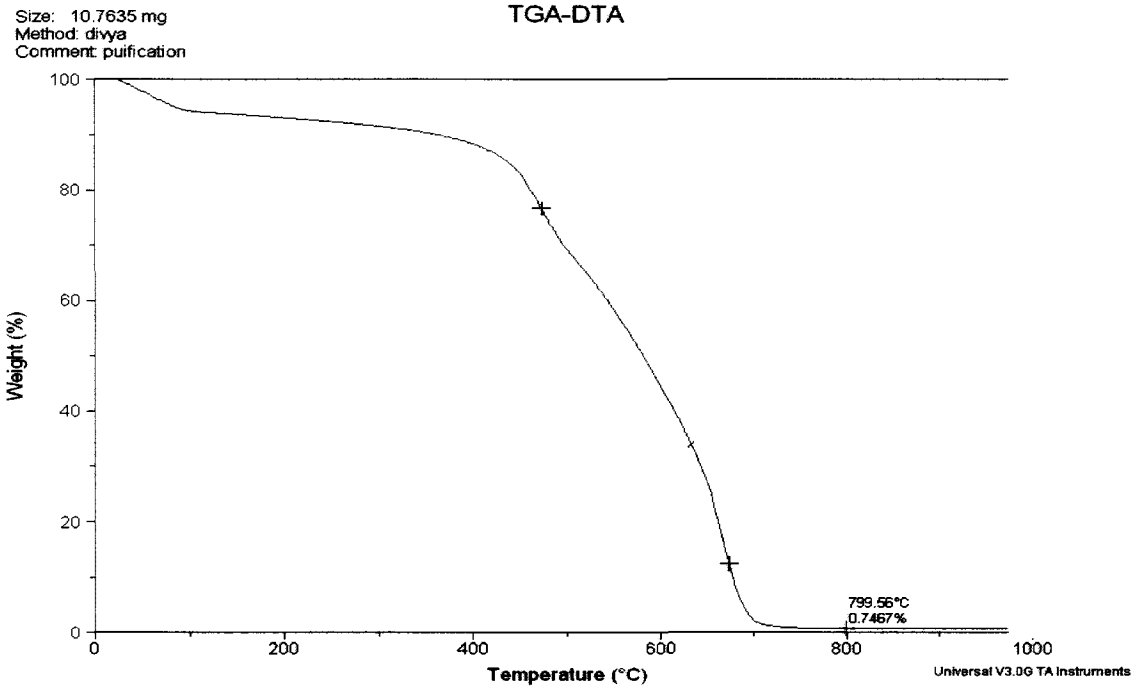

Figure 3.6. TGA of purified SWNTs (amount of metal content 0.7467%)

Figure 3.7 shows the Raman spectra of purified tubes. It can be seen that the D peak is very minimal indicating removal of defects and high level of purity which is confirmed by the TGA analysis. Figures 3.7 and 3.8 show the SEM images of purified SWNTs and SWNTs coated with nickel. It can be seen from the SEM images that Ni-SWNTs are better disentangled than purified nanotubes.

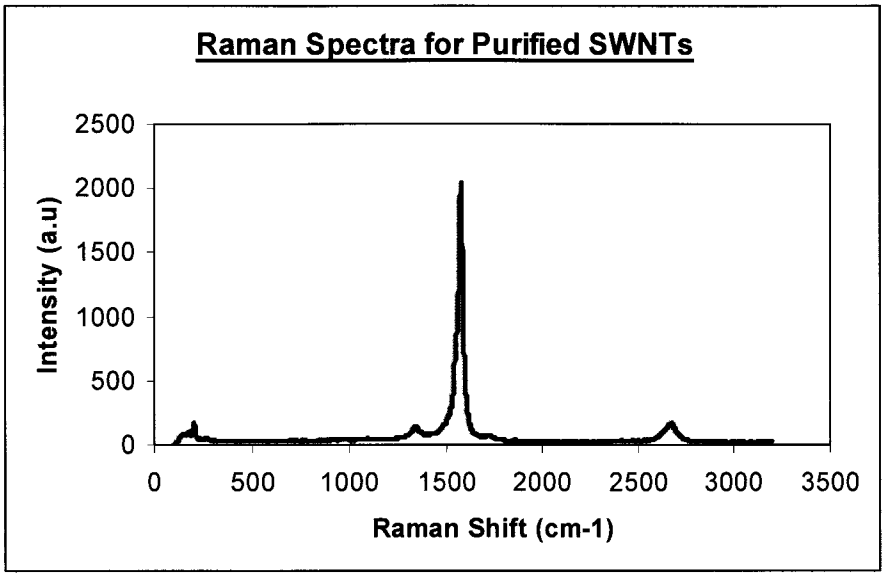

Figure 3.7. Raman spectrum of purified SWNTs.

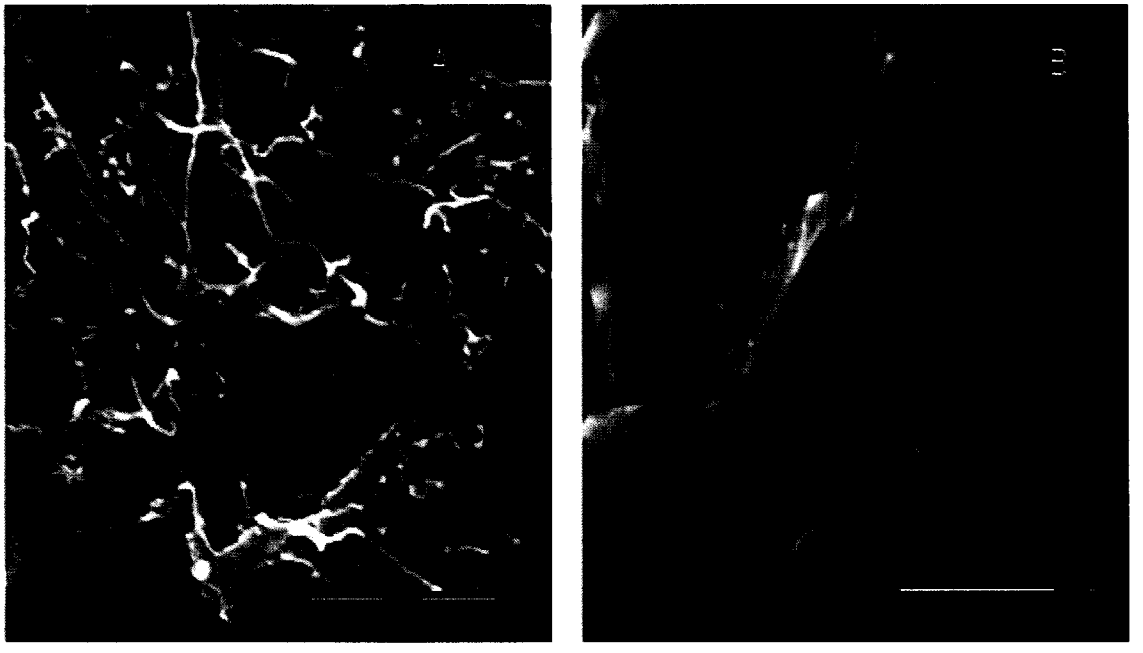

Figure 3.8. SEM images of A) Ni-SWNTs, B) purified SWNTs

3.3.2. Dispersion Studies.

Carbon nanotubes tend to aggregate due to their high surface energies and intrinsic Van der Waal's forces and are extremely resistant to wetting. In order to effectively utilize their unique mechanical and electrical properties, stable dispersions of carbon nanotubes in solvents are important. Hence, a number of studies have been carried out to determine the effect of solvents, surfactants, functionalization of nanotubes and energy in disentangling the tubes. Liu *et al* [61] and Ausman *et al* [62] demonstrated dispersions of nanotubes in N, N-dimethylformamide (DMF) and 1-methyl 2- pyrrolidone (NMP) respectively. Ausman *et al* also studied the dispersions in various solvents. Giordani *et al* [63] suggest that in order to effectively disperse the carbon nanotubes, a solvent should form a weak hydrogen bond and have a strong ability to donate electrons.

Attachment of chemical entities to the nanotubes not only improves their solubility in the solvents, but also enhances their interaction with the polymer. The two main types of functionalization are covalent and non-covalent. In the case of covalent functionalization, the chemical groups are covalently bonded to the sidewall or the end of the nanotubes. This results in the change of the hybridization from sp^2 to sp^3 resulting in the loss of conjugation. Covalent functionalization is mostly preferred as it enhances the mechanical properties of the polymer composites. This is due to a better interface between the matrix and the filler because of the improved dispersions and interactions. Non-covalent functionalization refers to wrapping of nanotubes mainly based on supramolecular complexation using various adsorption forces.[64] Figure 3.9 shows a schematic of the various types of functionalization. However, to preserve the unique electrical properties

of nanotubes, tip functionalization or non covalent wrapping of nanotubes is preferred as compared to sidewall functionalization.

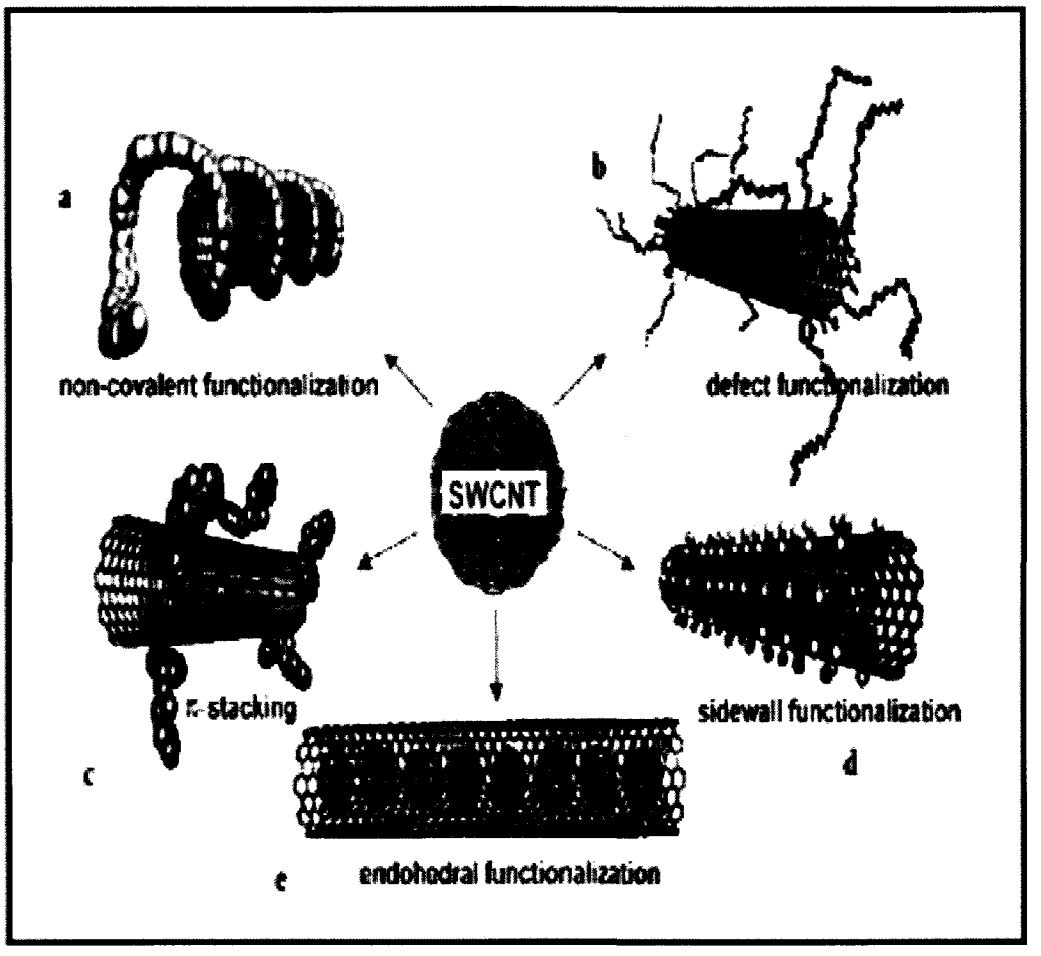

Figure 3.9. Various types of functionalization of SWNTs a) non – covalent functionalization b) defect functionalization c) functionalization through π stacking d) sidewall covalent functionalization and e) endohedral functionalization by filling the SWNTs [64].

In this section, dispersion analysis of purified and nickel coated SWNTs is discussed. The effect of solvent, surfactant and decanting on the dispersion efficiency is presented. DLS and AFM analysis were used for characterization.

3.3.2.1 Dispersion of purified SWNTs

After sonication, it was found that SWNTs suspended in toluene and ethanol were not stable and sedimented in 30 minutes, whereas suspensions of nanotubes in DMF (showed sedimentation after 3 hours) and NMP (was stable for over 24 hours) were stable for longer periods of time. Figure 3.10 shows optical micrographs (Zeiss Polarizing Optical Microscope using transmittive mode with a 20X objective) of suspensions of purified SWNTs in DMF and NMP. Large amount of agglomeration in the case of purified nanotubes / DMF suspensions compared to SWNT/NMP suspensions is observed. Dark patches seen in the optical micrographs indicate agglomeration.

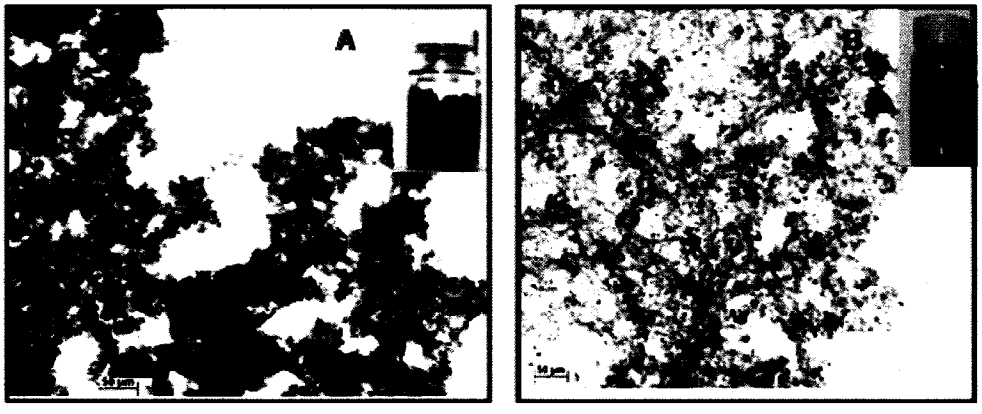

Figure 3.10. Dispersion of purified SWNTs in A) DMF indicating large amounts of agglomeration B) NMP indicating a uniform network along with some agglomeration and no sedimentation.

From the figures above, it can be seen that NMP is a better solvent to disperse the nanotubes. High lone pair donacity of NMP probably plays a role in better solvent – nanotube interaction. Also, Giordani *et al* [65] were certain that very high interaction energy between the NMP solvent and the nanotubes resulted in very small

positive or negative enthalpy of mixing which is favorable for nanotubes to be thermodynamically soluble in the solvent.

Suspensions containing SWNTs in NMP were centrifuged at 15000 rpm for 30 minutes to study the effect of decanting on the bundle diameters (Figure 3.11). Since direct imaging techniques such as AFM and TEM only give information on the dispersion of a very small fraction of the sample. DLS was used for a quick analysis of the diameter and length distributions of the SWNTs. Sano *et al* [66] discussed the efficacy of using DLS to analyze the nanotube bundle diameters and lengths. Quantitative analysis of diameters from DLS cannot be solely relied on since it is based on measurement of dispersion of light scattering caused from the particle motions in the solvent and it depends on the orientation of the particles. Hence DLS should be used in conjunction with other imaging techniques. Our results for SWNT / NMP suspensions are in agreement with Giordani et al [63], who also found stable dispersions of SWNTs in NMP at concentrations of 1 mg/ml when decanted at 6000 rpm for 90 minutes. The resultant SWNT diameters of their samples ranged from 1.2 to 6 nm.

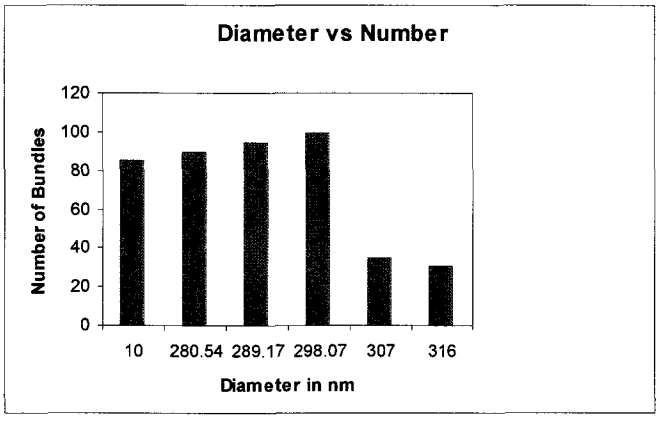

Figure 3.11. Diameter and length of SWNTs in NMP suspensions after decanting at 15000 rpm for 30 minutes.

3.3.2.2 Dispersion of Ni-SWNTs

Literature shows depending on the method used for coating of purified SWNTs with nickel, the diameters of the coated tubes ranged from 3 to 40 nm.[67,58,68,69]. The diameter of the nickel coated SWNTs processed in our lab ranged from 5 to 25 nm. The particles on the SWNTs in Figure 3.12 are nickel, and in some places it can be seen that instead of single SWNTs, ropes of SWNTs are coated with nickel. This can be due to entanglement of purified SWNTs before the coating, since most of the electroless plating takes place in DI water medium in which the SWNTs tend to agglomerate.

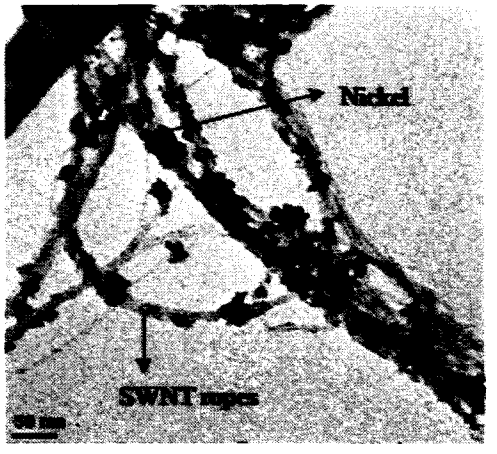

Figure 3.12. Nickel particles on the sidewall of the SWNTs obtained by electroless plating.

Amine based solvent (ethylene diamine) and amine based surfactants (oleylamine) were used to study the dispersions of Ni-SWNTs because amine groups form a complex with transition metals which will help in improving their dispersions. The structure of oleylamine is shown in Figure 3.13. Rostro [70] has shown that the interesting structure of oleylamine is very useful for enhanced dispersion of nanotubes in solvents by micelle formation. Oleylamine in combination with polar solvents like tetrahydrofuran (THF) and toluene can effectively disperse the metal coated SWNTs.

Figure 3.13. Structure of Oleylamine.

SWNTs are hydrophobic; they exhibit anisotropy and are fibrous. The π electrons in the SWNTs interact with the hydrophobic part of the oleylamine molecule and the amine groups interact with the nickel. Amine-amine interactions between oleylamine leads to micelle formation which helps in forming a network in the solvent. Figure 3.14 shows a photograph of the Ni-SWNT suspensions in THF, toluene and ethylene diamine. All suspensions were visibly homogeneous, dark colored and show no sedimentation even after two weeks, indicating a good dispersion.

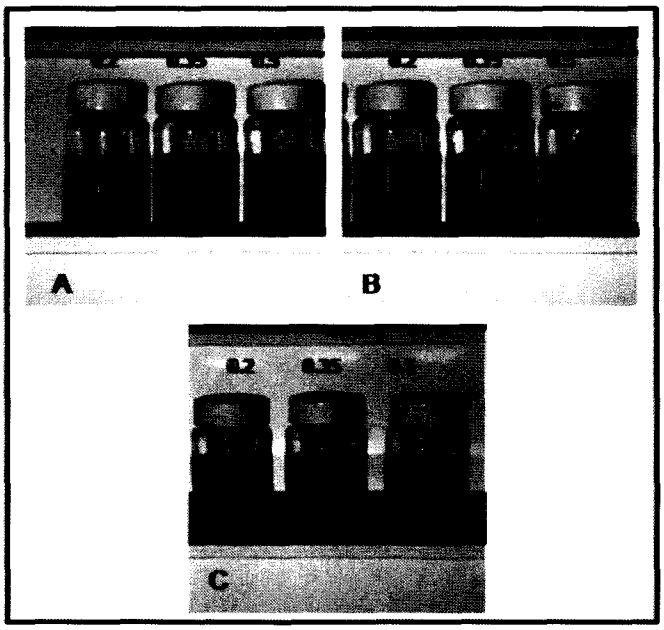

Figure 3.14. Dispersions of Ni-SWNTs in various solvents after 14 days (no visible sedimentation was observed: A) Ni-SWNTs dispersed in THF / Oleylamine B) Ni-SWNTs in toluene / Oleylamine C) Ni-SWNTs in ethylenediamine.

Figures 3.15 and 3.16 show the DLS analysis of Ni-SWNTs dispersed in THF with and without oleylamine surfactant after decanting at 13000 rpm for 30 minutes. The concentration of the Ni-SWNTs was maintained at 0.2 mg/ml and 0.35 mg/ml. It can be seen that the addition of oleylamine drastically reduced the bundle diameters and inhibits agglomeration. The diameter of the bundles/agglomerates was reduced from 80 nm to 3.5-5 nm when the Ni-SWNTs concentrations were maintained as 0.2 mg/ml and, from 101 nm to 11 nm for 0.35 mg/ml concentrations. The aspect ratios of the Ni-SWNTs (0.2mg/ml) increase from 10 to 228 approximately by addition of oleylamine indicating intercalation between the Ni-SWNTs and de-agglomeration. Furthermore, Rostro has shown that the combination of non-covalent interactions from the metal complex, hydrogen bonding from oleylamine, π stacking and hydrophobic forces leads to formation of a self assembled fibrillar network.

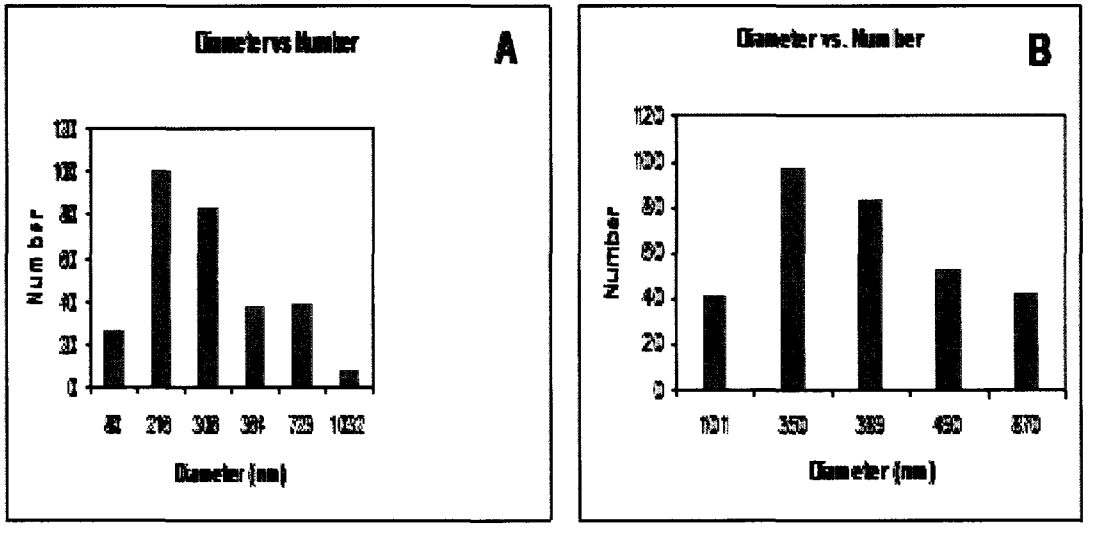

Figure 3.15. Decanted Ni-SWNTs-THF suspensions indicating agglomeration

A) 0.2mg/ml B) 0.35mg/ml.

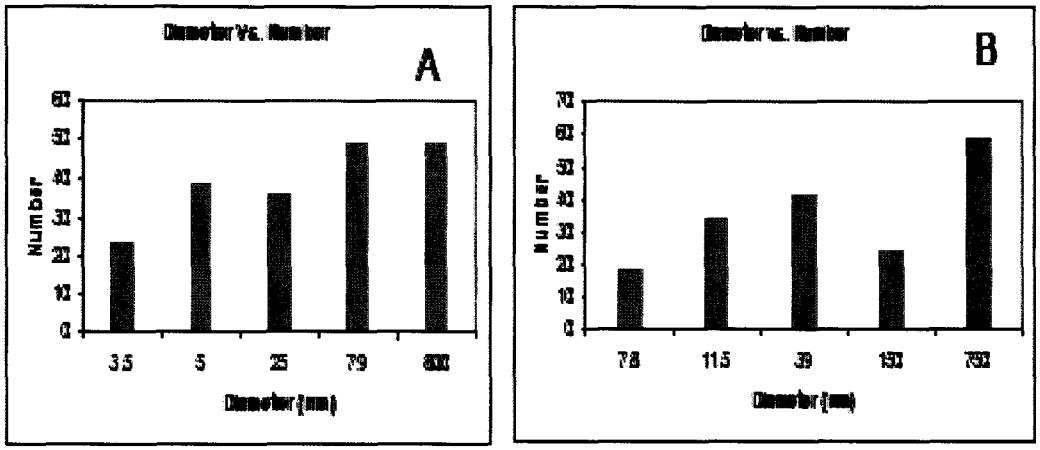

Figure 3.16. Decanted Ni-SWNTs in oleylamine and THF showing a reduction in the diameter of the agglomerates by addition of surfactant A) 0.2 mg/ml B) 0.35 mg/ml.

Similar behavior was found for Ni-SWNTs in toluene and oleylamine suspensions (as shown in Figures 3.17 and 3.18). However, the bundle diameters of Ni-SWNTs were slightly larger than the Ni-SWNTs/THF/oleylamine suspensions. This might be due to THF being more polar than toluene which leads to better interaction with oleylamine resulting in improved dispersions. Maeda et al [71] have also seen enhanced dispersions of SWNTs in THF with amine based surfactants.

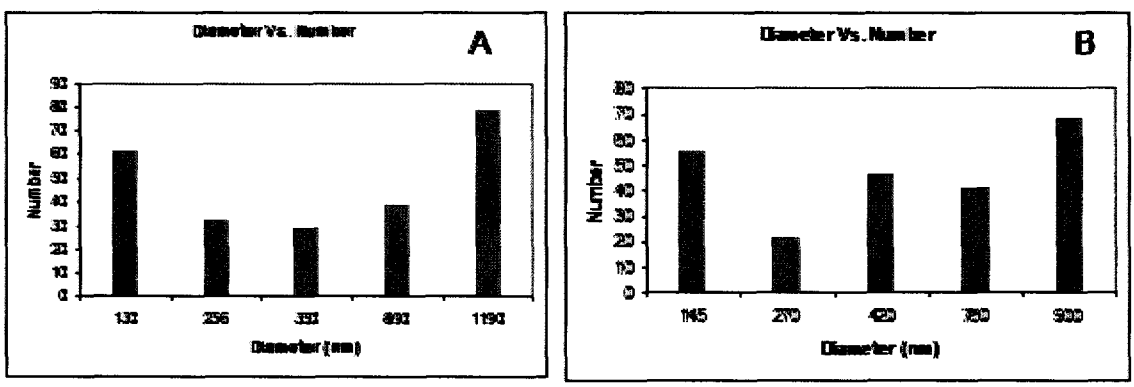

Figure 3. 17. Decanted Ni-SWNTs-Toluene suspensions indicating agglomeration A) 0.2mg/ml B) 0.35mg/ml.

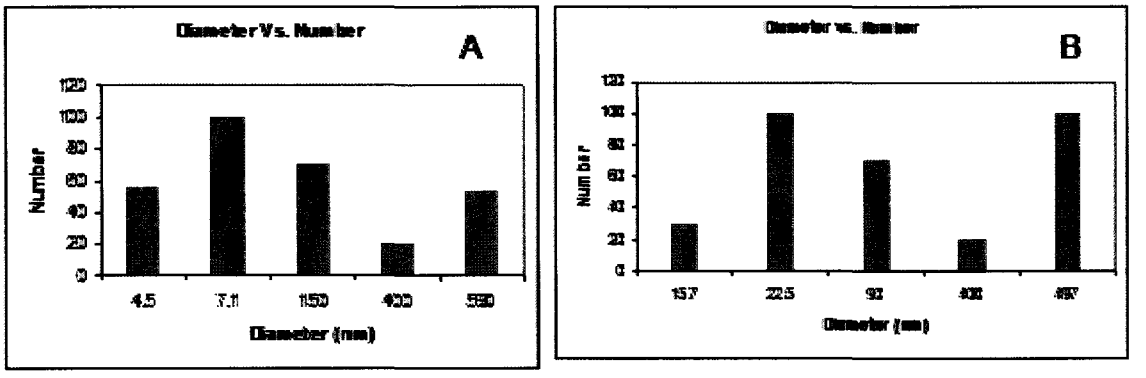

Figure 3.18. Decanted Ni-SWNTs in oleylamine and toluene showing a reduction in the diameter of the agglomerates by addition of surfactant A) 0.2 mg/ml B) 0.35 mg/ml.

It was observed that suspensions containing 0.2 mg and 0.35 mg of Ni-SWNTs per ml of the solvent were better dispersed than suspensions containing 0.75 mg of Ni-SWNTs/ml of the solvent. Hence, only the data for 0.2 mg/ml and 0.35 mg/ml Ni-SWNTs dispersions are shown. The diameters of the decanted Ni-SWNTs dispersed in ethylenediamine were around 4 – 6 nm and 5 – 12 nm in 0.2 mg/ml and 0.35 mg/ml concentrations respectively (Figure 3.19). The diameters of the Ni-SWNTs before decanting were in approximately 90 – 125 nm.

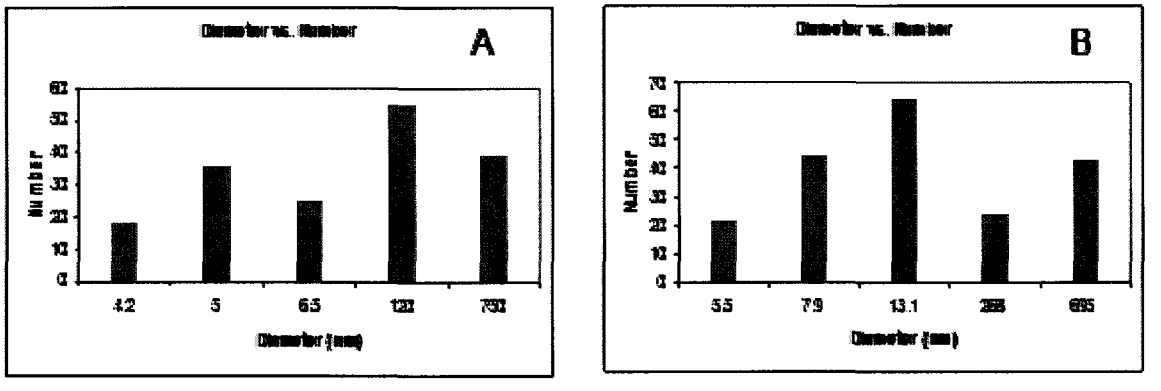

Figure 3.19. Decanted Ni-SWNTs in ethylenediamine showing a reduction in the diameter of the agglomerates by addition of surfactant A) 0.2 mg/ml B) 0.35 mg/ml.

AFM analysis on the decanted Ni-SWNTs-solvent suspensions is shown in Figure 3.20. It can be seen that the AFM diameters obtained are in fair agreement with the DLS data. The AFM images show bright spots on the backbone of the SWNTs which indicate the presence of nickel. The AFM measured diameters of Ni-SWNTs in suspensions ranged from 3 to 15 nm (in ethylenediamine), 4 to 35 nm (in toluene + oleylamine) and 4 to 15 nm (in THF + oleylamine).

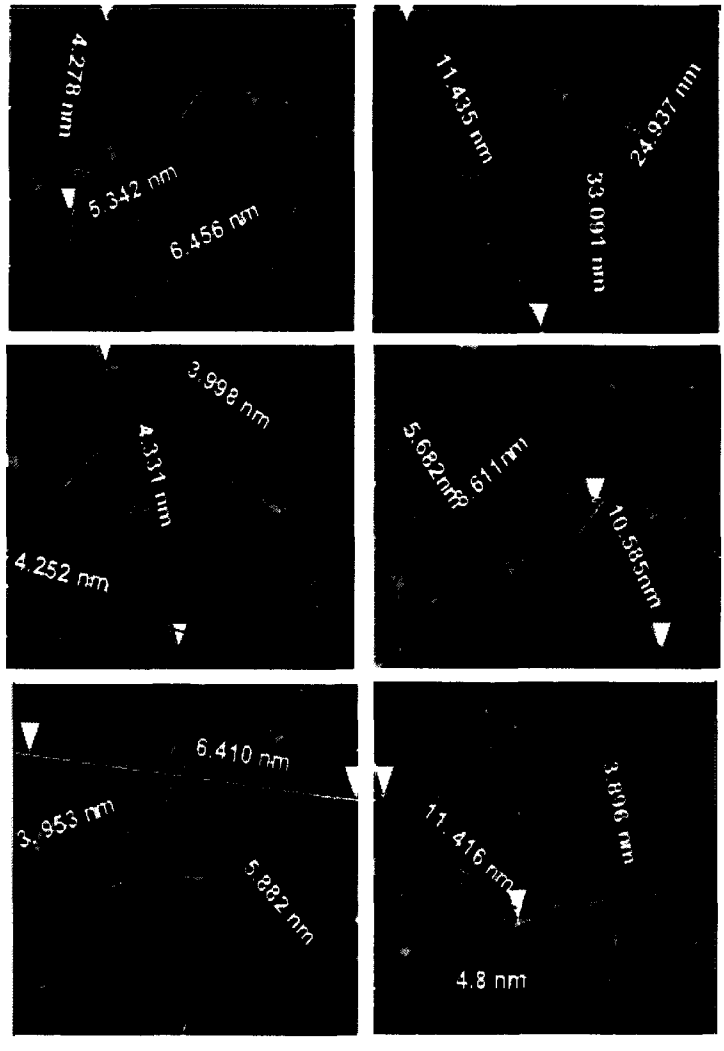

Figure 3.20. Cross sectional height analysis of dispersion of Ni-SWNTs: a and b) 0.2 mg/ml and 0.35mg/ml in toluene with oleylamine, c and d) 0.2 mg/ml and 0.35mg/ml in THF with oleylamine, e and f) 0.2 mg/ml and 0.35mg/ml in ethylenediamine.

3.3.2.3 Raman Analysis of the Ni-SWNTs suspensions

Raman spectroscopy is an exceedingly useful tool to study the vibrational properties and electronic structures of SWNTs.[72,73,74] The strongest features observed in the Raman spectrum of SWNTs are (i) Radial breathing modes corresponding to the vibration of the C atoms in the radial direction (RBM) are unique features in the CNTs (ii) high frequency G mode (tangential mode associated with the sp^2 hybridization) which usually occurs around 1590 cm^{-1} (iii) disordered induced D band. [72] D band is due to the presence of defects, any alteration or introduction of sidewall functionalization to the SWNTs will result in the increase in intensity of the D band. However, the limitation of Raman spectroscopy is that the amount of functionalization cannot be quantified. [75]

Raman spectra of decanted Ni-SWNTs in THF-oleylamine, in toluene-oleylamine and in ethylenediamine are shown in Figure 3.21. No increase in the intensity of D-peak is observed for samples suspended in ethylenediamine and a very small increase in the D peak is observed for samples suspended in solvents to which oleylamine was added. Oleylamine only wraps around the SWNTs and does not covalently bond to them. So, this minor increase in D peak does not necessarily indicate any sidewall functionalization. The Raman data indicates that the effect of sonication, decanting and addition of surfactant does not induce defects on the sidewall of the SWNTs.

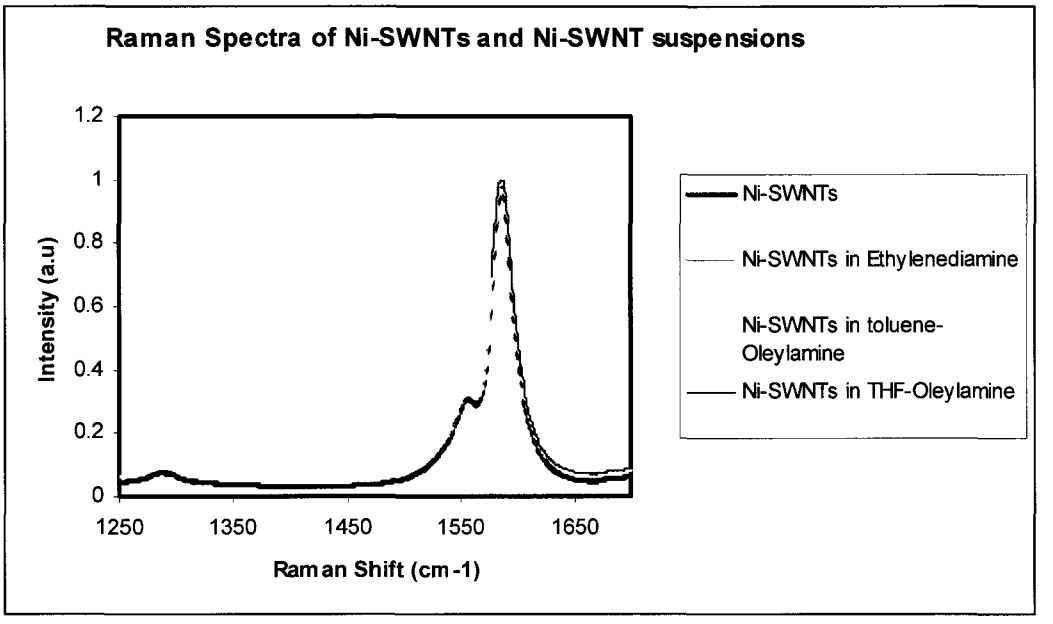

Figure 3.21. Raman spectra of Ni-SWNTs and Ni-SWNT suspensions

From the dispersion analysis it can be concluded that Ni-SWNTs disperse well as predicted in amine based solvent and surfactants. The concentration of Ni-SWNTs should be maintained between 0.2 mg/ml and 0.35 mg/ml to obtain a stable suspension.

3.3.3 Surface coverage of purified SWNTs and Ni-SWNTs on the surface of carbon plies.

Surface coverage of 1, 2 and 4 wt% SWNTs and Ni-SWNTs on the carbon plies was studied. Prior to spraying, all carbon plies were heated to 100°C, which prevented formation of large droplets of the suspensions and also improved the surface roughness of the carbon fiber to provide a better interaction with the filler and the matrix. The SEM micrographs are representative of the whole sample because different areas in the sample were used for analysis to ensure the reproducibility of the results. The most common method to introduce CNTs into fiber reinforced composites is mixing them with the resin

followed by resin infusion. It is well known that addition of CNTs increases the resin viscosity.[76,77,78] leading to processing difficulties. In our study we sprayed the SWNTs on the carbon fiber and then infused the resin. The latter is a better technique, since, it eliminates the viscosity issues which limit the high concentration of Ni-SWNT nanofillers that can be used and, their location on the fiber can be controlled depending on the properties desired. Hence, studying the surface coverage of carbon plies is important because (i) it helps in determining efficiency of the solvent in wetting the surface of the carbon fiber (ii) the dispersion and network formation can be gauged from SWNT coverage (iii) resistivity measurement of the carbon fibers along with SWNT can be used to determine the optimal nanotube concentration for electrical conductivity applications.

3.3.3.1 Surface coverage of Ni- SWNTs on carbon plies.

Figure 3.22 shows the effectiveness of the solvent in wetting the surface of the carbon fiber. Ni-SWNTs in THF and ethylenediamine show better coverage on the carbon fiber than toluene.[79] Partial coverage of Ni-SWNTs toluene suspensions may be a result of insufficient wetting of the carbon fiber by the solvent. Furthermore, mats of Ni-SWNTs cover the surface of the carbon fiber when THF is used as a solvent; this indicates that the Ni-SWNTs agglomerate once the solvent/surfactant evaporates. A clear network of reasonably dispersed Ni-SWNTs is seen when ethylenediamine is used as the solvent. Also, it can be seen that the Ni-SWNTs not only cover the surface of the carbon fibers, but also bridge the gaps between them forming a continuous network.

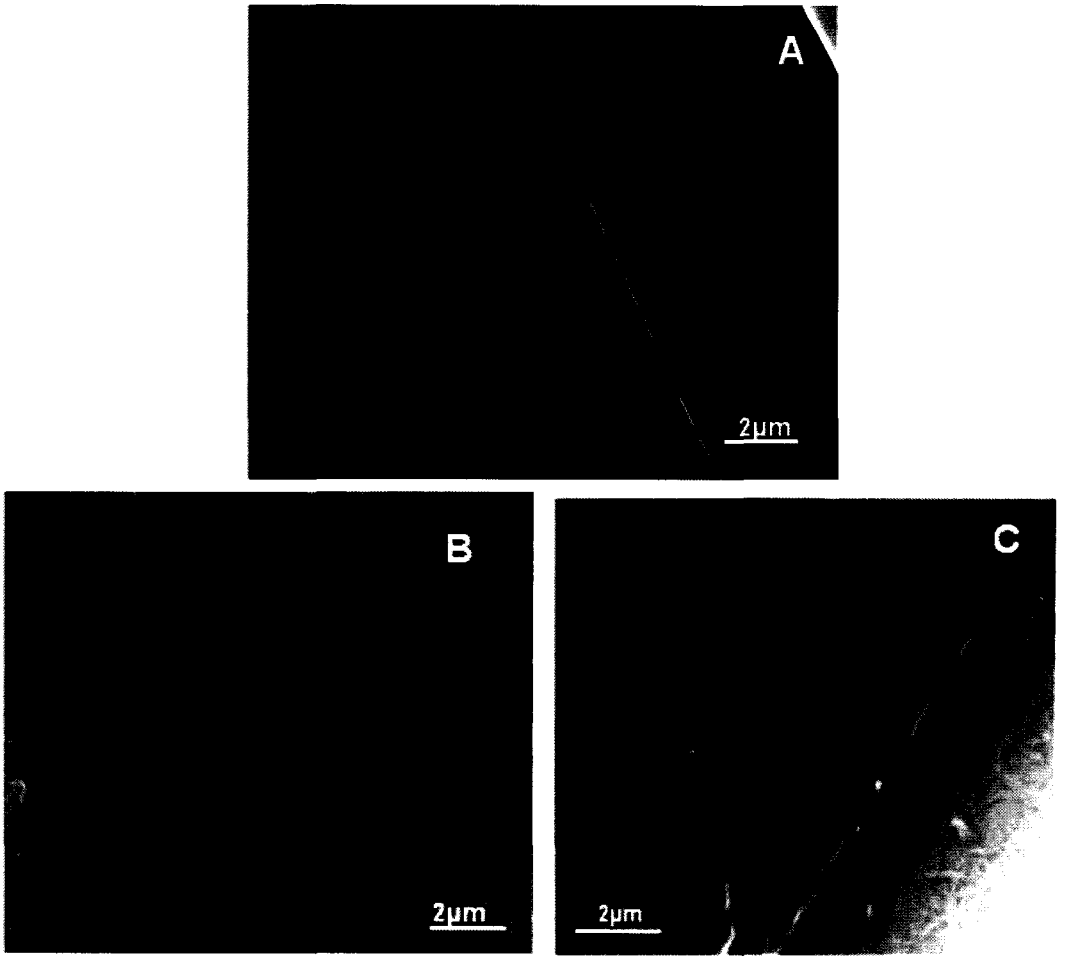

Figure 3.22. Surface coverage of Ni-SWNTs on the carbon fiber (A) dispersed in toluene-oleylamine suspensions (B) dispersed in THF-oleylamine suspensions (C) dispersed in ethylenediamine.

1, 2 and 4 wt% Ni-SWNTs in ethylenediamine were analyzed further since they showed an enhanced surface coverage and dispersion on the surface of the carbon fiber. Continuous surface coverage on the carbon fibers plies was seen when the concentration of the Ni-SWNTs was ~ 4wt%. Figures 3.23, 3.24, 3.25 and 3.26 show the coverage of various concentrations of Ni-SWNTs with respect to the weight of the carbon plies.

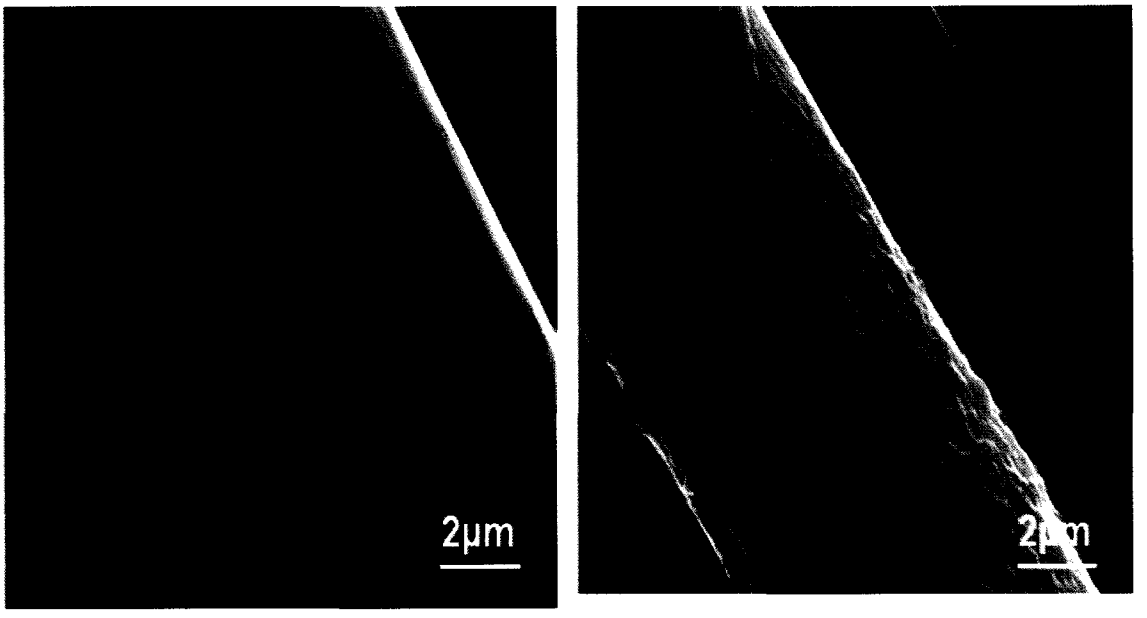

Figure 3.23. 1 wt% Ni-SWNTs suspended in ethylenediamine sprayed onto carbon plies showing a non uniform and discontinuous surface coverage.

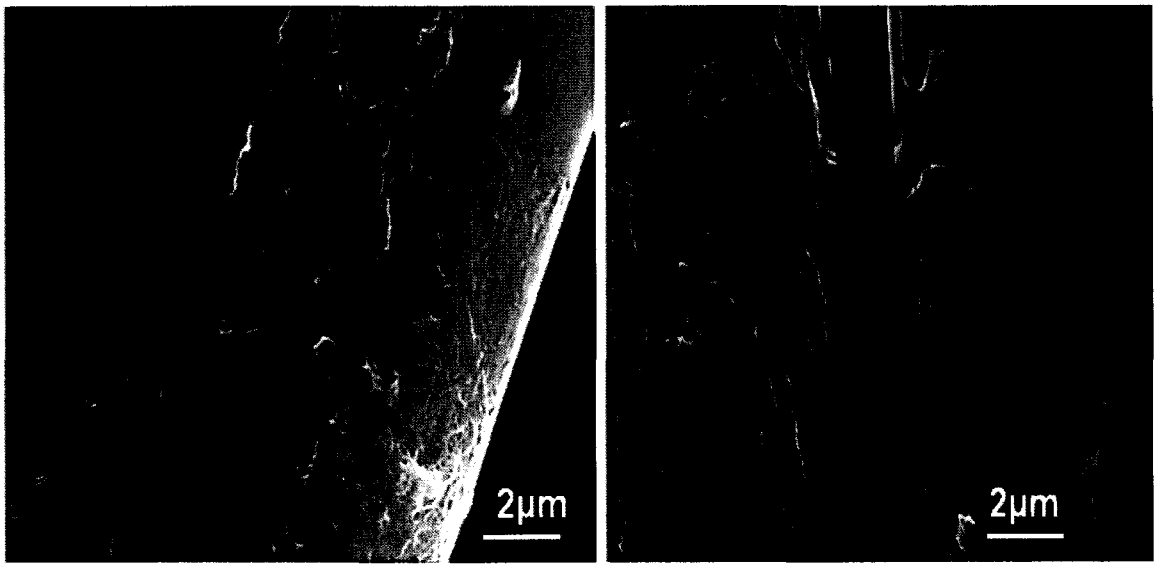

Figure 3.24. Partial surface coverage of 2 wt% Ni-SWNTs dispersed in ethylenediamine.

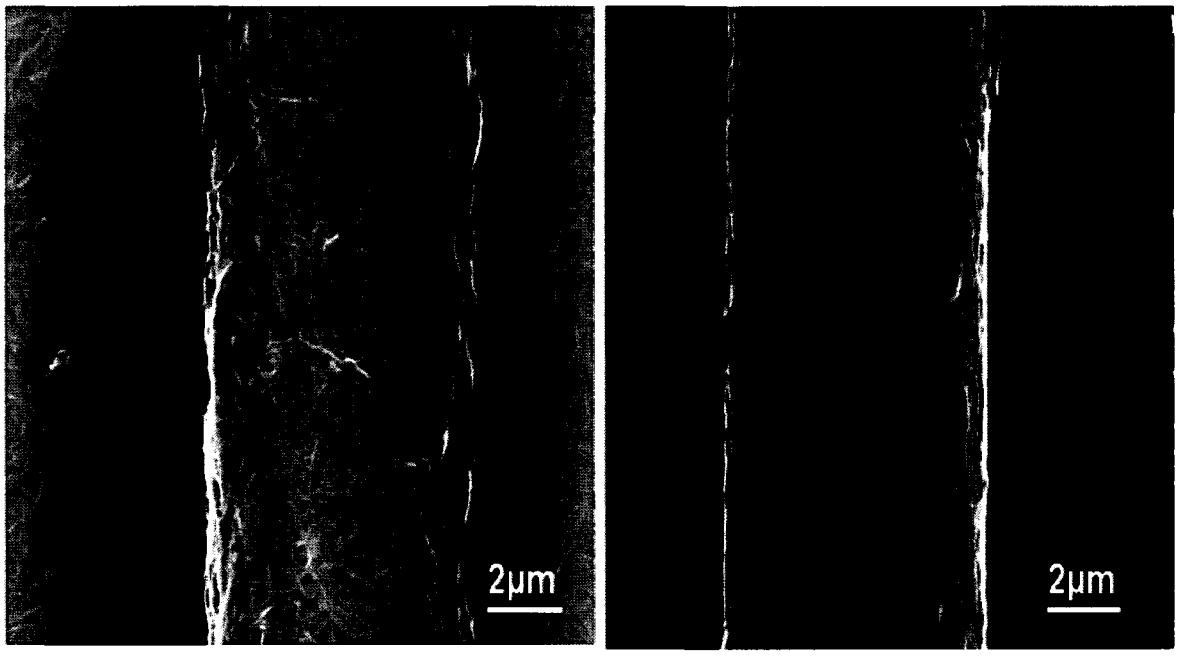

Figure 3.25. Ni-SWNTs in ethylenediamine (4 wt %) showing a continuous surface coverage on the carbon plies.

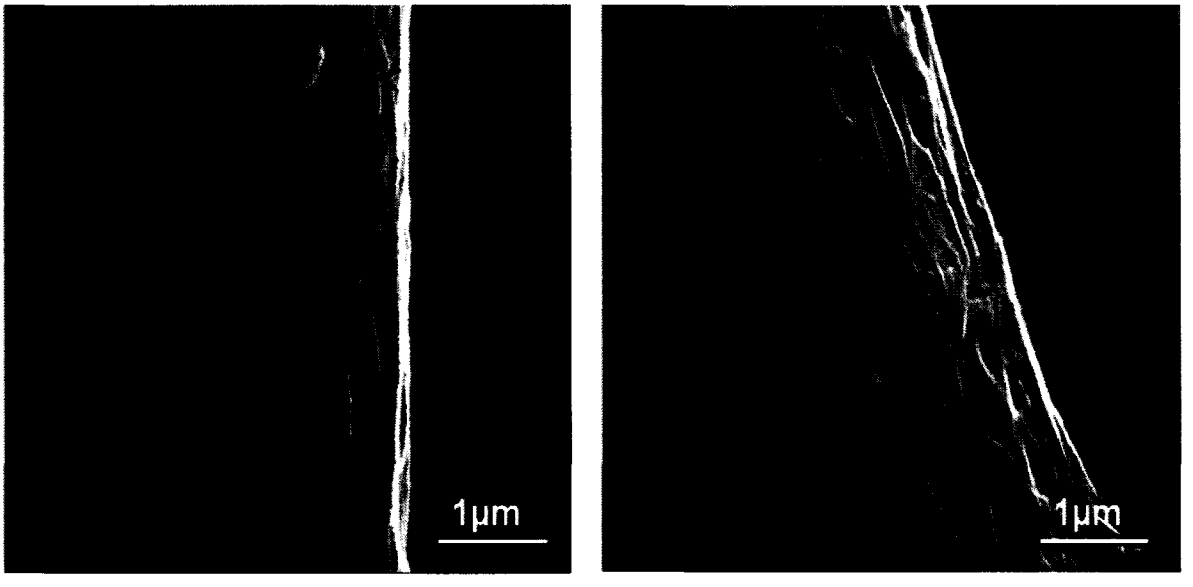

Figure 3.26. Higher magnification image of the carbon plies showing a uniform coverage of Ni-SWNTs.

3.3.3.2. Surface coverage of purified SWNTs on carbon plies.

In the case of purified SWNTs, similar behavior as seen with Ni-SWNTs was observed. 4 wt% SWNTs showed better coverage. Agglomeration of SWNTs was observed for all concentrations and mats of SWNTs were coated on the carbon fiber (as shown in Figure 3.27). If only electrical properties of the material are under consideration, this kind of network on carbon fiber by Ni-SWNTs/NMP suspensions is acceptable, but not for structural properties because agglomeration reduces effective load transfer between the fiber and the matrix.[80] The advantage of using high aspect ratio fillers is lost due to agglomeration.

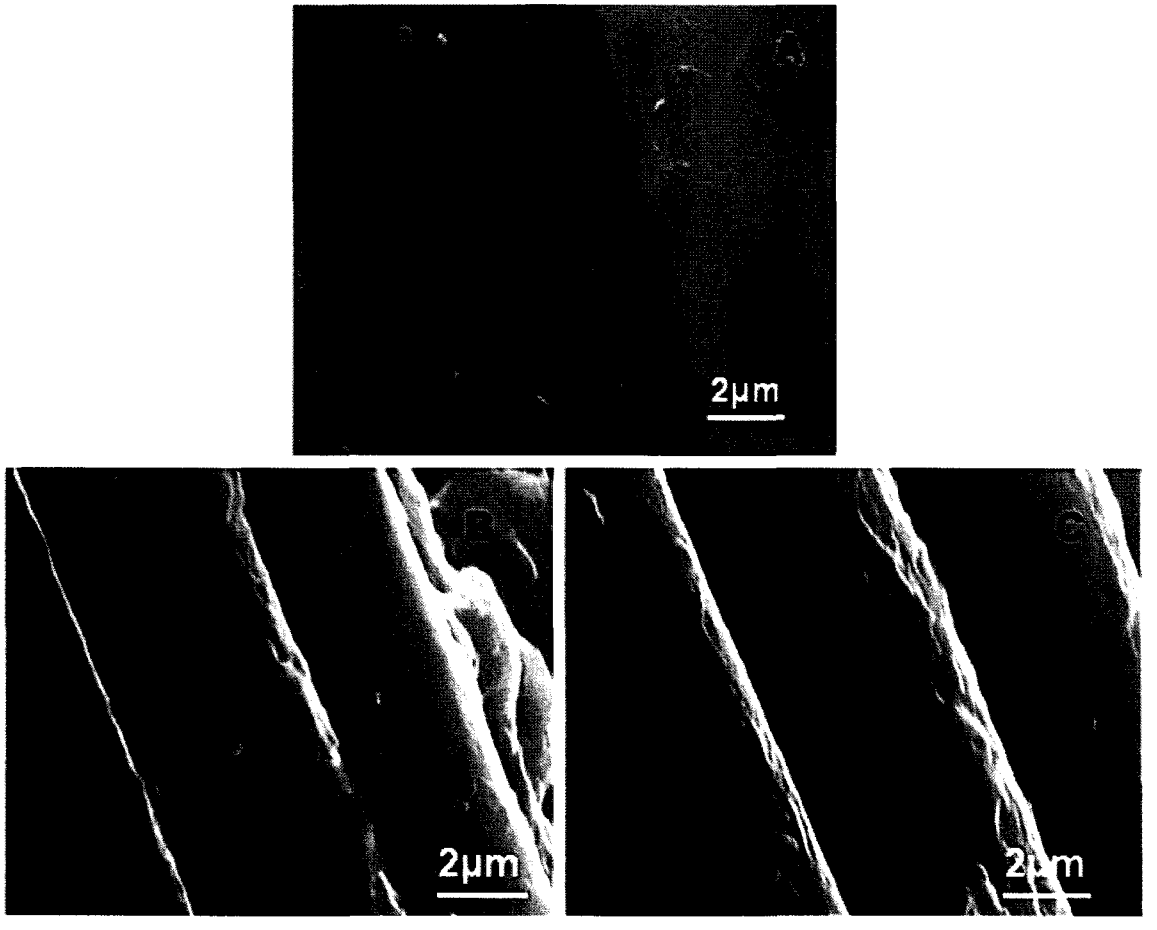

Figure 3.27. Surface coverage of purified SWNTs dispersed in NMP on carbon plies (A) 1wt% SWNTs (B) 2wt% SWNTs (C) 4wt% SWNTs.

3.4. BMI/carbon fiber/Ni-SWNT composites.

Bismaleimide resins (BMIs) are high temperature thermosetting polymers whose thermal curing characteristics are superior to conventional epoxy systems. Their ease of processibility combined with high thermal stability, modulus and flame retardant properties, make them the most sought after resins for high temperature applications.[81]However, one of the main drawbacks of these polyimide resins is their brittle behavior, and this can be attributed to their low tensile strength and strain to failure which is common to other brittle materials.[82] To combat the brittle nature of BMI matrices one of the main focus has been "reinforcement" as it has been proven to diminish the mechanical weakness. Carbon nanotubes and carbon fibers have been some of the most promising reinforcements that are being used to improve the mechanical properties of the BMI matrices.[83,84] In our research we have used T600 Toray carbon plies as reinforcements and SWNTs as fillers to study the electrical properties of the hybrid composite.

Tensile behavior of carbon fiber tows impregnated with BMI resin was studied as a function of temperature.[85] Reinforcing BMI with carbon fiber improves their mechanical properties remarkably and also enhances their glass transition temperature making them useful for aircraft applications. Zhang *et al* [86] have studied the mechanical properties of Toray T300, T800 and T700 carbon fiber reinforced modified BMI prepegs and laminates. They found that although composites with T700 had superior compression after impact (CAI), all three fiber reinforced composites showed very good mechanical properties. Figure 3.28 adapted from their paper shows the mechanical properties of the laminates.

Properties	5428/ T300	5428/ T700	5428/ T800
0° tensile strength/MPa	1670	2150	2700
0° tensile modulus/GPa	134	125	158
Poisson's ratio	0.30	0.32	
90° tensile strength/MPa	72	65	
90° tensile modulus/GPa	8.4	7.8	
Elongation/%	0.89	0.89	
0° compression strength/MPa	1230	1210	1760
0° compression modulus/GPa	115	107	148
0° flexure strength/MPa	1734	1640	1620
0° flexure modulus/GPa	122	120	150
Short beam shear strength/MPa	116	97	112

Figure 3.28. Mechanical properties of BMI / Carbon fiber laminates (adapted from Zhang *et a l*[86]).

Cheng *et al* [87,88] engineered BMI/MWNT composites with excellent mechanical and electrical properties. They used MWNT sheets (from Nanocomp Technologies) and impregnated them with a BMI resin solution to make BMI – 60 wt% MWNTs prepegs. Six prepegs were stacked on each other and cured under an extremely high pressure. Figure 3.29 shows the improvement in mechanical and electrical properties of these high temperature polymer composites as a function of the stretch ratio of the MWNT sheets. A remarkable improvement in electrical and mechanical properties was attributed to (i) length and concentration of the MWNTs (ii) Prepegging of BMI-MWNTs sheets (iii) Curing of stacked prepegs under extremely high pressure to ensure contact between the MWNTs. This improved the interface between the MWNT and BMI matrix which subsequently enhance load transfer.

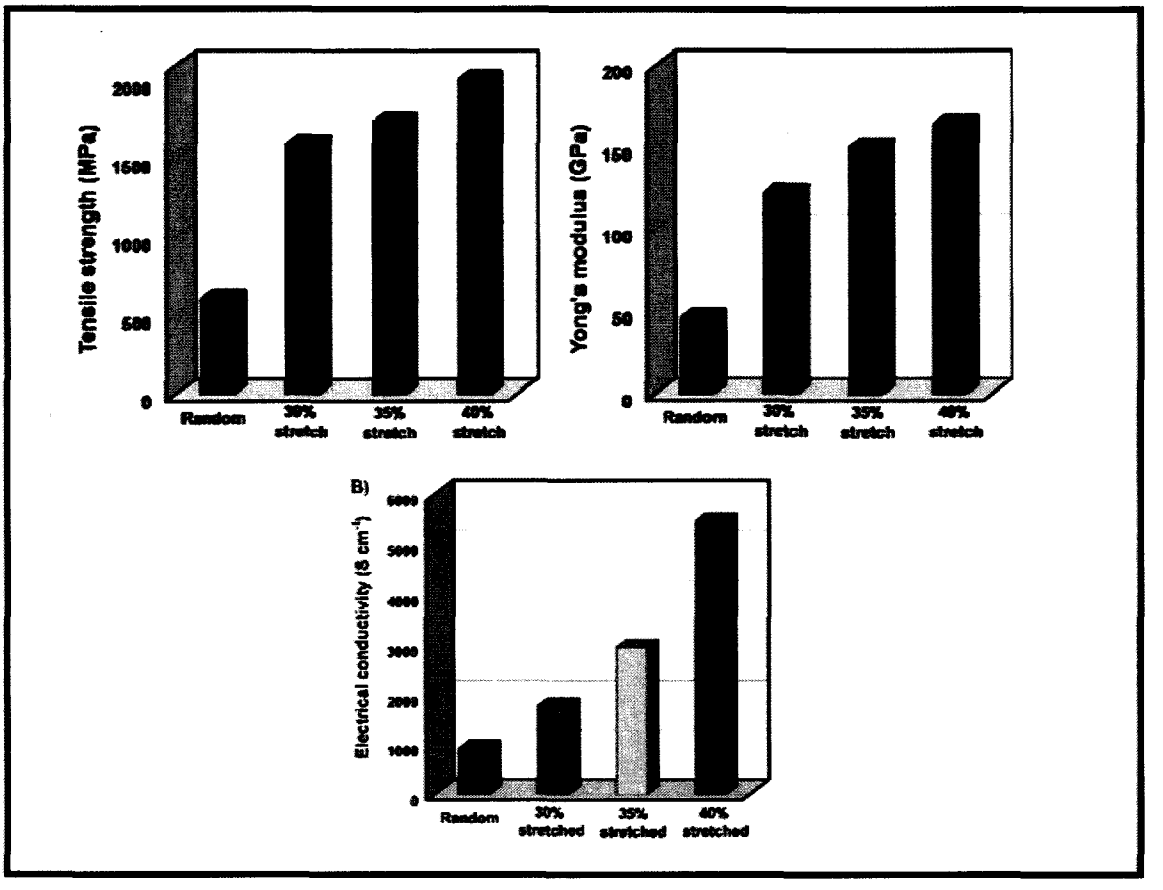

Figure 3.29. Mechanical and electrical properties of the MWNT / BMI composite as a function of the stretch ratio of the MWNT sheets (adapted from Cheng *et al*).

A recent review on electrical percolation of carbon nanotubes in polymer nanocomposites has been published by Bauhofer *et al* [89] . The paper throws light on the effect of various parameters such as CNT type, synthesis and treatment, dimensionality, processing and polymer type on the electrical conductivity of polymer composites. The best conductivities for epoxy composites filled with 2.5 wt% - 3 wt% SWNTs, ranged between 10^{-2} – 10^{1} S/cm. For MWNTs – epoxy composites with filler concentrations ranging from 0.01 wt% to 10 wt% , the highest conductivity reported is 5 S/m. For our studies 1, 2 and 4 wt% Ni-SWNTs and 4 wt% purified SWNTs BMI carbon fiber

composites were fabricated to study the effect of concentration on the electrical resistivity of the composites.

Ni-SWNTs filled BMI carbon fiber composites were fabricated at the Center for Composite Materials at the University of Delaware. The fabrics are laid on top of each other with the Ni-SWNT coated fabric being at the very bottom with the Ni-SWNTs side facing the tool plate as shown in Figure 3.4A. Powdered BMI is laid on the top most fabric and the whole set up is placed in a vacuum oven. Since the molten resin flows from top to bottom, it is expected that BMI will coat the Ni-SWNTs when flowing through them. Prior to characterization by SEM, the composite samples were washed in an ethanol isopropanol mixture to remove BMI debris.

In Figure 3.30, the area indicated is the region where the resin peeled off in the composite. Upon further characterization of the "resin peel off area" in Figure 3.30, the presence of Ni-SWNT network bridging the cracks between the BMI matrix and bonding of Ni-SWNTs with the resin is seen in Figure 3.31.

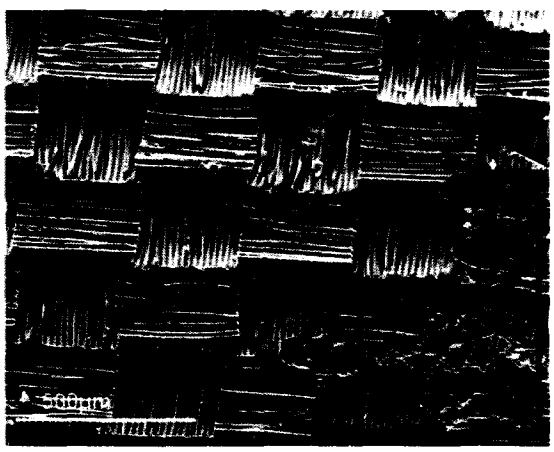

Figure 3.30. BMI/Carbon fiber/Ni-SWNT composite sample showing resin peel off indicated by the rectangle box.

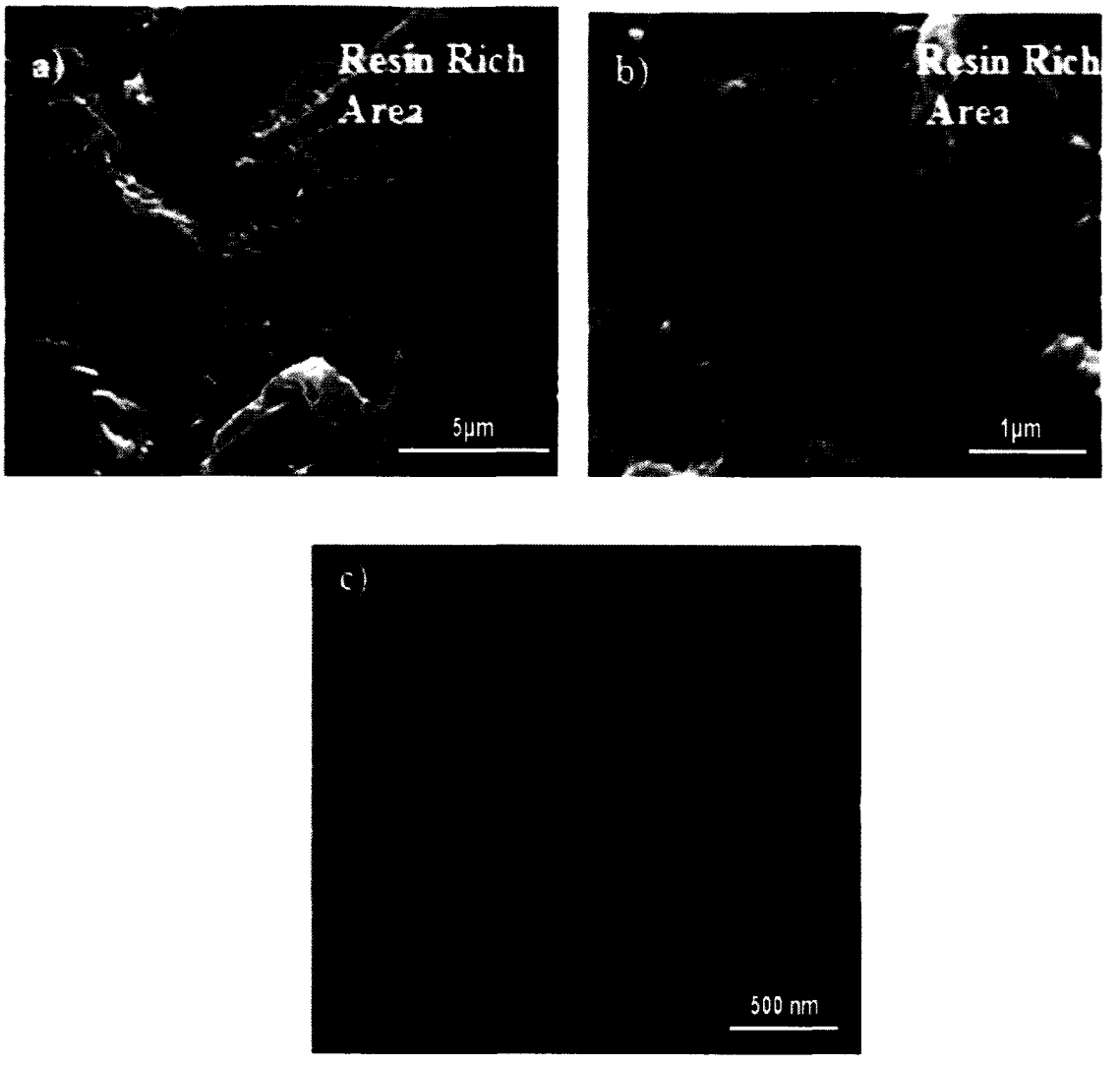

Figure 3.31.a) network of Ni-SWNTs in the BMI composite, b) adhesion of Ni-SWNTs to the BMI resin, c) diameter and length of the Ni-SWNTs that bridges the cracks in the BMI matrix.

The approximate diameter and length of the Ni-SWNTs used, as shown in Figure 3.31c are 36 nm and 2.3 microns respectively. Furthermore, it can be seen that the Ni-SWNTs are coated with the BMI resin in accord with the well-known adhesion of BMI resin to metals which is facilitated by formation of a transition metal complex bonding with the

electron-rich BMI polymer building units. The adhesion of Ni-SWNTs to BMI explains the observed bridging of composite matrix cracks by the Ni-coated nanotubes. Figure 3.32 shows additional images of the Ni-SWNTs in the composite; in some areas nanotube and polymer bundles are found. As expected, Ni-SWNTs form a network under the BMI layer and this network along with high nanotube aspect ratios will enable better electrical properties of the composite.

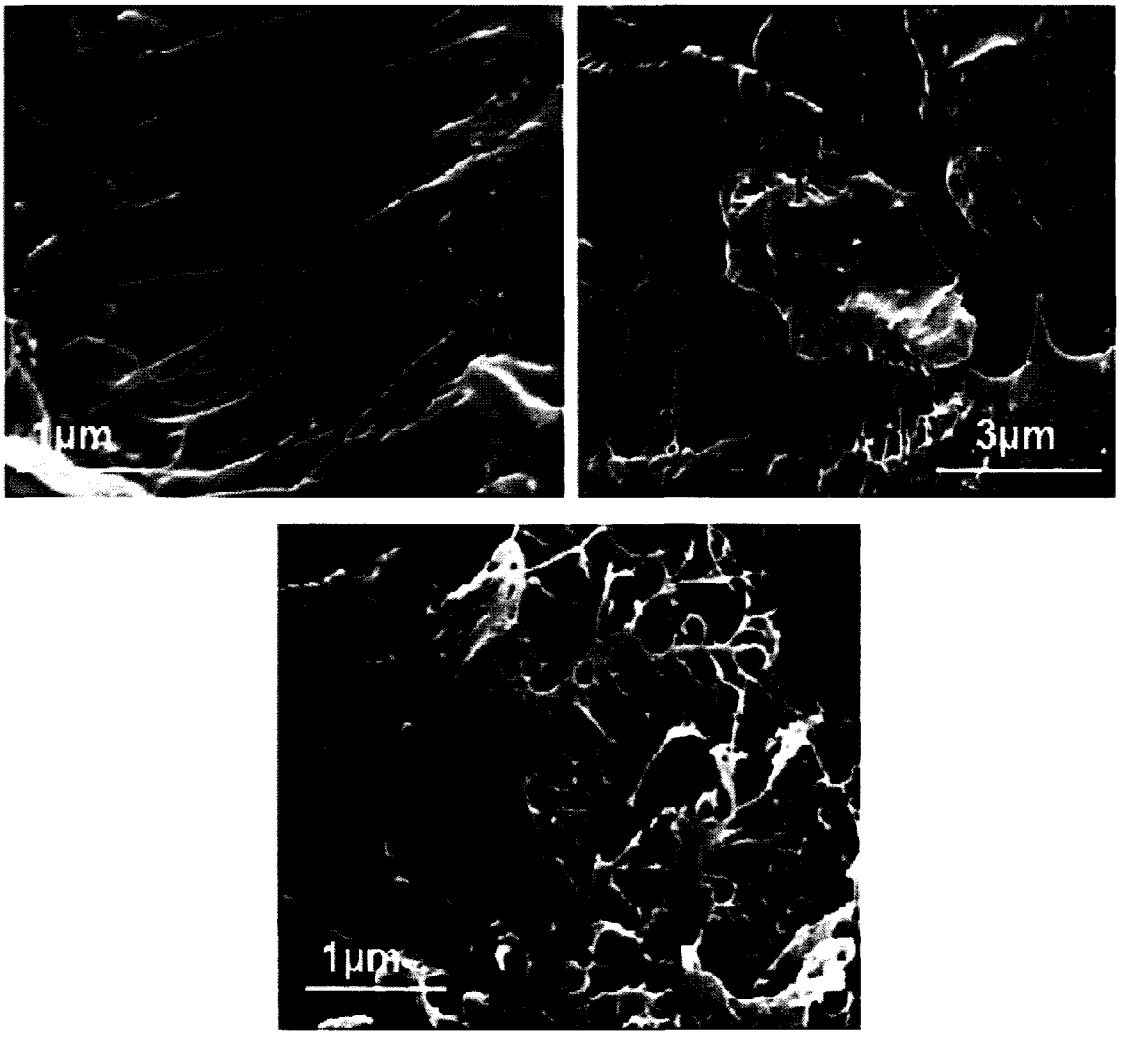

Figure 3.32. Ni-SWNTs BMI interaction in the composites showing a polymer coating of the Ni-SWNTs.

3.4.1. Resistivity of BMI/Carbon fiber/ Nanotube composites.

The surface resistance of the composites processed is shown in Table 3.3. The surface resistance of the baseline composites (without nanotubes) is 10^{12} ohms per square and addition of 4 wt% purified SWNTs reduced the surface resistance to 10^{8} ohms per square. By using 4 wt% Ni-SWNTs the surface resistance reduces further by 6 orders of magnitude to $2 - 4 * 10^{2}$ ohms per square and the surface resistivity ranging between 15 – 30 Ω.cm. Since nickel is coated on the nanotubes in a 1:1 wt. ratio, the amount of nanotube constituent in Ni-SWNTs added into composite is half the amount of purified tubes. This further emphasizes that coating the SWNTs with nickel aids in enhanced dispersion and surface coverage which in turn improves the electrical conductivity of the final composite.

Table 3.3. Resistance and Resistivity of the composites measured using cylindrical and four point probe.

Sample	Resistance (Surface resistance meter, ohms per square). (Limitation : 10^{4} ohms per square)	Resistance (four point probe) (Ohms / Square)	Amount of SWNTs in Ni-SWNTs.	Thickness of the surface layer	Surface Resistivity of the composite (Ohm.cm)
1 wt% Ni-SWNTs in BMI carbon fiber composites.	$10^{7} - 10^{10}$ (Lot of fluctuation)	0.075	0.075	0.075	$7.5*10^{5} - 7.5*10^{8}$
2 wt% Ni-SWNTs in BMI carbon fiber composites.	$10^{4} - 10^{8}$ (Lot of fluctuation)	0.075	0.075	0.075	$7.5*10^{2} - 7.5*10^{6}$
4 wt% Ni-SWNTs in BMI carbon fiber composites.	10^{4} (Consistent)	$4*10^{2} - 2*10^{2}$	2 wt%	0.075	30 - 15
4 wt% Purified SWNTs in BMI carbon fiber composites	10^{8}	10^{8}		0.075	$7.5*10^{8}$

3.5. Lightning Strike Testing and Characterization of Composites.

Fielding *et al* [48] performed a statistical analysis to analyze the current waveform applied to the samples. The changes in peak current and continued current applied to the samples show that the damage was caused by the material configurations and not the changes in current waveform applied to the composites. Figure 3.33 shows the schematic of the test up used.

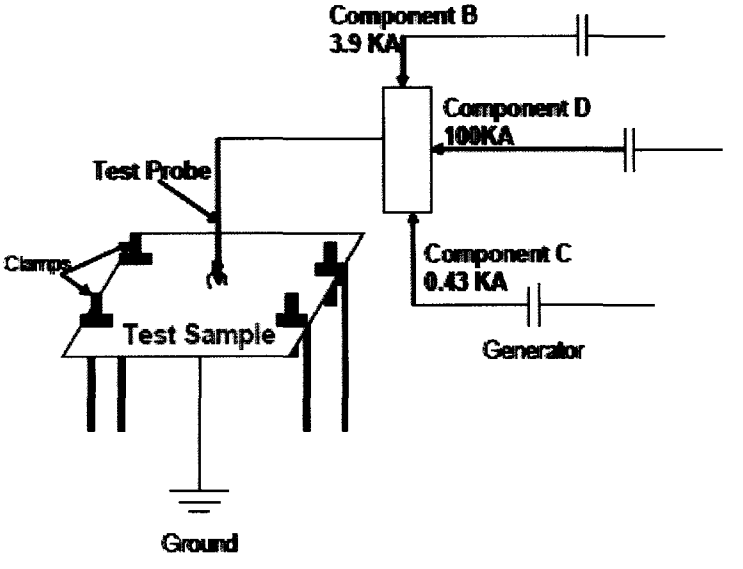

Figure 3.33. Schematic of the test probe used for simulated zone 2A lightning strike (adapted from Fielding *et al* [48]).

Two areas on the composite test sample were considered for characterization: central region where the arc hits the sample, and the region away from the lightning strike. Figure 3.34 shows photographs of the damages inflicted on composite samples (with and without Ni-SWNTs) and also the nomenclature of the two areas that are being discussed. Carbon fiber pull out is observed for the baseline composite shown in Figure 3.34b where

the top layer subjected to the arc is completely damaged. Since this composite is highly resistive, thermal energy build up in the localized area resulted in its damage. However, it can be seen from Figure 3.34a that the Ni-SWNTs/BMI composites show reduced amount of damage compared to the baseline composite. A rough estimate of the central fiber damage areas for composites filled with and without Ni-SWNTs were 5.17 cm^2 and 32.85 cm^2 respectively (indicated by carbon fiber pull out area).

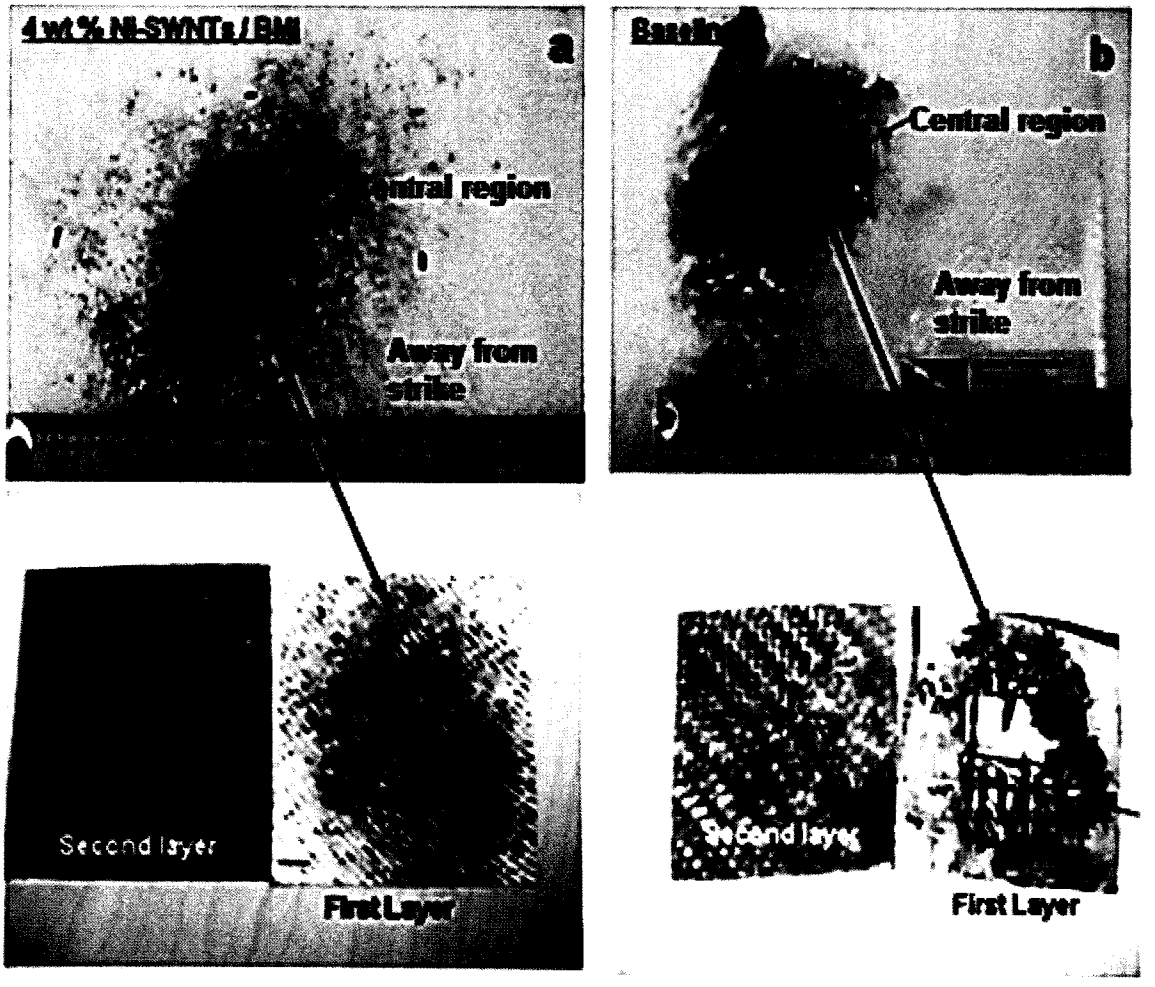

Figure 3.34. Photographs of BMI composite samples hit by simulated lightning showing a) minimal damage to the top layer of the Ni-SWNTs filled composite b) carbon fiber pull out in the baseline composite damaging the top layer.

An approximate analysis showed that the damage penetrated into the second layer and the depth of damage for the composites filled with Ni-SWNTs was 0.15 cm. Figure 3.35 shows a comparison of the depth of damage and the area of damage of various reinforcements used by Fielding *et al.* For comparison purposes, we added our data to their data set. The data points of our sample are encircled in a red boundary.

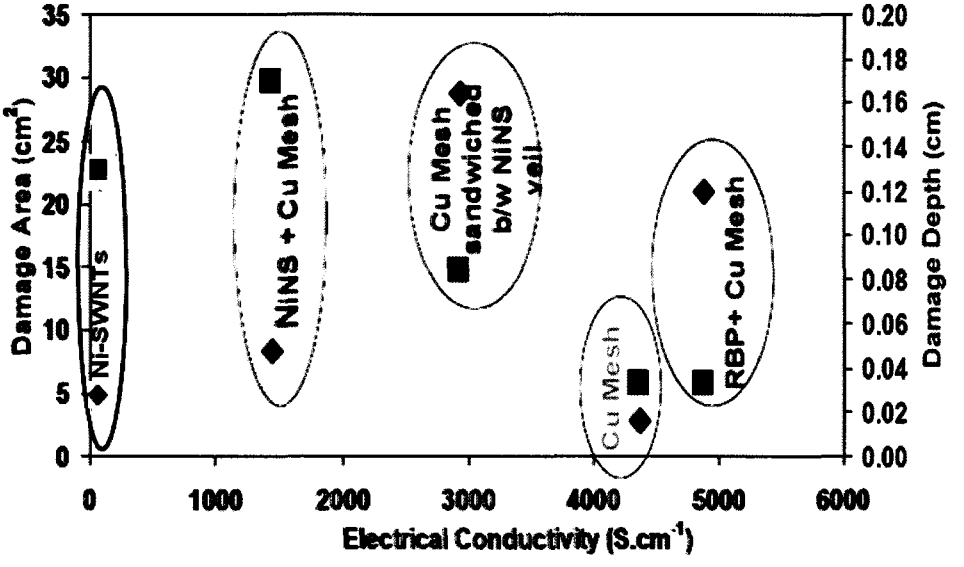

Figure 3.35. Electrical conductivity, depth of damage and area of damage of composites with various reinforcements (adapted from Fielding *et al* and modified to add our data to the figure for comparison purposes).

It can be seen that though copper mesh + nickel nanostrand (NiNs) veil conduct much better than our composites, the area and depth of damage are higher compared to our samples. Fielding *et al* discuss the reason for higher damage in nickel nanostrand based composites may be due to their porous morphology. The porosity blocked the current flow by rendering a dielectric layer. The results for nickel coated carbon fiber composites

(NiCCF) are shown in Figure 3.36. They found that the BP reinforced NiCCFs performed better than the NiNS counterparts. Aligned bucky paper composites showed the highest resistance to damage. Also, no correlation between electrical conductivity, depth and area of damage was found for these composites.

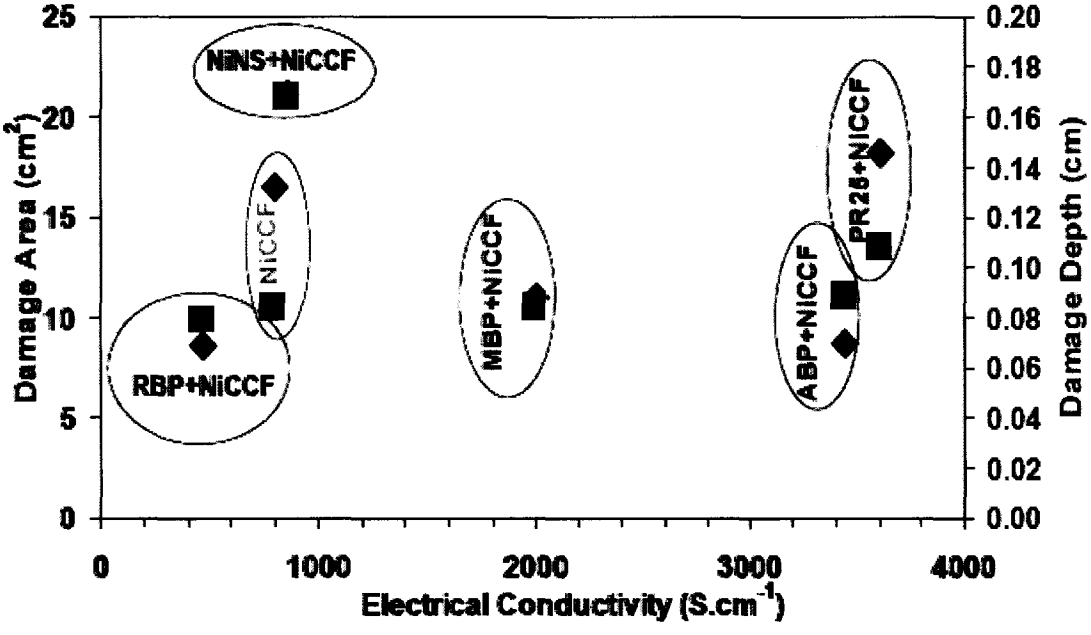

Figure 3.36. Electrical conductivity of NiCCF composites filled with various nanomaterials and their depth and area of damage due to simulated zone 2A lightning strike (adapted from Fielding *et al*).

Carbon nanofiber and nickel nanostrand papers were used as surface layers for composites panels tested for lightning strike mitigation by Gou *et al.*[52] These hybrid papers were incorporated to the surface of the carbon fiber using an RTM process. They found that the electrical conductivity of the surface layer had an effect on the degree of damage caused by simulated lightning strike.

3.5.1 Raman spectroscopy analysis of the samples.

It is proposed that in the Raman spectra of sp^2 nanocarbons, the G-band is highly sensitive to strain effects such as the strain induced by external forces or even by the curvature of the side wall in SWNT; therefore, the G-band can be used to probe modification of graphene structure.[90] For instance, the Raman shift in the G peak for functionalized SWNTs can be explained by the bond lengths and angles of graphene structure modification by strain caused by the interaction with sidewall moieties. In the Raman spectra shown in Figure 3.37, the G band for purified SWNTs shifts from 1579.2 to 1587 cm^{-1} when coated with nickel. For Ni-SWNTs, the observed upshift of the G band can be attributed to the strain created by charges injected by Ni into SWNT by the electron transfer from Ni to the SWNT sidewall to result in stiffening of the tangential (G) mode [91]. Spraying of Ni-SWNTs on the carbon fiber brings no change in the surrounding environment for the nanotubes, since they do not chemically bond to the fiber. Hence, no shift in the G peak position is seen. Table 3.4 shows the corresponding G peak positions of all the samples; the areas of samples away from lightning strike region are similar to the composites processed before the exposure to lightning strike. In the Raman spectra of these samples, the G peak upshifts further by about 5 cm^{-1}. This can be due to: (i) interaction and bonding of Ni-SWNTs to the resin, so their further modified sidewall moieties shifts the peak, (ii) In the BMI composites, the nanotubes bridge the polymer matrix cracks, as seen in the SEM images (Figures 3.31, 3.32). When Ni-SWNTs are bonded to BMI resulting in stiffening of the tangential G mode. Schadler *et al* [92] observed an shift of the G peak in the Raman spectra of the SWNT-filled composites under both tensile and compressive strain. Also, BMI has a positive coefficient of thermal

expansion; hence it expands on heating stretching the Ni-SWNTs. For the sample area hit by simulated lightning, the G peak shifts further by 4 cm^{-1}. However the presence of the radial breathing modes and G peak indicate the presence of carbon nanotubes after the lightning strike.

Table 3.4. Position of the G peak in the Raman spectra of the samples, showing the effect of coating, processing of composites and simulated lightning strike on the tangential G mode of the SWNTs.

Type	G Peak
Purified	1579.2
Ni-SWNTs	1587
Ni-SWNTs on carbon fiber	1587.2
Ni-SWNTs BMI before lightning strike	1592.5
Ni-SWNTs BMI LS far end	1592.5
Ni-SWNTs BMI LS central	1596.6

From the Raman analysis it can be concluded that no major damage to the Ni-SWNTs is caused by simulated lightning strike hit since no pronounced D bands indicating sidewall defects are observed. This affirms our experimental findings that Ni-SWNTs can be proposed as a promising nanofiller candidate for lightning strike protection of composites.

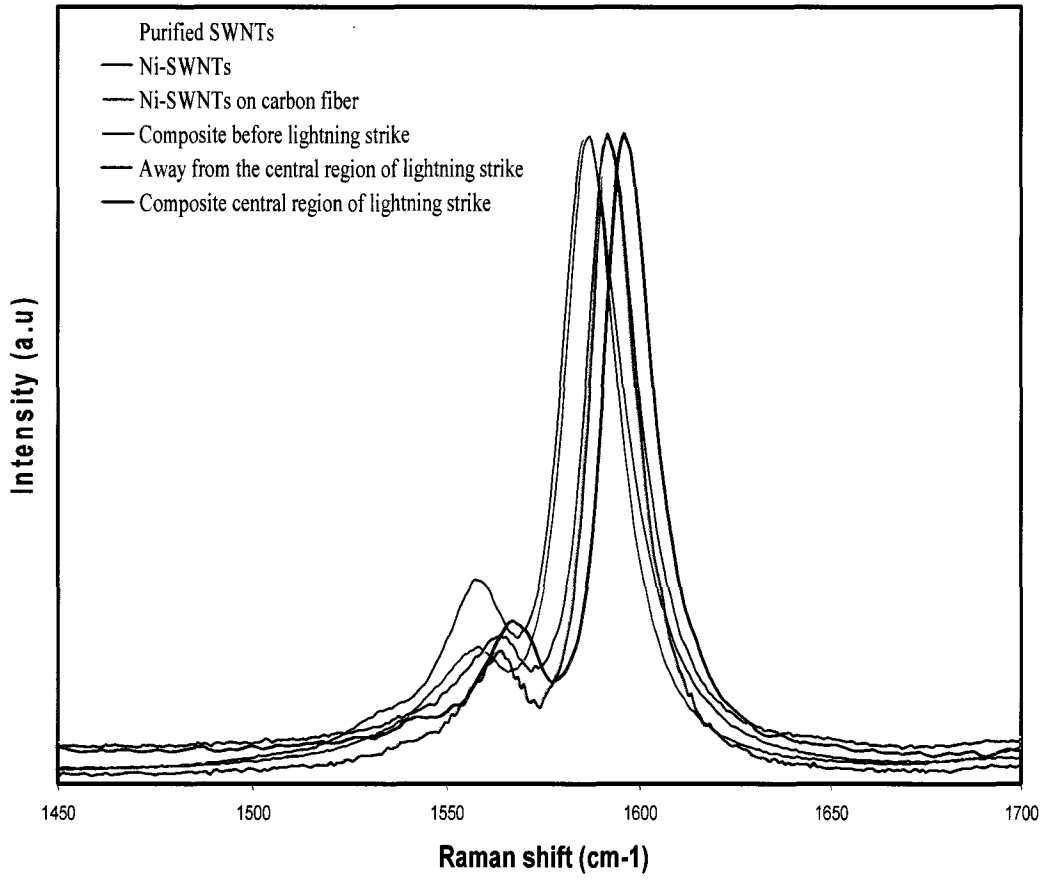

Figure 3.37. Raman spectra of the samples showing a shift in G peak after each processing.

3.5.2 Characterization of damage using SEM

Figure 3.38 shows SEM images of sample areas away from the lightning strike region. A rich network of Ni-SWNTs and bridging of cracks all along their length can be seen on the images. These images indicate that the damage was concentrated at the point of

simulated lightning strike hit and did not spread far away from the central region because they look similar to the samples before lightning strike.

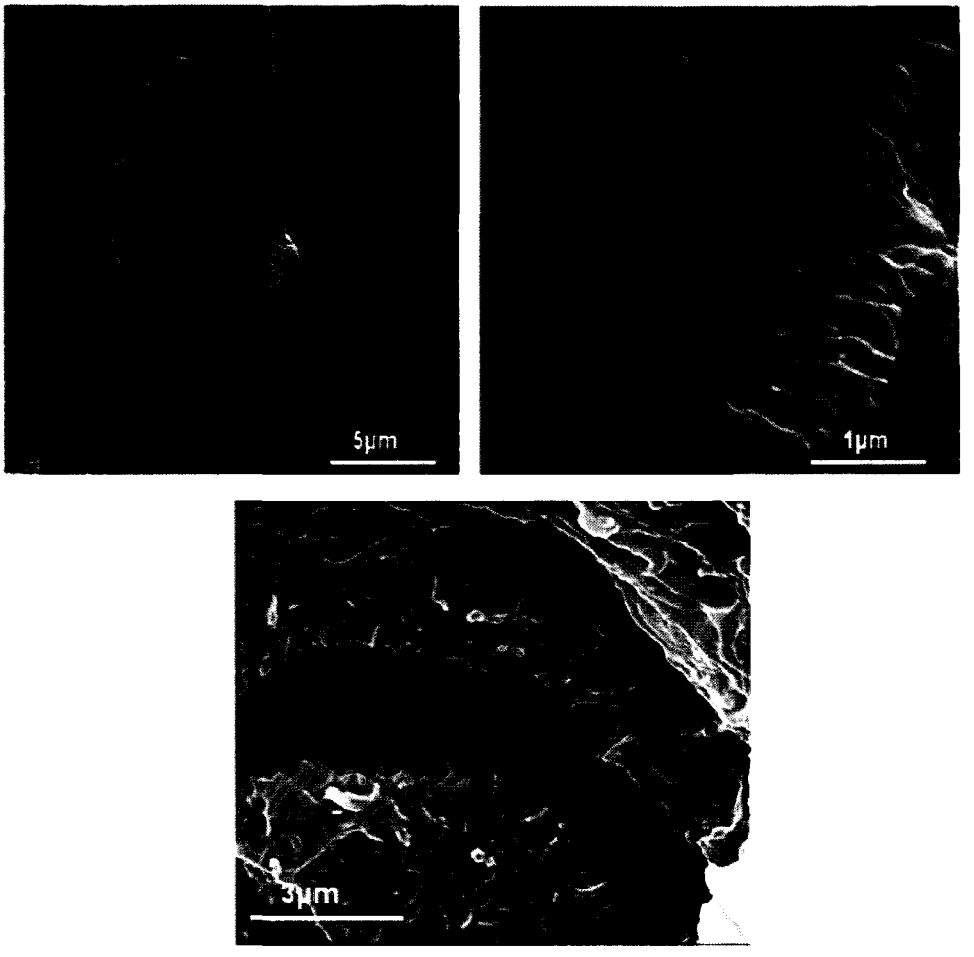

Figure 3.38. Regions away from the central region of the lightning strike showing no damage.

The effect of strike on the BMI resin is seen in Figure 3.39. Charring and pulverizing of BMI resin along with pulling of nanotubes bonded to the resin is observed in the image. Since the resin has a very high electrical resistance, instant thermal energy build up degrades the resin. TGA analysis of the resin showed that most of the resin degrades

approximately around 600 °C. SEM analysis on the TGA residue revealed images similar to those shown in Figure 3.39, and is shown in Figure 3.40.

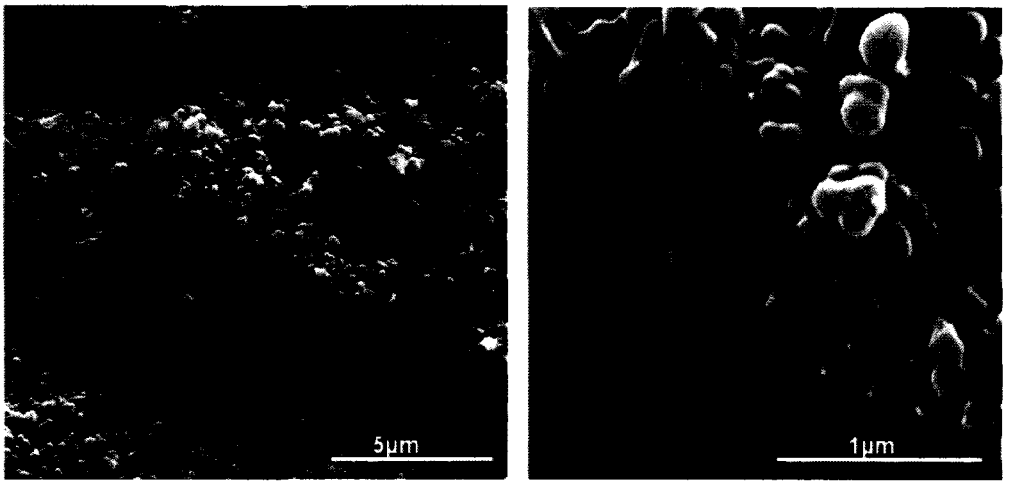

Figure 3.39. Effect of strike on the BMI resin showing charring and pulverizing of the resin and pulling of nanotubes.

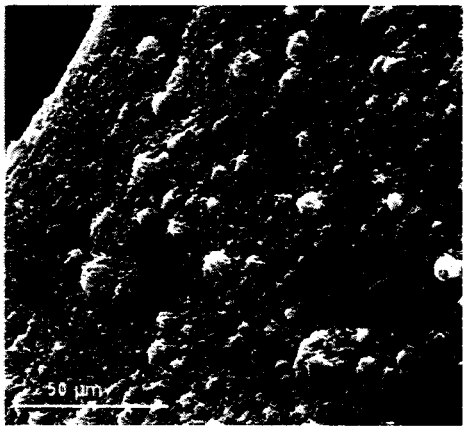

Figure 3.40. BMI residue after TGA showing complete degradation of the resin similar to the lightning strike sample.

SEM images in Figure 3.41 show that the simulated lightning strike has no adverse effect on the carbon fiber coated with Ni-SWNTs, since no major damage in the nanofiller rich area is seen. The resin on top of the Ni-SWNTs probably chipped off after composite

processing and hence, no resin can be seen in Figure 3.41. Because the carbon fiber coated with Ni-SWNTs is not resistive; when lightning hits the sample, the charge is immediately dissipated through the network of SWNTs causing no thermal energy build up and damage to the carbon fiber.

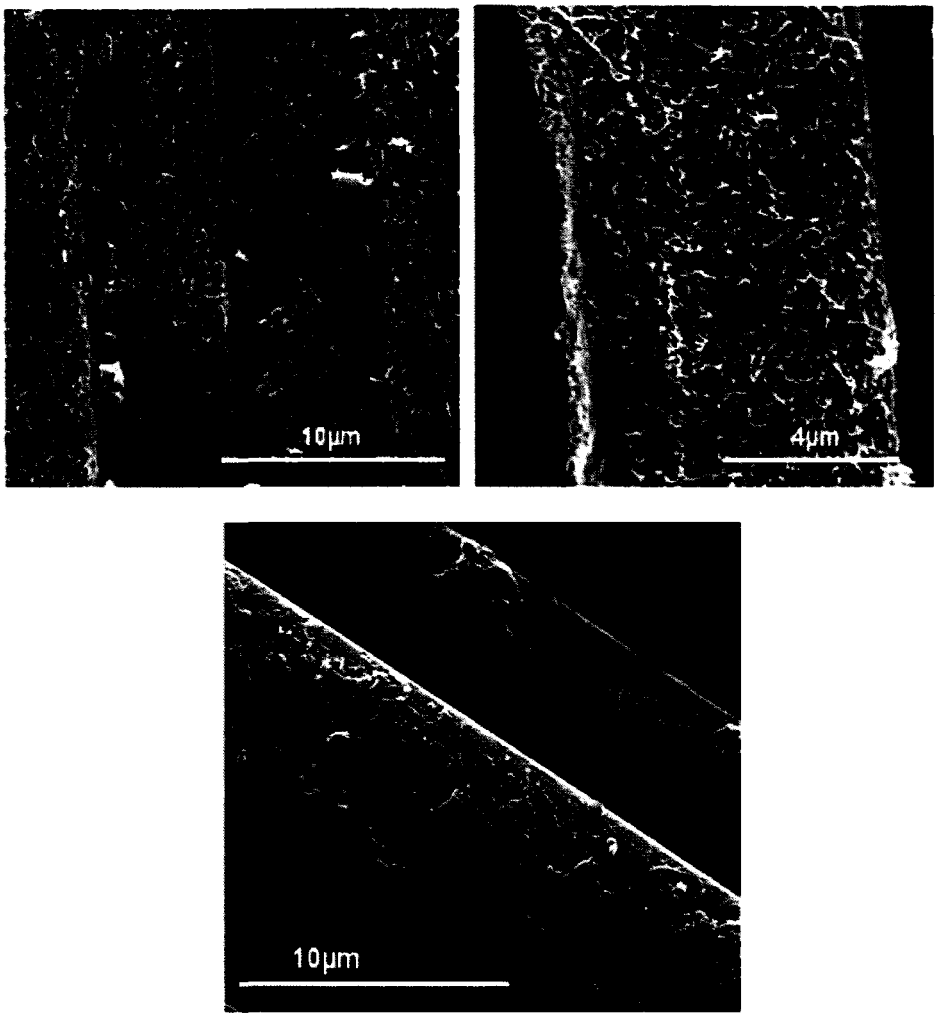

Figure 3.41. Carbon fiber and SWNT rich regions of the composite after exposure to simulated lightning strike.

3.5.3 Analysis of the presence of nickel after each processing step

XPS analysis was used to determine the presence of nickel after each processing step from coating of nickel to simulated lightning strike hit on the sample. EDS and XPS did

not show pronounced signals since the nickel is underneath the BMI layer and the penetration depth for both these techniques is approximately 10 nm. The signature XPS peak for Ni $2p_{3/2}$ is shown in Figure 3.42.[93] Figure 3.43 shows the XPS data for Ni-SWNTs, Ni-SWNTs on the carbon fiber and Ni-SWNTs in the BMI composite (only the nickel peaks are shown in figure).

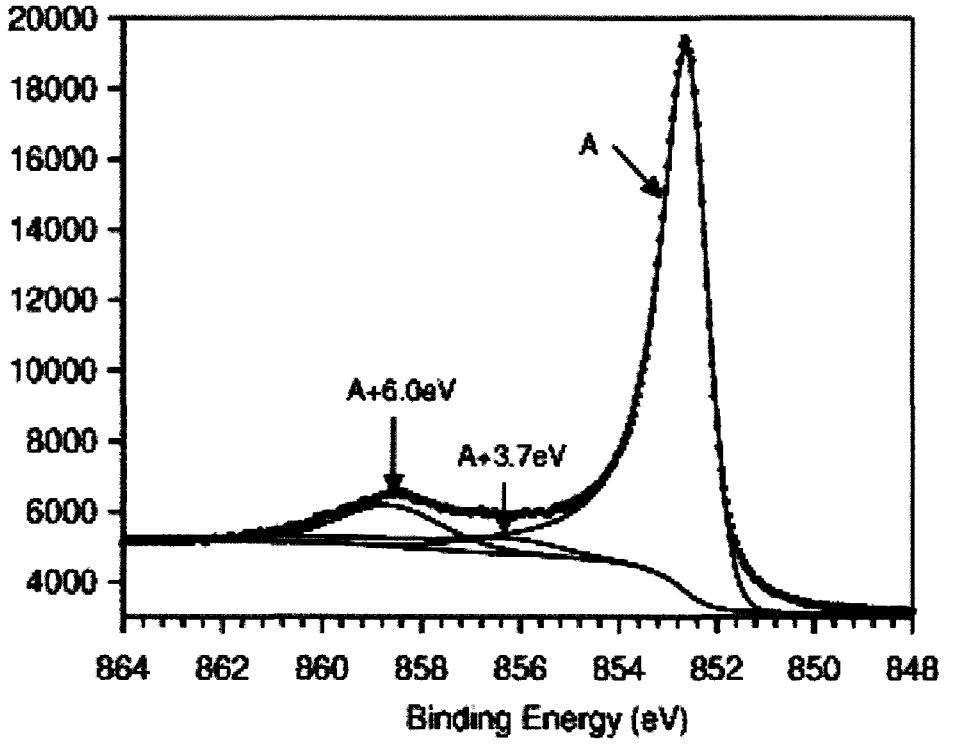

Figure 3.42. XPS spectrum of pure nickel showing the signature peak for Ni $2p_{3/2}$.

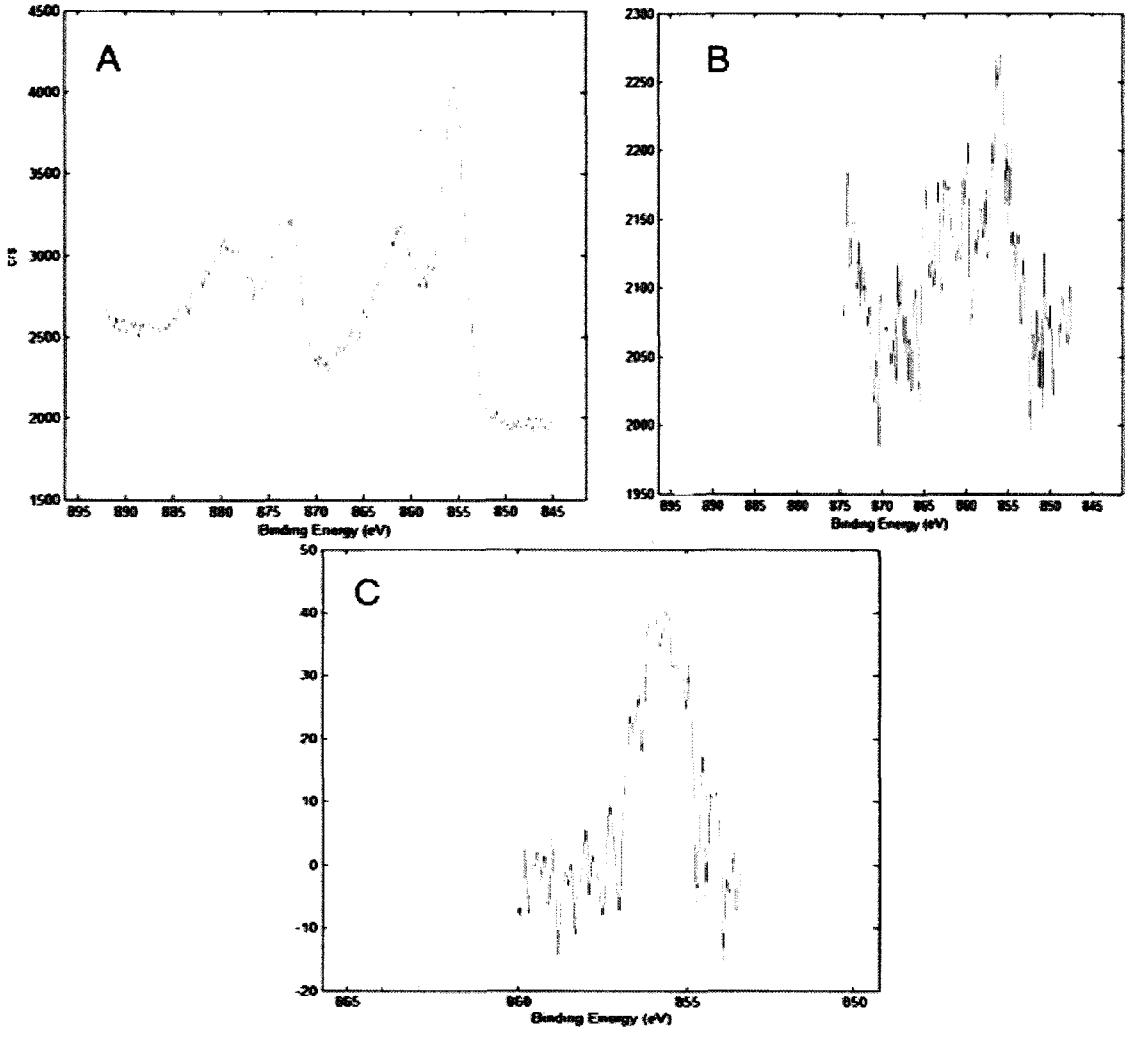

Figure 3.43. Presence of nickel indicated by the Ni $2p_{3/2}$ in A) Ni-SWNTs B) Ni-SWNT BMI carbon fiber composites C) Ni-SWNTs sprayed on carbon fiber.

No nickel peak was observed for samples analyzed after lightning strike. Hence, ICP analysis was used to determine the amount of nickel after the composites were hit by simulated lightning strike. After selectively dissolving and filtering out the BMI and carbon fibers, the sample was analyzed using ICP-MS and for every 0.8 mg of the sample, the amount of nickel detected was approximately 0.5 micrograms. One of the

possibilities would be that the nickel vaporized since its heat of vaporization is lower than the heat of graphitization of carbon, taking away the major effect of the current.

3.6. Conclusions.

Nanotubes were used as a template to coat nickel which improved the interface between the carbon fiber and the matrix. Dispersion, surface coverage and electrical conductivity results show that Ni-SWNTs outperform purified SWNTs in dispersion and conductivity in BMI composites. From the technical reference given in Torayca's website, the carbon fiber sizing that is compatible with epoxy is Bisphenol A diglycidyl ether (BADGE). Assuming we have the BADGE sizing, it makes it clearer as to why the Ni-SWNTs show a better dispersion and distribution on the carbon fiber compared to the purified SWNTs. The sidewall of the nanotubes is very smooth at the atomic level which makes it a bad interface between the carbon fiber and the CNTs. One of the methods to improve the interface is sidewall functionalization. However, for our application any functional group would disrupt the sp^2 hybridization as discussed. Nickel being a transition metal will form a coordination complex with the lone pair electrons provided by the oxy ligands in the BADGE molecule which may result in a strengthened interface between the Ni-SWNTs and carbon fiber along with good distribution. Hence, electroless plating of nanotubes with nickel is a novel technique to improve the interface. Addition of 4 wt% Ni-SWNTs reduced the electrical resistivity of the composite by 10 orders of magnitude. From our results, Ni-SWNTs show a good potential as nanofillers for high temperature polymer composite systems which can be used for lightning strike protection.

CHAPTER 4: Achieving High Electrical Conductivities in Polyethylene – Carbon Nanotube Composite Systems.

4.1. Introduction

Improving the electrical, thermal and mechanical properties of polymers composites by addition of carbon nanotubes has been a topic of extensive research since their discovery. Their remarkable mechanical, electrical and thermal properties make them the most sought after nanofillers for composite applications. Carbon nanotubes possess a very high electrical conductivity close to $10^5 - 10^8$ S/m [94, 95] and aspect ratios greater than 1000.

The electrical conductivity of an insulating matrix filled with conductive fillers depends strongly on the filler loading as described by the percolation theory. [96] When filled with conductive fillers at low concentrations, the distance between them is larger than their size and hence the resistivity is close to that of the insulating matrix since there is no conductive pathway. However, at a critical concentration a network of connected fillers is formed resulting in a sharp drop in resistivity of the composite; such concentration is called the percolation threshold. There exist disparities in the percolation threshold and composite electrical conductivity reported by different groups due to the method of production of carbon nanotubes, their purification, functionalization, degree and level of dispersion, polymer used, processing techniques used and also the amount of amorphous carbon present in the nanotubes. Also, the electrical properties of the composite are affected by waviness of CNTs, [97] the resistance at the contact junctions between the nanotubes, [98,99,100,101,102] and the nanotube – polymers junctions. [103] Evaluating and optimizing each of these parameters is essential in understanding the electrical properties of the polymer nanocomposites. The effect of the parameters and

various processing methods on the electric properties of various polymer systems is discussed in section 4.2

4.2 Background on improving the electrical conductivity in polymer composites

4.2.1 Effect of dispersion and process optimization.

Grossiord *et al* [96] present a detailed study on the electrical conductivity of MWNT powders (IPCNTs) and MWNTs from vertically aligned films (VGCNTs) in polystyrene composites. They optimize the CNT exfoliation process by using UV Vis spectroscopy and relate the dispersion in the matrix to the electrical conductivity of the nanocomposite. Maximum exfoliation was indicated by a point on the UV Vis spectra where additional energy does not change this point. This characterization ensured that the energy used to exfoliate the nanotubes did not damage them or produce defects which will affect the final properties. Figure 4.1 shows the optical absorbance spectra of the MWNT-SDS suspensions (the samples were diluted so that the content of the CNT was $3.33*10^{-4}$ wt %).

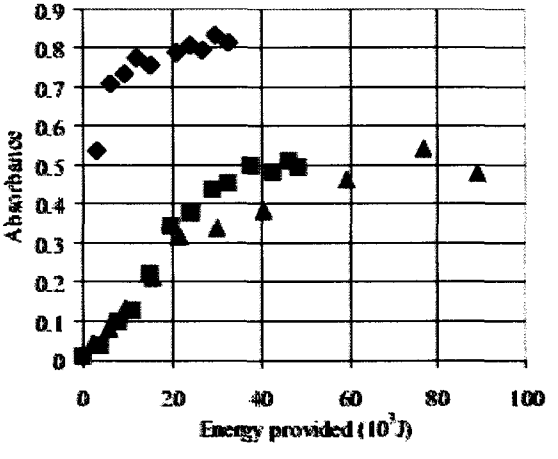

Figure 4.1. Optical absorbance spectra of (a) IPCNTs (◆) (b) VGCNTs (▲,■) showing the maximum energy required for exfoliation. (adapted from Grossiord *et al*).

The electrical conductivity values obtained as a function of the filler concentration is shown in Figure 4.2. They observed that VGCNT based composites conduct better and have a lower percolation threshold compared to the IPCNT counterparts though both of them showed uniform and stable dispersions in the polymer. The performance of IPCNTs was attributed to their aspect ratios which were roughly 3 times smaller than the VGCNTs. Also a measurement of the electrical conductivity of the bucky papers processed from IPCNTs and VGCNTs showed that the conductivity of the former was 2 times lower than the conductivity of the latter and they attributed this to the intrinsic quality of the CNTs. Hence they have clearly shown that the intrinsic quality of the CNTs and their aspect ratios in the composite play a role in enhancing or diminishing its electrical properties.

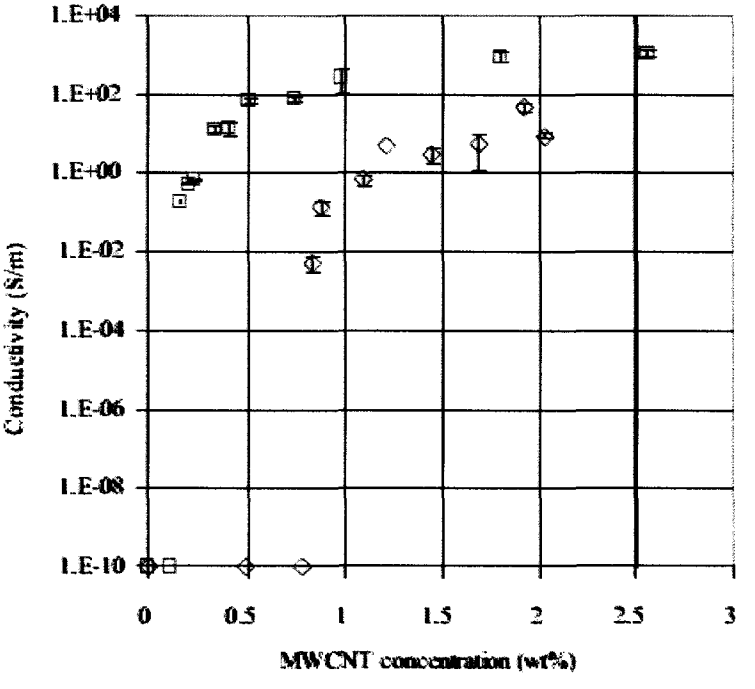

Figure 4.2. Conductivity of the PS composites filled with a) VGCNTs (■) (b) IPCNTs (◆). (adapted from Grossiord *et al*).

Effect of dispersion of poly (phenyleneethynylene) (PPE) functionalized SWNTs on the electrical properties of polystyrene composites was studied by Ramasubramaniam *et al.* [104] They used a non-covalent chemistry to functionalize the CNTs so their inherent properties were not damaged. PPE-SWNTs were dispersed in chloroform and various polymer composite (polystyrene and polycarbonate) films with SWNT concentrations ranging 0.01 to 10 wt% were prepared. The electrical conductivity of these composite films is shown in Figure 4.3. The conductivity of the polystyrene composites at 7 wt% SWNT loading is around 7 S/m and for polycarbonate composites the conductivity reaches 4.81 * 10^2 S/m. This study shows that the polymer matrix plays an important role in determining the electrical conductivity of the composites.

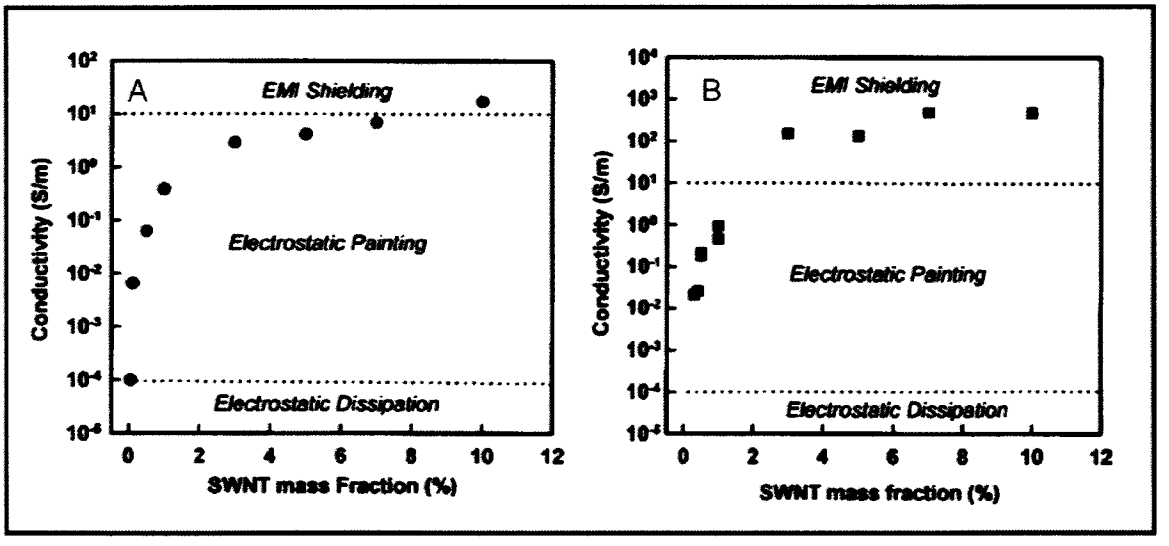

Figure 4.3. Electrical conductivity of PPE functionalized SWNTs in A) polystyrene matrix B) polycarbonate matrix (adapted from Ramasubramaniam *et al*)

Skakalova *et al* [105] used pristine and thionyl chloride doped SWNTs to study the electrical and mechanical properties of CNT filled polymethylmethacrylate (PMMA) composites. They found that doping the SWNTs with thionyl chloride increased the initial conductivity of the bucky papers by factor of 5. At 10 wt% pristine SWNTs and 13.5 wt% $SOCl_2$ doped SWNT concentrations, the measured composite conductivity was 17 S/cm and 100 S/cm respectively. Figure 4.4 shows the electrical conductivity of the composites with the fillers as a function of their concentration. Hence, doping is one of the methods that can be used to improve the conductivity of the polymer composites as it enhances the initial conductivity of SWNTs fillers.

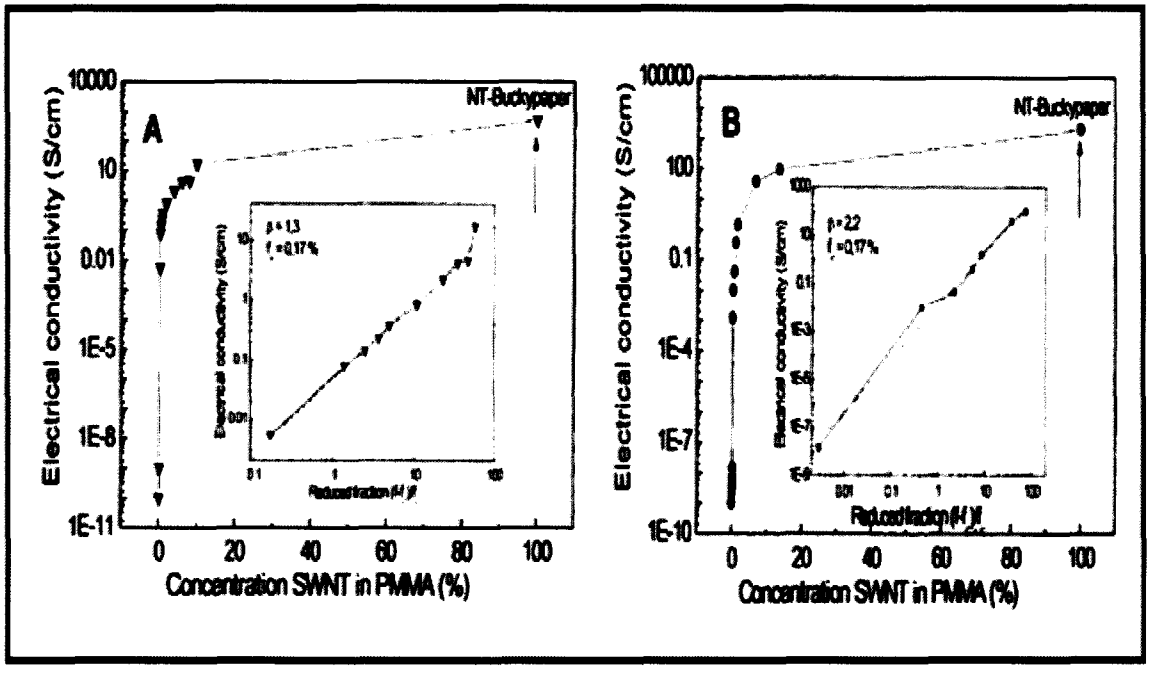

Figure 4.4. Electrical conductivity of PMMA composites filled with A) Pristine SWNTs B) $SOCl_2$ doped SWNTs. (adapted from Skakalova *et al*)

The influence of synthesis method, entanglement state, dimensionality of the nanotubes, and sample preparation on the electrical conductivity of epoxy carbon nanotube composites was studied by Kovacs *et al.* [106] Each parameter was varied while keeping the rest constant to assess its influence. Non-entangled and aligned MWNTs processed by aerosol chemical vapor deposition (ACVD) and catalytic chemical vapor deposition (CCVD) were used. They found that the polymer layer in between the nanotubes blocks their path for conduction and the initial conductivity of the nanotubes did not play a role in improving the electrical conductivity of the composite. Their studies showed at higher concentrations, the entanglement improved the conductivity while the shear forces did not contribute to the increase in conductivity.

Grossiord *et al* [107] studied the effect of processing conditions on the electrical properties of the composites. MWNTs / polystyrene composites were fabricated using a latex based approach where both the polymer and filler were stabilized using an ionic surfactant. The diffusivity of CNTs in the polymer is dependent on the polymer viscosity because it determines the extent of reorganization of the CNTs within a given amount of time. They showed that by changing the processing conditions, such as extending the temperature and time of compression, lower percolation threshold and higher conductivities can be obtained by pushing the system towards equilibrium state. Hence, by using high temperatures and sufficient time to reach equilibrium they concluded that the polymer size had a limited impact on the electrical percolation threshold and conductivity of the composites.

4.2.2. Effect of nanotube type and electric field.

An extensive review on the electrical percolation in carbon nanotube polymer composites

was published by Bauhofer *et al.* [89] They reviewed the effect of nanotubes type and production, polymer type, dispersion methods, composite processing methods, entanglement and non entanglement of the nanotubes on the percolation and the resulting conductivity of the composites.

Figure 4.5 shows the maximum conductivities achieved for polymer systems using different kinds of fillers (entangled SWNTs, entangled and non-entangled MWNTs, unknown state of SWNTs and MWNTs).

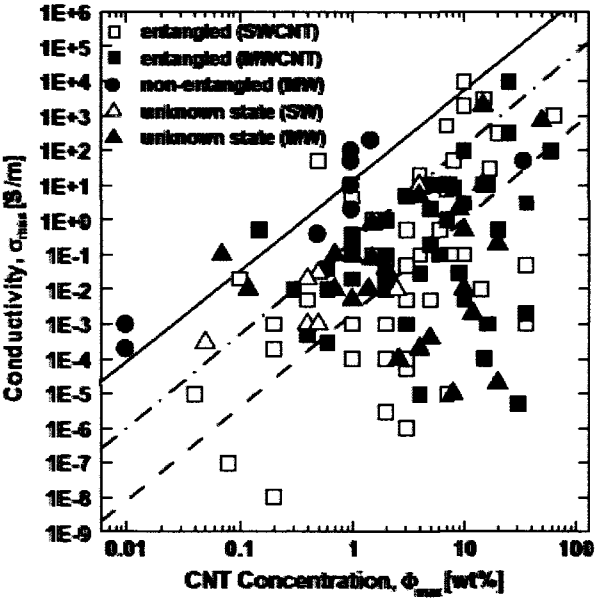

Figure 4.5. Maximum conductivities achieved in polymer composites using various types of fillers (adapted from Bauhofer *et al*).

Non-entangled MWNT systems showed conductivity values 50 times higher than their entangled counterparts and also, an indirect proportionality exists between the percolation and maximum conductivity reached for a given CNT concentration.

Effect of using AC electric field during the curing of composites is shown in Figure 4.6. Electric field helps in alignment of nanotubes and also increases the attractive forces between the neighboring CNTs which enhance the conductivity of the composite. They also discussed that AC field showed better effect than DC electric field on the composite conductivity. Also, the viscosity of the polymer/solvents along with nanotube concentration plays a role in how effectively the nanotubes align.

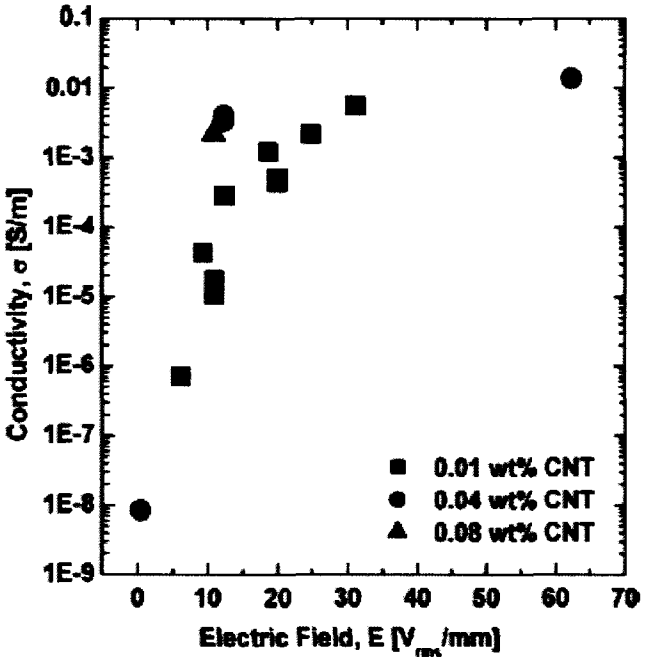

Figure 4.6. Effect of electric field on the composite conductivity for various concentrations of MWNTs (adapted from Bauhofer *et al*).

Alignment of SWNT suspended in quaternary ammonium based salt and THF was studied using a DC electrical field by Kamat *et al.* [108] THF has a very low viscosity of 0.48 cP which is one of the primary requirements for nanotube alignment. 40 V and 100 V DC field were applied to the suspensions to study the alignment. When a low DC field was used they found that carbon nanotubes in the suspension move towards the positive

electrode and with time, they deposit as a thin film on the electrode. At high DC fields, they aligned themselves perpendicular to the electrodes. Dispersion, viscosity of the solvent and the electric field play a role in the alignment of nanotubes.

Martin *et al* [109] studied the effect of alignment of MWNTs in an epoxy system using application of both AC and DC electric fields during nanocomposite curing to induce formation of aligned conductive nanotube networks between the electrodes. They used in-situ optical microscopy and current density measurements during the curing to evaluate the network formation. Effect of field strength and the concentration of MWNTs used were studied. Optical micrographs of 0.01 wt% aligned CNTs in epoxy composite are shown in Figure 4.7

.

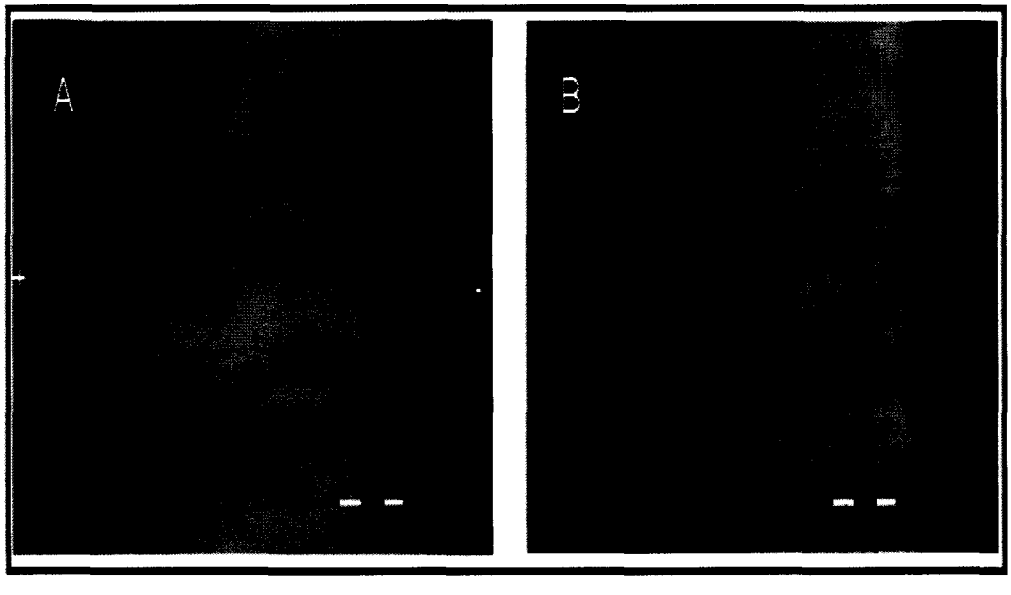

Figure 4.7. Optical micrographs of 0.01 MWNTs in bulk composites (a) DC field 100 V/cm (b) AC field (adapted from Martin *et al*).

AC field induced alignment was more uniform compared to DC field induced alignment as seen in Figure 4.7. They found that both AC and DC field help in alignment of the nanotubes in the composite; however use of AC field showed uniform alignment. In spite of achieving good alignment, conductivity of the composite did not reach the conductivity of MWNTs. This is due to the presence of polymer barriers which increases the junction resistance and also disrupts the path for conduction.

Alignment of MWNTs in bulk epoxy composites using an external electric field and layer by layer approach was studied by Zhu *et al.* [110] A 2000 V_{AC} voltage with peak to peak frequency 2000 Hz frequency was used. UV light was used to irradiate the samples and to lock the alignment of nanotubes by instantaneously polymerizing the epoxy. Figure 4.8 shows electrical conductivity of the composites at different frequencies.

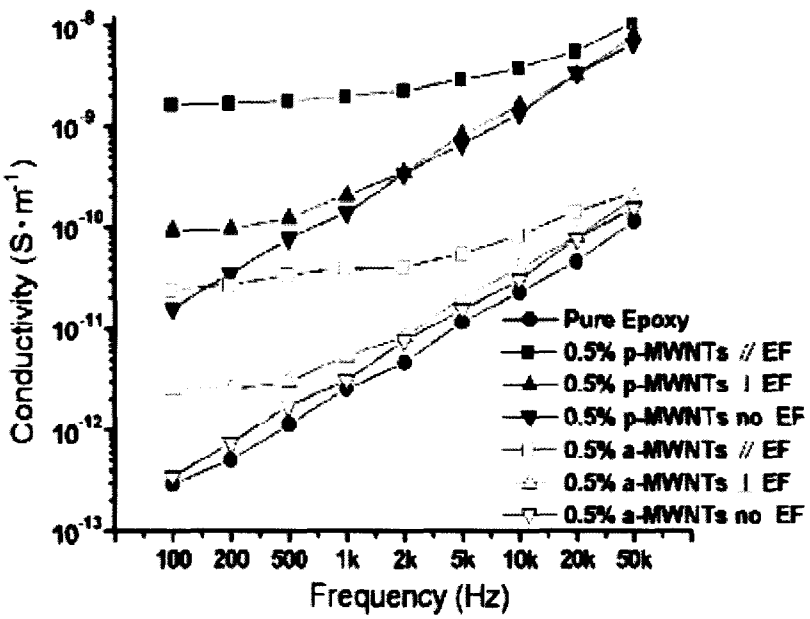

Figure 4.8. Electrical conductivity of the composites at different frequencies and configurations of electric field (adapted from Zhu *et al*).

They observed both lateral and longitudinal alignment of nanotubes in the composite. The degree of alignment strongly depended on the strength and the frequency of the field. Functionalized MWNT composites showed lower electrical conductivity values as compared to pristine MWNT composites which was attributed to the shortening of MWNTs due to functionalization. Hence, they showed that alignment, length of the nanotubes and rapid polymerization help in improving the electrical conductivity of the epoxy composites.

Ma *et al* [111] studied the alignment and dispersion of MWNTs and oxidized MWNTs in polymer composites. They reported the response of functionalized MWNTs to the AC field and compared it with the pristine MWNTs. Oxidized MWNTs showed enhanced and uniform dispersions, however their length was about half of the pristine MWNTs. In situ high resolution digital camera and optical microscope showed that the pristine MWNTs aligned rapidly under the influence of electric field. They were not stable and formed bundles over a period of time.

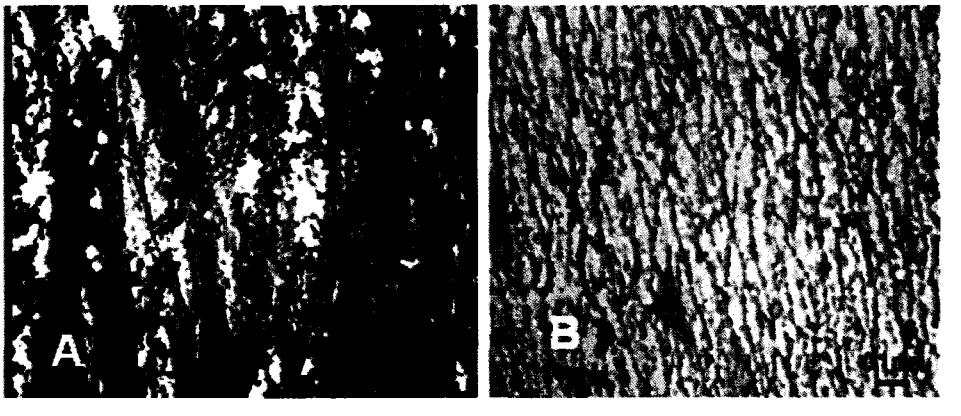

Figure 4.9. Alignment of (a) pristine MWNTs (b) oxidized MWNTs in an AC electric field showing a more uniform alignment of the latter. (Adapted from Ma *et al*).

In the case of oxidized MWNTs, the presence of polar functional groups resulted in larger dipole moments and also repulsive forces between them, leading to a better non-entangled alignment as shown in Figure 4.9.

The electrical conductivity of these composites and polarized Raman spectra is shown in Figure 4.10. Though the oxidized MWNTs were shorter in length, they showed a higher conductivity as compared to the pristine tubes which is very contradictive to the previously discussed research. They observed end cap functionalization of the CNTs preserves the sidewall structure and improves the dispersion of MWNTs in the matrix reducing the disentanglements. This reduced the contact resistance between CNT – CNT.

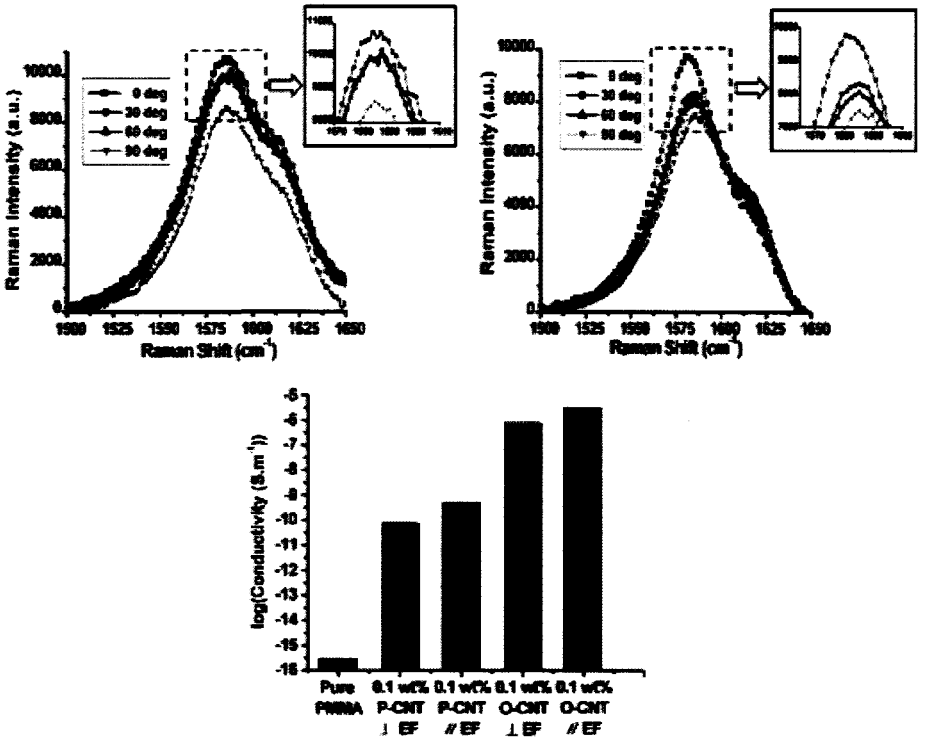

Figure 4.10. Polarized Raman spectra of pristine MWNTs composites (left) and oxidized MWNTs composites (rights). The electrical conductivity of various composites is also shown (adapted from Ma *et al*).

The effect of alignment on the percolation conductivity of PMMA / SWNT composites was studied by a group of researchers at the University of Pennsylvania.[112] Purified SWNT / PMMA composites were prepared by hot coagulation method prior to melt spinning. Alignment was characterized using small angle X-ray scattering (SAXS). Increase in full width half maximum (FWHMs) from 0° to 180° correspond to the increase in alignment of the SWNTs. The electrical conductivity as a function of concentration and also the degree of alignment is shown in Figure 4.11.

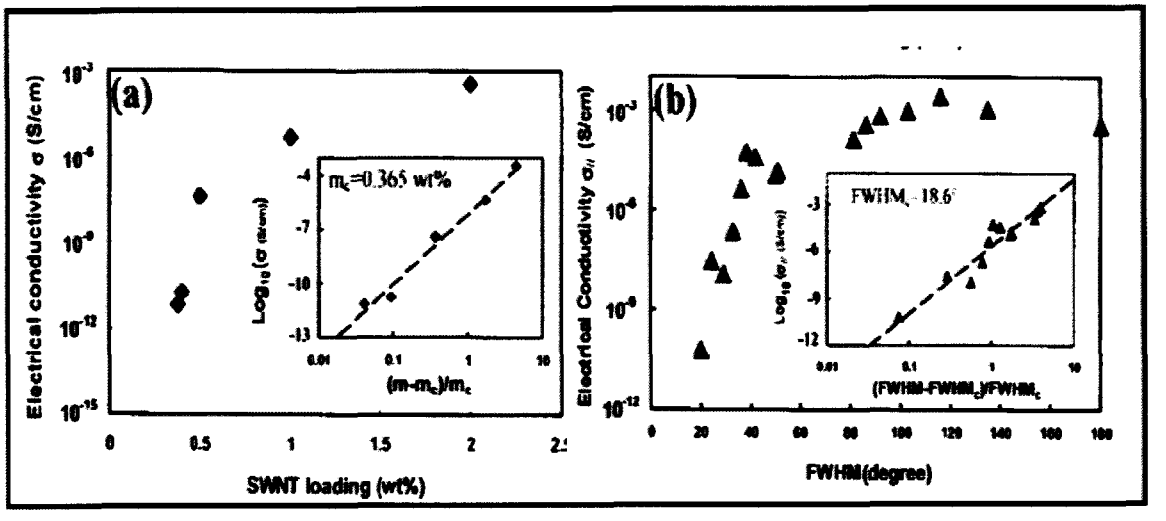

Figure 4.11. Electrical conductivity of SWNT / PMMA composites as a function of (a) concentration (b) alignment of SWNTs indicated by the FWHM. (adapted from Du *et al*).

Figure 4.11b shows that the electrical conductivity reached a maximum at a certain orientation and then decreased when the SWNTs were aligned perfectly. At such alignments, the SWNT networks do not touch each other and there is no network for electron flow. Increase in concentration of SWNTs did not lead to an increase in the electrical conductivity. They found that at lower concentrations small changes in isotropy of SWNTs resulted in enhanced conductivity of the composite.

Park *et al* [113] were among the initial group of researchers to study the alignment of SWNTs in a polymer matrix using an external electric field. An AC field was used and the distance between the electrodes was maintained at 1 mm. They analyzed the effect of varying the electric field, the time to cure and the frequency on the alignment of SWNTs. The structure of alignment of SWNTs due to the electric field was different from that of shear induced alignment. They observed that the SWNTs not only align but also migrate to form thick columns between the electrodes. An improvement in the electrical properties of the composite was related to the effect of alignment which can be controlled by optimizing the applied field parameters.

4.2.3. Effect of magnetic field on the alignment of CNTs

Walters *et al* [114] studied the alignment of SWNTs dispersed in DMF (10 mg/l) using varying magnetic field (0–19T). They reported that permanent magnets and superconductive magnets are effective in aligning the nanotubes. The amount of magnetic field required to align bundles was less compared to aligning single nanotubes. Figure 4.12 shows the in plane alignment of SWNTs at 25 T magnetic field.

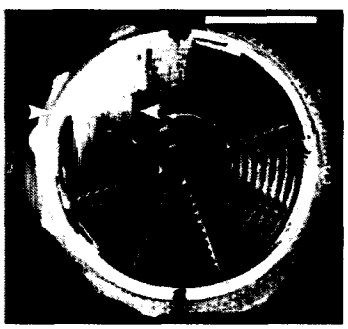

Figure 4.12. Inplane alignment of SWNT films using a high magnetic field (adapted from Walters *et al*).

Choi *et al* [115] processed polymer composites with enhanced electrical and thermal properties by aligning the nanotubes using magnetic fields. The concentration of SWNTs in the epoxy composites was maintained at 3 wt% and magnetic fields varying from 0 to 25 T were used. The magnetic fields were applied for 4 hours; 2 hours at room temperature and 2 hours at high temperature. They observed an increase in the localized length of SWNTs due to the increase in the bundle diameters of aligned SWNTs and attributed to the effect of magnetic field. The thermal and electrical properties along the magnetic field alignment direction increased by 10 and 35 % as compared to the non - aligned composites. However, both the papers point out that viscosity plays a major role in the alignment of CNTs.

4.2.4. In-situ polymerization and melt spinning techniques for alignment in thin films.

Synthesis of thickness aligned carbon nanotube PMMA composite thin films by infiltration of the monomer into aligned arrays of CNTs followed by in situ polymerization was studied by Raravikar *et al.* [116] They found that the wetting of the polymer solution against nanotubes walls was important and the low viscosity governed the infiltration of the monomer that affects the ultimate properties of the composite.

Feng *et al* [117] also showed well aligned carbon nanotube in polyaniline (PANI) by in situ polymerization of the monomer. A good interaction between the nanotubes and the polymer was proven by FTIR spectroscopy. The electrical conductivity as a function of temperature is shown in Figure 4.13. Addition of MWNTs increased the conductivity of the conductive polymer by one order of magnitude. Increase in temperature lead to

increase in conductivity owing to semiconductor like behavior of the composite. Delocalization of charges by addition of MWNTs to PANI was explained by the dependence of resistivity on the temperature before and after adding the filler. They suggest that these composite films can find their use in molecular electronics and other fields.

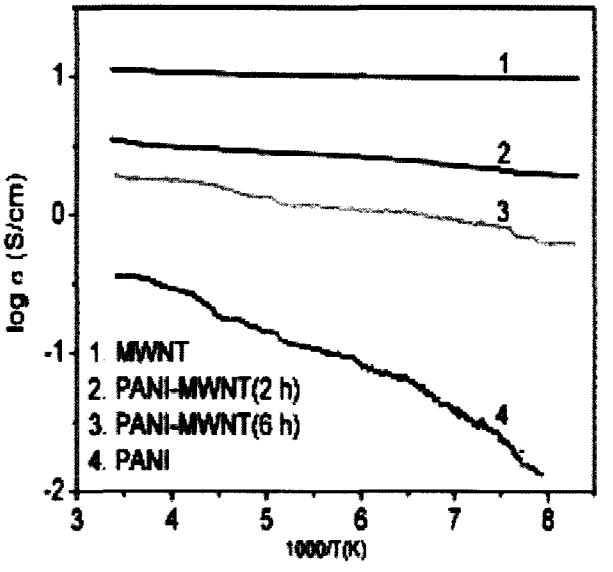

Figure 4.13. Electrical conductivity of MWNT-PANI composite films as a function of temperature (adapted from Feng *et al*).

Haggenmueller *et al* [118] at the University of Pennsylvania used melt processing methods to align the SWNTs in polymers. Prior to melt spinning they used two method to form the composite films: (i) A mixture of PMMA in DMF and SWNTs suspensions were sonicated for 3 hours and poured into Teflon dishes heated to 20 °C for drying (ii) the films from the previous method were hot pressed a number of times and dried. Composites from method 2 showed a more homogenous and uniform dispersion as compared to the ones fabricated by method 1. At draw ratios close to 4 the conductivity

increased in the melt spun direction. However, at higher drawing ratios the increase in conductivity was lower than expected.

4.2.5. Theoretical studies on nanotube conductivity in the polymer composites.

Kyrylyuk and Schoot [119] used a continuum theory to study the percolation of carbon nanotubes in polymeric and colloidal media. Using this model they predicted the effect of polydispersity, bending flexibility and also attractive interactions between the carbon nanotubes on the percolation threshold of the carbon nanotube polymer systems. Their predictions assumed that equilibrium was achieved during the processing of composites. The properties that affected the percolation threshold were:

(1) Small quantities of larger rods, meaning high aspect ratio CNTs reduced the percolation substantially.

(2) Bending of nanotubes resulted in smaller effective aspect ratios thereby increasing the percolation threshold.

(3) The stickiness as they termed it is the medium induced interaction between the nanotubes, also played a major role in determining the percolation threshold. They found that weak interactions between the nanotubes dropped the percolation. So by optimizing the stickiness by choosing the right polymer, the percolation threshold can be lowered.

(4) They discussed that the network formation depends on the tunneling distance of charge carriers which further depends on the host polymer and nanotube material properties. A high dielectric constant polymer is preferable since it allows higher conduction by reducing the potential barrier between adjacent tubes.

Hence, by using the connectedness percolation theory, by making the right choice of host polymer, one can reduce the percolation and increase the electrical conductivity of the composite since it influences the behavior of nanotubes in the composite during the processing stage.

The effect of filler concentration and the degree of alignment on the electrical conductivity of composites beyond the percolation threshold was studied was by White *et al* [120] using a three dimensional simulation. The aspect ratio of the fillers considered was 10, 20 and 80 and a random resistor model was used to calculate the electrical conductivity of the composites by addition of conductive fillers. The simulated conductivity as a function of axial orientation parameter was studied. They found that the conductivity increased up to a certain degree of orientation and then dropped; this was related to loss in network at high degree of alignment. Also, fillers with higher aspect ratios showed a wider range of concentration and alignment orientation parameter at which the electrical conductivity was high as compared to the fillers with lower aspect ratios. In lower aspect ratio fillers even a small degrees of alignment is required to disrupt the percolation system. They found that axial orientation played a pronounced role in determining the electrical conductivity of the composite regardless of the concentration or the aspect ratio of the fillers used.

In this research, the effectiveness of using SWNTs beyond the percolation threshold to improve the electrical conductivity of polyethylene composites is presented. As strongly discussed in the literature; the effect of dispersion, nanotube aspect ratios, polymer nanotube interactions and the degree of alignment were studied.

4.3. Experimental Methods and Materials.

4.3.1. Materials

Purified HiPco and Southwest CG 100 SWNTs were used as conductive fillers. Low, medium and high density polyethylene (Purchased from Sigma Aldrich) were used as the matrices. Dichlorobenzene (DCB) and N-methylpyrrolidone (NMP) used as solvents were purchased from Sigma Aldrich. For application of electric field two different kinds of set up were used, for the wire set up 8 gauge copper wire was used and for the vacuum spray process set up ITO glass electrodes were used. SEM, TGA and Raman analysis of the SWNTs is shown in Appendix- A.

4.3.2. Processing of polyethylene / SWNT composites and electric field studies.

The composites were processed using two methods: (i) hot coagulation method[121] (ii) Electric field vacuum spray process.

A. Hot coagulation method

In this method, the SWNTs were sonicated in DCB (0.2 mg/ml) using a probe sonicator (Cole Parmer ultrasonic homogenizer) for 2 hours, and heated to the respective melting temperature of the polymer used (110°C for MDPE). The polymer was then dissolved in dichlorobenzene at its melting temperature and this mixture was added to the heated nanotube suspension. The mixture was cooled to below 70°C while simultaneously sonicating allowing for the polyethylene to crystallize which preserves the dispersion of nanotubes. The cooled mixture was then filtered using a vacuum set up and the composites were dried at 150°C under vacuum. The concentration of the nanotubes was limited to 10%.

The dried sample was pulverized into a fine powder and placed in a quartz tube (4 mm and 2 mm diameter) which was further sealed with two copper wires connected to a DC power supply. The sample was melted to 20°C above the melting point before applying the electric field. A schematic of the set up is shown in Figure 4.14. The distance between the copper leads was maintained at 1.5 cm using a clamp on system. Low DC voltage was applied to the sample after melting it.

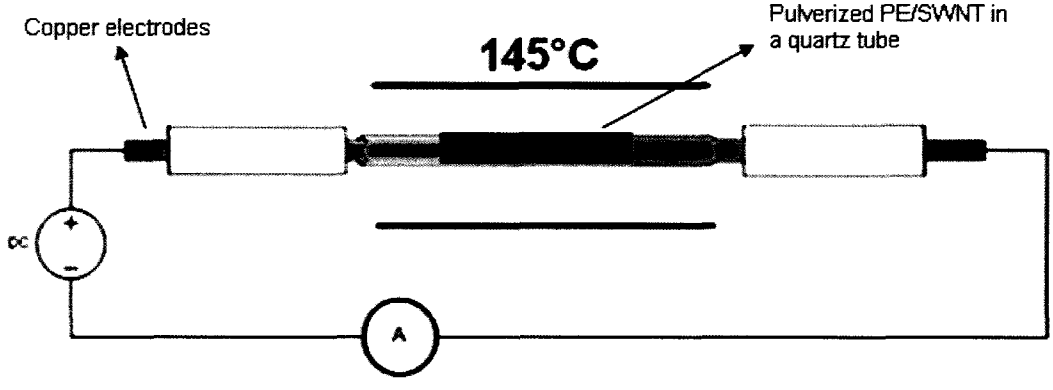

Figure 4.14. Electric field set up used for hot coagulated polyethylene / carbon nanotube composites

Several challenges were encountered and resolved during the electric field conditioning of the SWNT/MDPE composite.

a) For SWNTs to effectively align in the MDPE polymer, the polymer must have low viscosity. To combat this challenge, the composites were heated to 145°C to reduce the viscosity of the MDPE by melting it.

b) For the applied electric field to take effect, direct contact must be made between the copper leads and the composite. The samples were compacted between the leads using applied pressure and the leads were clamped in place to ensure effective contact between the composite and the copper leads.

c) The formation of voids or air pockets within the composite was another major challenge. This was addressed by heating, electrically conditioning and compressing the sample composite to reduce the void formation.

d) The final challenge posed by the process was the ability to harden the MDPE matrix while retaining the SWNT network formed by the electric field. After several conditioning runs were performed to condition the SWNT/MDPE composite, a low voltage electric field was maintained while allowing the composite to cool. This retained the SWNT network while the MDPE matrix hardened.

B. Electric field vacuum spray method

In this method, the nanotubes were first dispersed in N-methylpyrrolidone (NMP) at a concentration of 0.2 mg/ml. The suspensions were sonicated for 2 hours using a probe sonicator followed by 4 hours using a bath sonicator (Branson 5200 ultrasonic cleaner). Simultaneously MDPE was dissolved in DCB at 110°C. In the vacuum system shown in Figure 4.15, two ITO glass electrodes parallel to each other were attached to the Buchner funnel and connected to a high voltage power supply. Nanotubes were sprayed onto the porous plate on which a 0.2 micron PTFE is placed, and the electric field was switched on. Once the electric field was switched on, the nanotubes aligned in the direction of the applied field. Immediately, the polymer solution was sprayed and the vacuum pump was turned on for the solvent filtration. The polymer locks the alignment of the nanotubes and the solvent was filtered into the Buchner flask. This process was repeated a number of times to obtain the desired

thickness of the composite film. Figure 4.15 shows a schematic of the set up designed for processing of composite thin films.

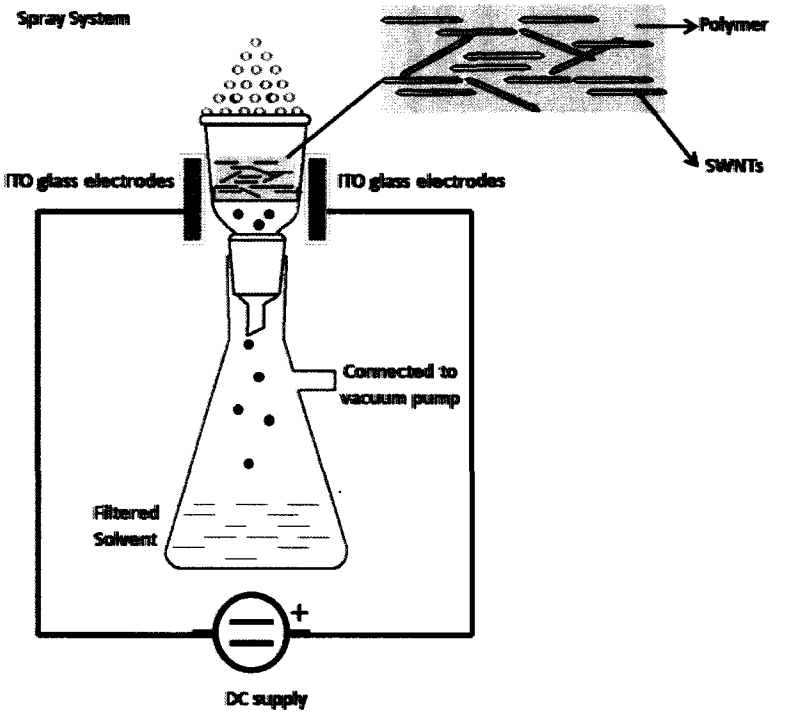

Figure 4.15. Schematic of the electric field vacuum spray set up used to process polyethylene/carbon nanotube composites.

4.3.3. Characterization of PE / SWNT composites.

The dispersion of CG-SWNTs in the solvents was characterized using TEM (JEOL 2100 Field Emission Gun Transmission Electron Microscope) and in the polymer matrix it was characterized using SEM (FEI Quanta 400 ESEM). Electrical resistivity measurements were made using an in-lab four point probe connected to a Keithley 580 micro ohmmeter. Raman spectroscopy with Renishaw Micro Raman system operating with a 780 nm AlGaAs diode laser source was used to verify the alignment of nanotubes. Raman

mapping was used to determine the effect of dispersion and the uniformity of nanotube distribution in the composite. SWNT-MDPE composites were also analyzed using Differential Scanning Calorimetry (DSC) thermograms acquired from 35 to 600 °C using a TA Instruments Q2000 analyzer at a heating rate of 20°C min^{-1}.

Using the data obtained for the samples processed by hot coagulation method which were subjected to electric field, a matrix was set up to find out which are the parameters that would affect the electrical conductivity of the polyethylene nanotube composites and also the interaction between them. Tests were conducted by varying the levels of factors namely: (1) Decanting - with or without – 2 levels (2) Electric field - with or without – 2 levels (3) viscosity – high, low and medium – 3 levels. The matrix set up used for analysis of variance is shown Table 4.1. The response variable for this set up was the measured resistance.

Table 4.1. Basic matrix used for the analysis of variance study (ANOVA).

Class	Levels	Values
Decanting	2	0 1
Efield	2	0 1
Viscosity	3	H L M

Decanting	1
No Decanting	0
Electric Field	1
No Electric Field	0
Viscosity	HDPE (H), MDPE (M), LDPE (L)

4.4 Results and discussion.

4.4.1 Composites processed by hot coagulation method and subjected to electric field.

Initially, before subjecting the composites to electric field test, the amount of time required to obtain an optimal dispersion of SWNTs in DCB was studied. The time of sonication as a function of the resistance of the composite was studied. Figure 4.16 shows the effect of sonication on the electrical resistance. It can be seen that the resistance increases from ~ 2500 ohms to 3000 ohms beyond 2 hours sonication indicating over sonication. It has been shown in the literature that over sonication leads to nanotube scission and induces defects on the sidewalls owing to reduction in overall properties of the polymer nanocomposite. [122, 123,124,125] Both CG-SWNTs and HiPco SWNTs showed a similar behavior; hence the sonication time was fixed at 2 hours for all samples.

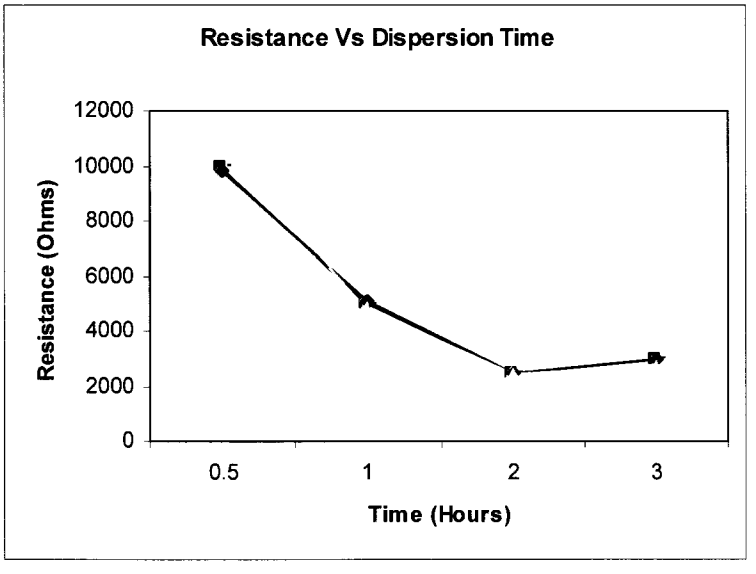

Figure 4.16. Effect of sonication time of SWNTs on the resistance of MDPE-SWNT composites.

To remove the larger agglomerates, the samples were centrifuged at different forces (*g*) for varying lengths of time. To separate out the catalyst particles, amorphous carbon and larger agglomerates, the CG-SWNTs in DCB samples needed to be centrifuged at 85000 *g* for 15 minutes. Figure 4.17 shows the TEM images of the CG-SWNTs before and after decanting. The red arrows indicating dark spots in the TEM image of the sample before decanting shows the presence of left over catalyst particles and it can also be seen that the nanotubes are heavily agglomerated before decanting as compared to after decanting process. A weight analysis on the pellet showed that 30% of the original sample, sediment out of the solution.

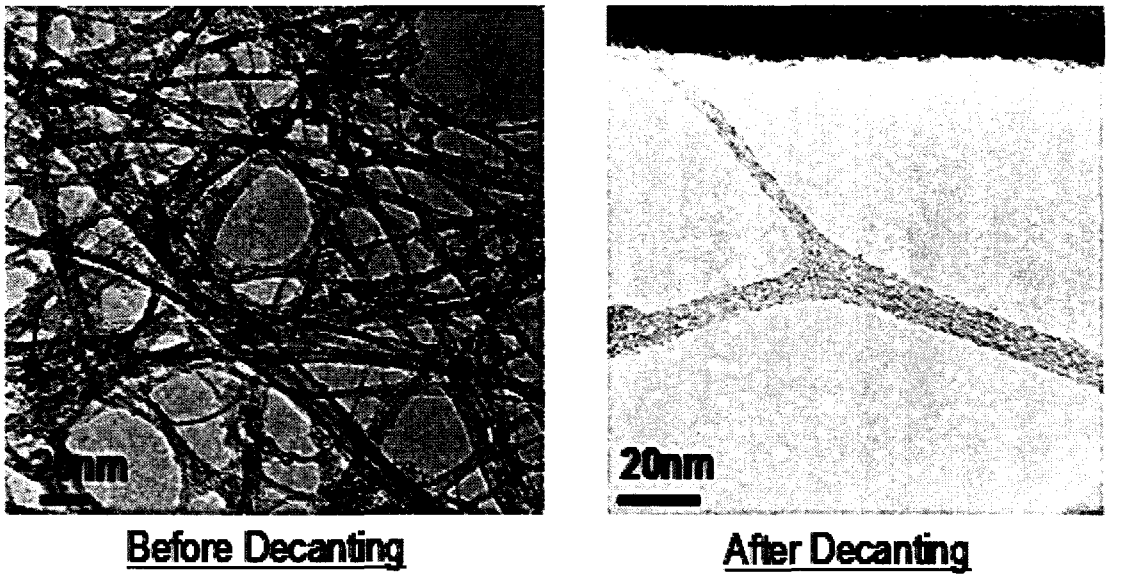

Figure 4.17. TEM image of the CG-SWNT/DCB suspensions before and after decanting showing the removal of catalyst and heavily bundled SWNTs after the centrifugation process.

As discussed previously in the background section, in order for the electric field to take effect the viscosity of the polymer / solvent in which the nanotubes are dispersed should be low enough to allow for their translational and rotational motions. Hence, the effect of

temperature on the resistance of the composites was studied prior to applying the electric field. Table 4.2 shows the resistance of the composites at different temperature for varying lengths of time.

Table 4.2. Optimizing the temperature of the samples prior to application of the electric field.

CNT in MDPE	Resistance room temperature (ohms)	Resistance at 110°C for 30 minutes (ohms)	Resistance at 145°C for 30 minutes (ohms)
10 wt% CG-SWeNTs	1500 ± 300	500 ± 50	150 ± 10
10 wt% HiPco SWNTs	1250 ± 175	500 ± 50	100 ± 10
10 wt% Ni-SWNTs	5000 ± 100	3500 ± 125	1950 ± 300
10 wt% Ag-SWNTs	2000 ± 500	600 ± 100	200 ± 50

The temperature has a major effect on the resistance of the composites; the resistance dropped from 2500 ohms at room temperature to 150 ohms when heated to 145°C. It is well known that the conductivity of the carbon polymer composites is sensitive to temperature changes [126]. Bin *et al* [127] reasoned this behavior by describing the mobility of the polymer chains beyond the melting point of the polymer. The polymer chains are more mobile when heated beyond the melting point resulting in their active movement and rearrangement which increases the nanotube to nanotube contact, thereby decreasing the resistivity of the composite. Also, they pointed out that the thermal expansion of the polymer was not significant enough to disrupt the conductive contact between the

nanotubes and the mobility of the polymer is controlled by the CNTs. Hence to improve the nanotube contacts, the samples were heated to 145°C for 30 minutes prior to application of electric field.

Figure 4.18 shows the behavior of SWNTs due to the effect of electric field. SWNTs in a liquid behave as dipoles when subjected to an external electrical field and over a period of time, they tend to align in the direction of the field.[112,128] For our study, electric field was used to improve the CG-SWNT network formation in the composite and also to reduce the polymer – carbon nanotube contact junctions. This is believed to reduce the electrical resistivity of the composite. The samples were conditioned 3 to 4 times which minimized the voids and improved the current carrying capability of the composite.

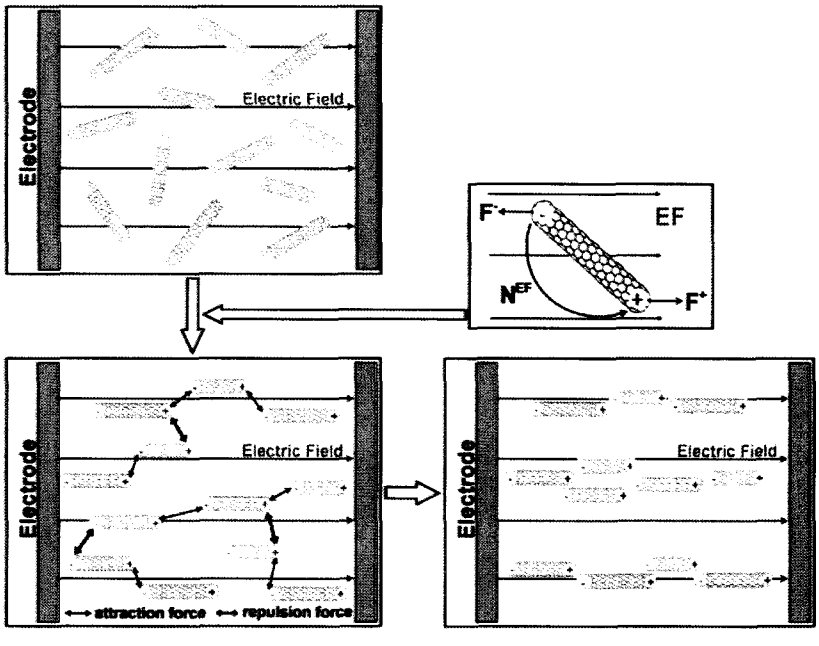

Figure 4.18. Mechanism of alignment of SWNTs when subjected to an electric field (adapted from Du *et al*).

Heat released from a single-walled CNT under microwave irradiation leads to temperatures close to 2000 °C as shown by Imholt *et al* .[129] Wang *et al* [130] showed use of microwave radiations leads to a large amount of heat release by MWNTs which melts the surrounding polymer within seconds. The approach of microwave welding is extremely useful in improving the intercalation of CNTs in the polymer matrix and improvement of polymer nanotube bonds without the use of adhesive and surfactants. They found that since the irradiation is for a short amount of time, no damage of the polymer occurs. Heat dissipation from MWNTs occurs instantaneously by conduction and radiation to the polymer and the damage of the polymer is prevented due to its thermal resistance and lower heating rate. By doing so they found the electrical resistance of the composite dropped to 10-50 ohms/square where as the sample before irradiation was insulating. Combining the principles of electrical field alignment and nanotube welding using heat, we studied the effect of applied electric field on the resistivity of the composites.

Figure 4.19 shows the current voltage statistics of 10 wt% CG-MDPE composites at 145°C and with each conditioning run, the resistivity of the composite decreased further. The peak temperature on the quartz tube was measured when the sample carried 1.2 amps of current and it was around 250°C which is much below the degradation temperature of polyethylene measured (480°C) by the differential thermograms shown in Appendix-1. However, any further increase in current rapidly shoots up the peak temperature and even irradiating the sample for very little time leads to degradation of the polymer.

Figure 4.20 shows the values of resistivity obtained for various samples processed (the values are representation for an average of 15 samples optimized to the best conditions). The resistivity of the composite increased by almost an order of magnitude when the

samples were cooled to room temperature. The possible explanations to this behavior are the presence of voids in the composite after cooling due to uneven size distribution of the pulverized composite and the contact resistance of the copper electrodes. Reduction in resistivity was attributed to improved SWNT-SWNT contacts between nanotubes and local heating of the polymer caused by the electric field. However in very few regions, alignment of the nanotubes was seen.

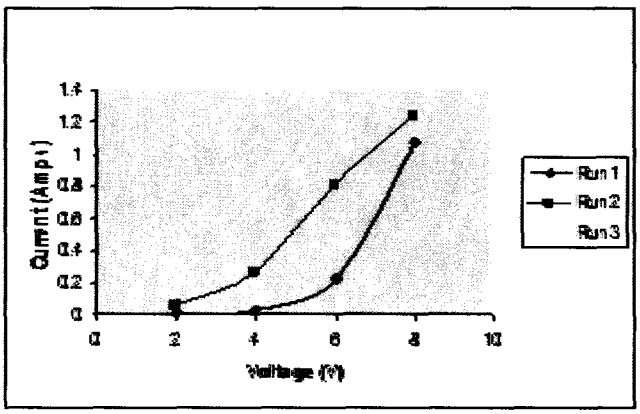

Figure 4.19. Current voltage statistics for 10 wt% CG SWNT / MDPE composites after each conditioning run showing an improvement in the current carrying capability of the composite.

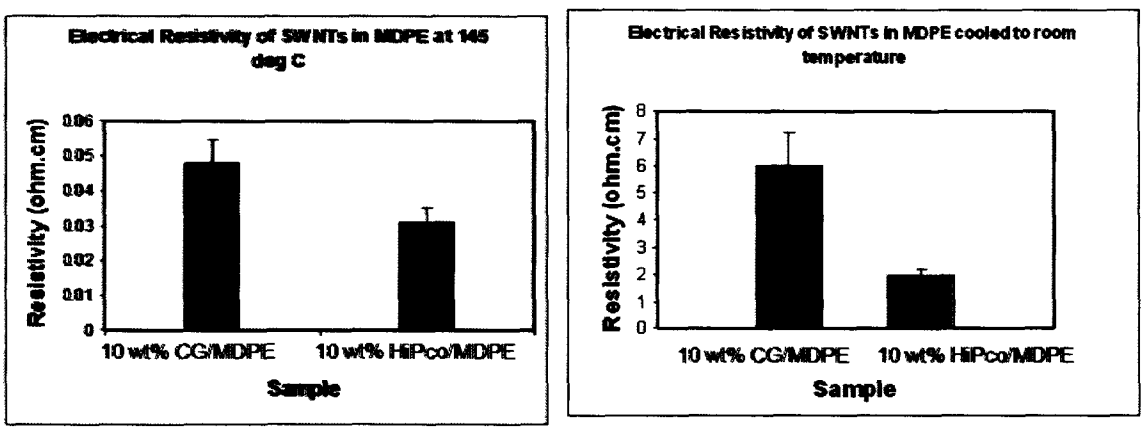

Figure 4.20. Electric resistivity of SWNT / MDPE composites (A) subjected to electric field at 145°C (B) subjected to electric field at 145°C and cooled to room temperature.

Figure 4.21 shows the SEM images of the composites before and after application of electric field. A better network of nanotubes is seen after the application of electric field.

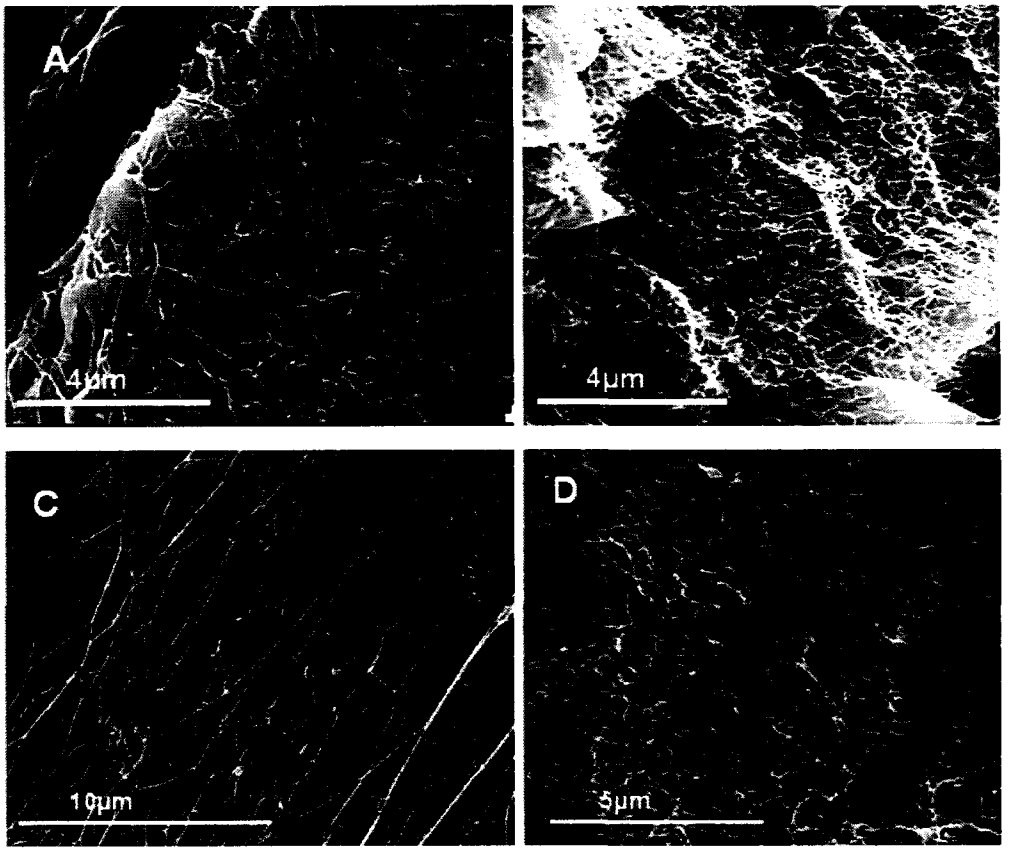

Figure 4.21. MDPE / HiPco composites (A) processed by hot coagulation method before the application of electric field. (B, C and, D) after the application of electric field showing an improved network and contact between the nanotubes.

HiPco SWNT filled composites show a lower resistivity compared to the CG-SWeNTs filled counterparts due to their better disentanglement and dispersion combined with lower defects confirmed by the SEM and Raman analysis shown in Appendix 1.

Samples subjected to high currents lead to polymer degradation shown in Figure 4.22 indicated by the enclosed areas. High amount of current instantly heats up the sample with peak temperatures exceeding 500°C which damages the polymer.

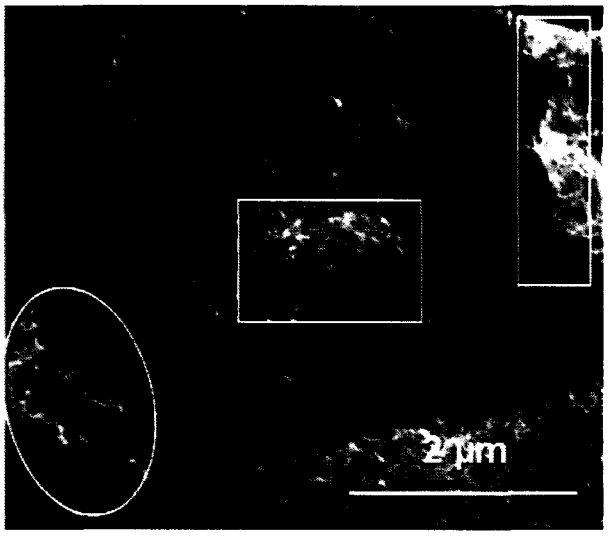

Figure 4.22. Samples subjected to current greater than 2 amperes showing polymer degradation (indicated by the area enclosed in white).

Du et al [131] developed a Raman imaging method to quantitatively characterize the dispersion of nanotubes in a composite. They quote that "Given that the G band intensity is exclusively from SWNTs and the laser penetration depth exceeds the thickness of the sample, the Raman intensity is to a very good approximation proportional to the number of SWNTs in a volume of $1 \times 1 \times t$ mm^3, where t is the thickness". Since the G mode corresponds exclusively to the tangential motion of the carbon atoms on the cylindrical surface of the nanotubes, for a uniform distribution of nanotubes the Raman map is featureless, and with non uniformity the map shows non uniform features. One of the requirements for this is the surface of the sample has to be smooth. Hence, the smooth portions of our samples were analyzed for nanotubes dispersion. Figure 4.23 shows the

Raman maps for three samples (a) composites before electric field (2) composites after electric field (c) composites subjected to high currents. It can be seen from the image that the map is featureless before being subjected to electric and current conditioning indicating a uniform dispersion of CNTs. However, a non uniformity is seen in the map after the sample is being subjected to electric field; this is because both polymer melting and application of electric field result in increased contact between the CNTs and also some agglomeration as seen in the SEM images in Figure 4.23. After the application of current, the map is extremely non uniform indicating uneven distribution of CNTs.

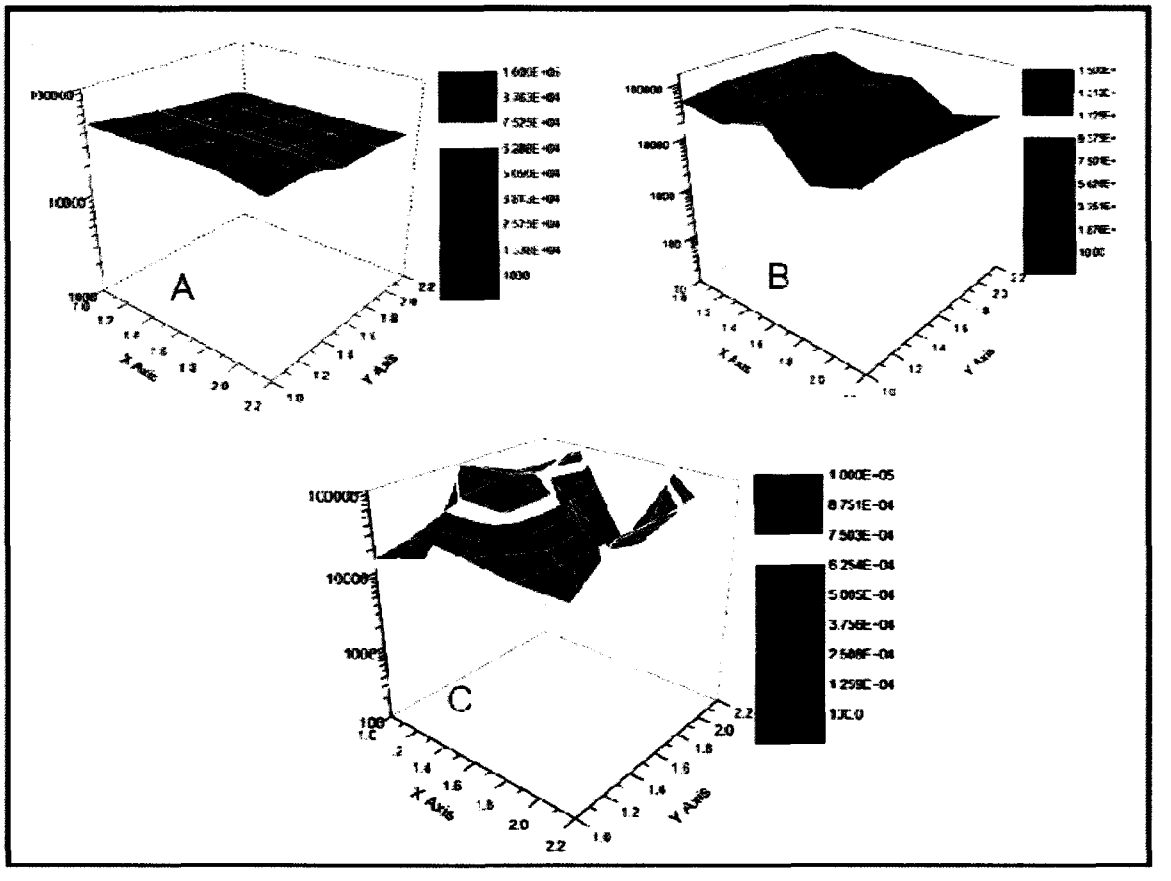

Figure 4.23. Raman mapping for SWNTs / MDPE composites (A) processed by hot coagulation method before subjecting to electric field. (B) samples subject to electric field and cooled to room temperature (C) samples subjected to high currents.

The standard deviation of the G peak intensity was calculated for all the plots (the Raman intensity was normalized to a mean of 100).The standard deviation (S.D) gives an approximate estimate of the variation in the G peak intensity of the samples. Higher variations resulted in higher standard deviations. The S.D of samples before subjecting them to electric field conditioning was 18.5 and that of samples subjected to electric and high currents increased to 24.6 and 35 respectively.

Hence, samples processed by hot coagulation method when subjected to low DC fields help in a modest reduction in the electrical resistivity of the composite without polymer degradation.

4.4.2 Composites processed by Electric Field Vacuum Spray process and their characterization.

4.4.2.1 Dispersion of SWNTs

Dispersion of the CNTs and alignment leading to better network formation, has a strong effect on the electrical properties of the composite.[132,133,134] From the previous studies on dispersion (discussed in chapter 3), it was concluded that NMP is a very good solvent that helps in exfoliation of SWNTs. In order for the SWNTs to be soluble in a medium, the free energy of mixing should be negative. The Gibbs free energy of mixing [135] ΔG_{mixing} is given by

$$\Delta G_{mixing} = \Delta H_{mixing} - T\,(\Delta S_{mixing})$$

Due to their structure and large attractive forces, the enthalpy of mixing of nanotubes in various systems is generally positive and the entropy is very small, owing to a positive free energy of mixing. However, Bergin *et al* [136] demonstrate that the free energy of

mixing is negative for the NMP / SWNT system since the enthalpy of mixing is almost zero. Hence, the SWNTs instantly exfoliate in the NMP solvent since it physisorbs onto them which is a requisite for any good solvent.

AFM and DLS analysis were used to study the dispersions and obtain an approximate value of the aspect ratio of the SWNTs used. The samples were decanted at low *g's* (10000 rpm) to get rid of the heavy agglomerates and catalyst particles. The analysis of the sediment showed approximately 5 to 8% of the sample settled down. SWNT suspensions were diluted before the analysis and APTS functionalized silicon chips were used as substrates for AFM. From the AFM images shown in Figure 4.24, both individual and bundled SWNTs can be seen, the diameter of the bundles range from 4 nm to 13 nm. Figure 4.25 shows the DLS data which gives an approximate estimate of the length of SWNTs from which the aspect ratios can be calculated.

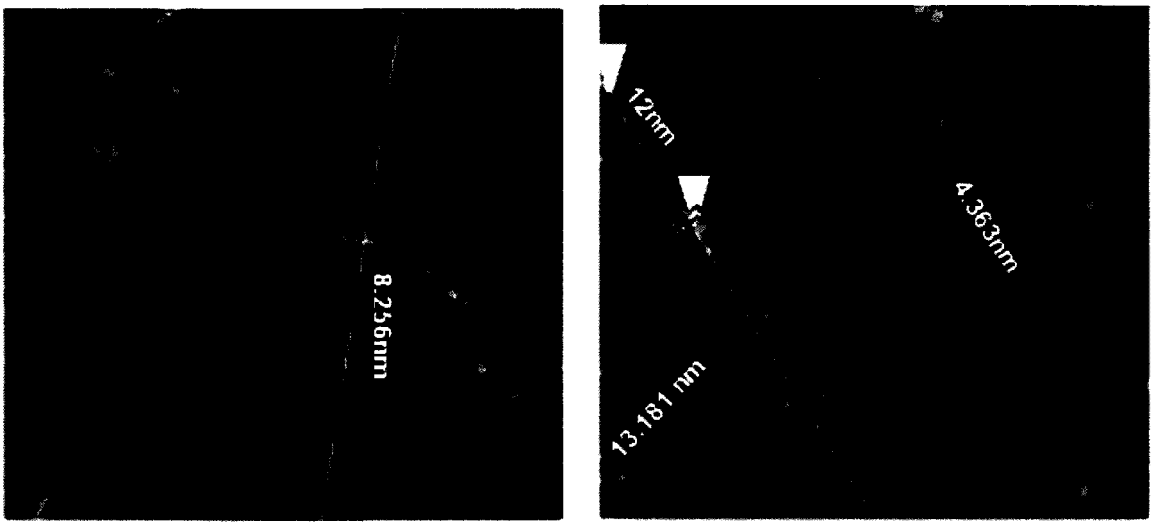

Figure 4.24. SWNT / NMP suspensions after decanting at 10000 rpm showing the presence of: (A) bundles (B) bundled and individually dispersed SWNTs.

Four samples were diluted from the master batch, for the DLS analysis to ensure the reliability of the results. It can be seen that the AFM diameters are comparable to the DLS diameters.

From the DLS analysis an approximate value of the aspect ratio determined is 85.9 (considering 4.48 nm as the diameter and 385 nm as the length).

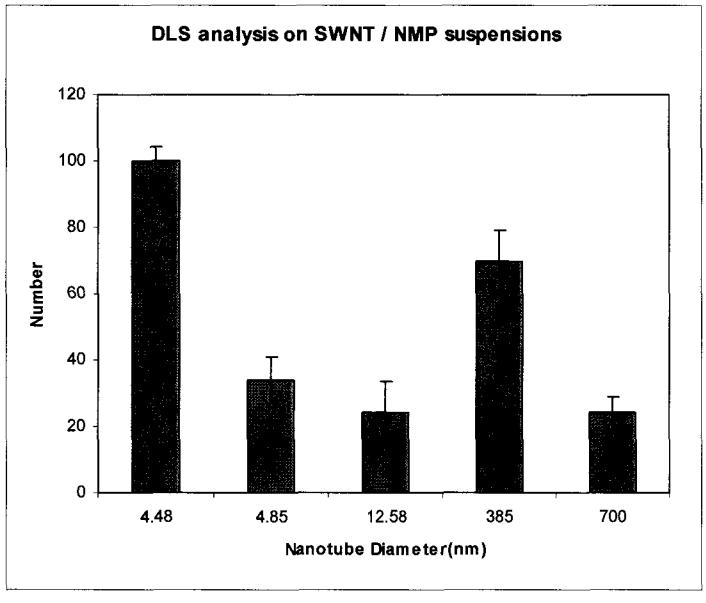

Figure 4.25. DLS analysis on the SWNT suspensions showing bundle diameters ranging from 4 to 13 nm and length from 385 – 700 nm.

4.4.2.2 Processing of composites.

The effect of diffused layer processing (spraying) as opposed to batch layer processing (pouring) was studied for 5 wt% HiPco-MDPE composites. SEM characterization of the both the samples is shown in Figure 4.26. The dependence of electrical resistivity of the sample on the processing, concentration, dispersion and alignment is discussed in the next section. Spraying has an advantage over batch layer processing due to the better

control of the layering process and also, the direction of spray helps preferential network formation and alignment of SWNTs. Also, our previous studies on surface coverage showed that spraying helps in keeping the SWNTs dispersed in the solvent and results in better surface coverage.

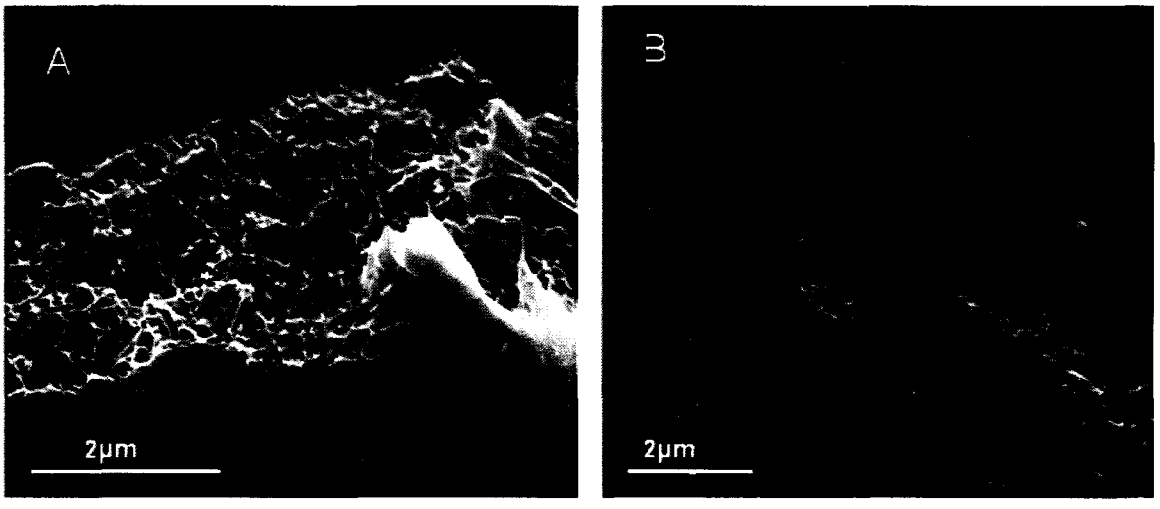

Figure 4.26. The difference in network formation when the samples were subjected to electric field (A) batch layer processing (B) diffuse layer processing.

To study the uniformity of the distribution Raman mapping was used. The standard deviations of the "G" band normalized to a mean of 100 were also calculated. The standard deviation for samples processed by spray method was approximately 2 and that of samples processed without spraying was around 10, indicating that the spray method helps in uniform distribution of SWNTs in the composite. Also, it can be seen from Figure 4.27 that the map for spray method is featureless and more uniform as compared to its counterpart indicating that the SWNTs are well distributed in the PE matrix.

The interaction between polyethylene and SWNTs was also studied using Raman spectroscopy. The increase in ratio of normalized intensities of the D and G bands in the

spectra is an indicator of sidewall functionalized or disruption in sp^2 hybridization of SWNTs.

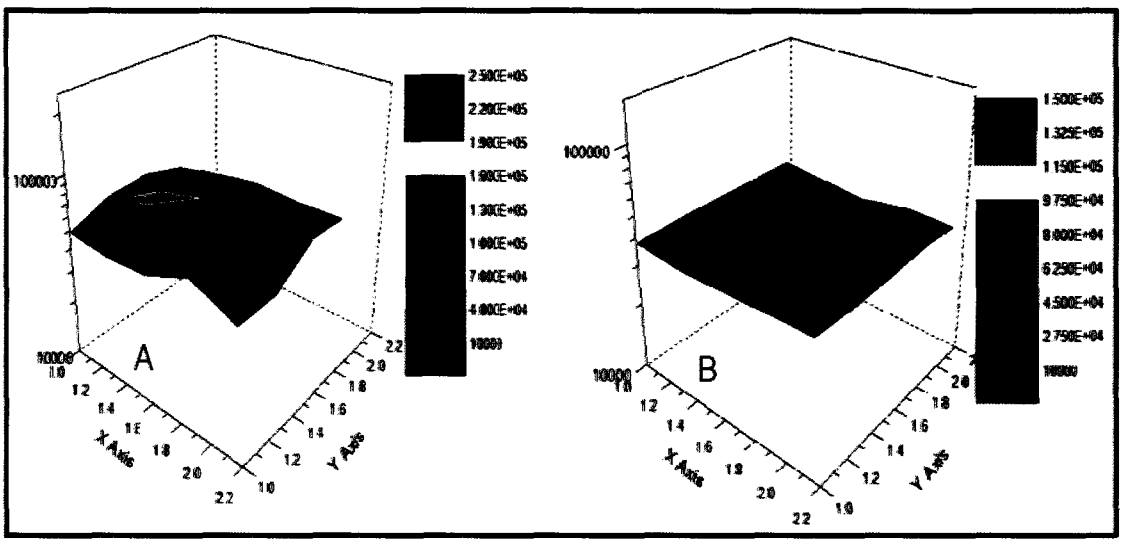

Figure 4.27. Raman map of G peak intensities of the samples processed by (A) pouring the SWNT suspension (B) spraying.

Figure 4.28 shows the Raman spectra of the SWNTs with and without MDPE; the D/G ratios of HiPco SWNT composites was 0.0627 and that of plain purified SWNTs was 0.041 indicating a modest interaction between the SWNTs and polyethylene. Pulikkathara *et al* [137] observed a similar behavior for fluorinated SWNTs (F-SWNTs) and MDPE composites. They observed that the D/G ratios increase for F-SWNTs/MDPE composites as compared to plain F-SWNTs and attributed this to the interaction between the polymer and the filler.

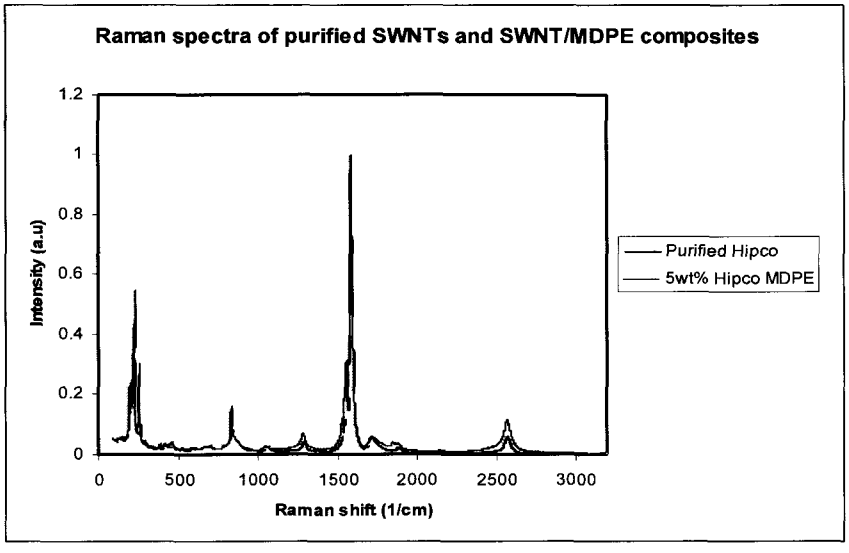

Figure 4.28. Raman spectra of purified SWNTs and SWNT/ MDPE composites.

4.4.2.3 Electrical Resistivity of the polyethylene / SWNT composites.

The effect of processing, concentration and, electric field on the electrical resistivity of the composites was studied. The effect of each parameter keeping the other two constant was evaluated. Weight percent of the SWNTs in MDPE ranged from 2 to 20 wt%.

A. Effect of processing

For the processing studies by the methods discussed above, 5wt% SWNT-MDPE composites were used and two different DC voltages were used. The calculated DC voltages maintained across the electrodes were 166.6 V and 333.3 V (though the initial voltage applied were 600 and 1200 V, the dielectric Buchner funnel reduces the effective voltage between the electrodes). The distance between the electrodes was ~ 4 cm. The amount of voltage applied was limited to the values specified due to the limitation of the power supply. Table 4.3 shows the electrical resistivity values obtained for the samples. It can be seen from the table that the samples processed by the spray method perform better than their non-spray counterparts. This is due to better dispersion and alignment

obtained by the spray process. By increasing the voltage, a decrease in the electrical resistivity is observed.

Kamat *et al* [108] observed that at a low DC voltage close to 40 V/cm the nanotubes move from the solution, and are deposited at the electrode. At a high DC voltage of 100 V/cm the nanotubes align perpendicular to the electrode surface.

Since the highest voltage applied for our experiments was ~ 75 V/cm, it can be concluded that the alignment and network formation are enhanced by increasing the field between the plates. Also, alignment reduces the waviness of the SWNTs, which is one of the factors that reduces the electrical conductivity of the composite due to increased contact junctions between the SWNTs.

Table 4.3. Influence of processing and electric field on the resistivity of the SWNT/PE composites.

Resistivity at	5 wt% Pouring	5 wt% Spray
37.5 V/cm	34 ± 4.8	0.9 ± 0.19
75 V/cm	12.5 ± 4.2	0.75 ± 0.04

Since the samples processed from the spray method performed better than the samples processed without the spray; for further studies all the samples were processed using the spray method.

B. Effect of concentration

The effect of concentration of SWNTs on the electrical resistivity was studied. Figure 4.29 shows the resistivity of the composites as a function of the SWNT concentration. There are two plots, one represented in logarithmic scale to accommodate resistivity values obtained and the other is an approximate plot showing the resistivity values at each concentration

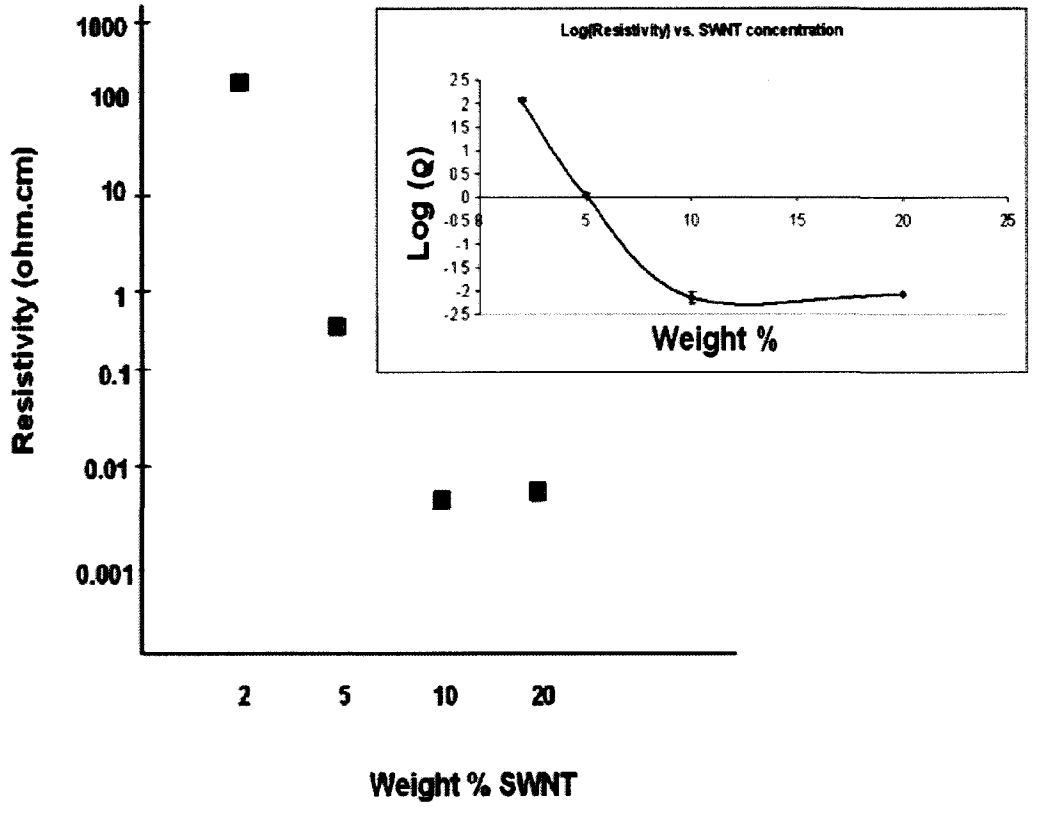

Figure 4.29. Resistivity of HiPco/MDPE composites as a function of the SWNT concentration.

From the plot (Figure 4.29) the observed resistivity of the composites reaches a minimum when the SWNT concentration is 10 wt% and above. Any further change in concentration does not reduce the resistivity. Stronger electric fields are required at high concentration

for enhanced alignment and network formation. Hence, for further studies 5 and 10 wt% SWNTs were used.

C. Effect of electric field

As discussed in the background section, partial alignment of SWNTs helps in enhanced network formation leading to better nanotube contacts thereby improving the electrical properties of the composite. However, for the nanotubes to align in an electric field

(1) The viscosity of the medium has to be low enough to allow for their translational and rotational motions.

(2) The concentrations of nanotubes should not be very high that they begin to bundle and form agglomerates which impede the alignment.

The new process meets both the requirements; 166 VDC and 333 VDC were used to study the effect of electric field on the alignment of 5 and 10 wt% SWNTs in MDPE. Resistivity of the composites in the aligned and non aligned directions is shown in Figures 4.30.

The resistivity of pure HiPco SWNTs bucky papers subjected to electric field was calculated initially to find the effect of polymer addition to the electrical resistivity of the composite. The electrical resistivity of bucky paper was close to 0.0009 Ω.cm – 0.001 Ω.cm . For the composites filled with 5 and 10 wt% SWNTs the values ranged from 0.3 ~ 0.75 Ω.cm and 0.0075 ~ 0.015 Ω.cm respectively in the aligned direction. The spray process is a layer by layer approach and hence it has the advantage of using low concentrations of SWNTs to effectively form an aligned network and subsequent

spraying of the polymer locks the alignment, thereby resulting in conductive polyethylene nanotube composite films.

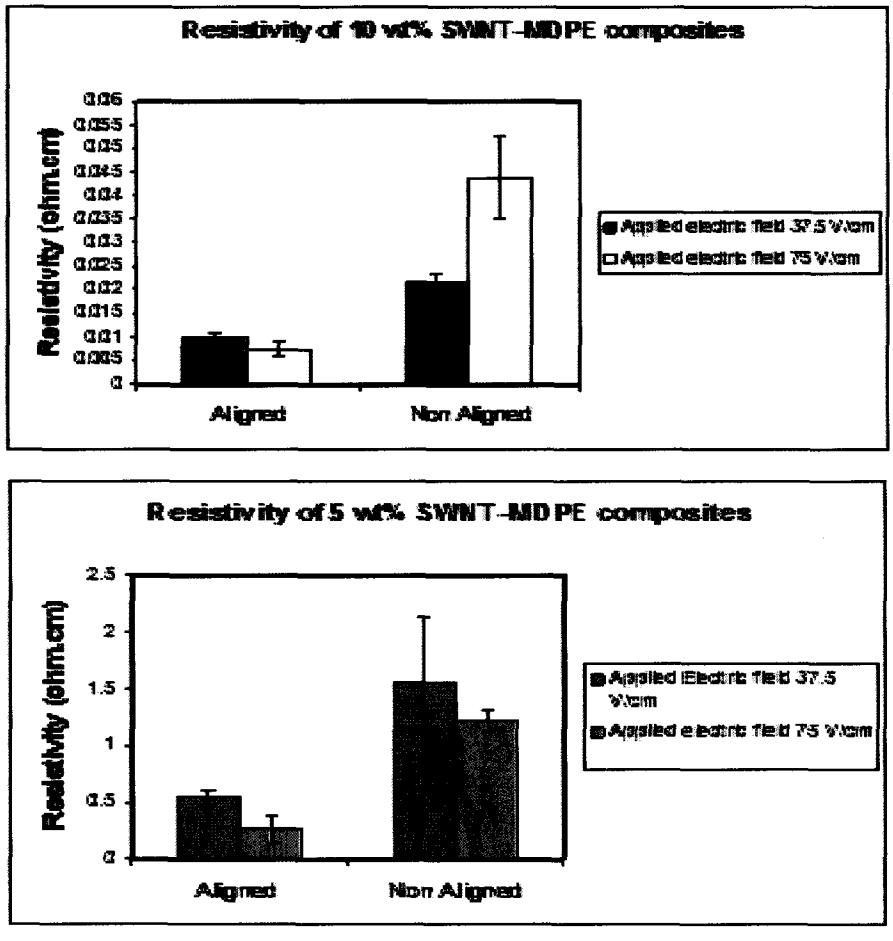

Figure 4.30. Effect of electric field on the resistivity of HiPco / PE SWNTs.

Fuhrer *et al* [38] measured the resistance between crossed nanotube junctions and found that the values can reach to the order of kilo ohms. Grossiord *et al* [96] discussed that the addition of polymer induces polymer nanotube contact junctions which will increase the resistance further. Hence, one of the main goals behind designing this process was to reduce the polymer nanotube contact junctions which control the conductivity of the composite. Another factor as discussed that affects the electrical resistivity is the waviness of the nanotubes in the composite. Li *et al* [138] studied the effect of waviness on

the electrical conductivity of nanotube polymer composites. Wavy nanotubes have more contact points than straight nanotubes in the polymer and this increases the electrical resistivity of the composite due to contact resistance. Large aspect ratios, low bending stiffness and processing induce waviness of the nanotubes in the composite. They report that the waviness affects both the percolation threshold and conductivity of the composites. The conductivity as a function of curl ratio is shown in Figure 4.31.

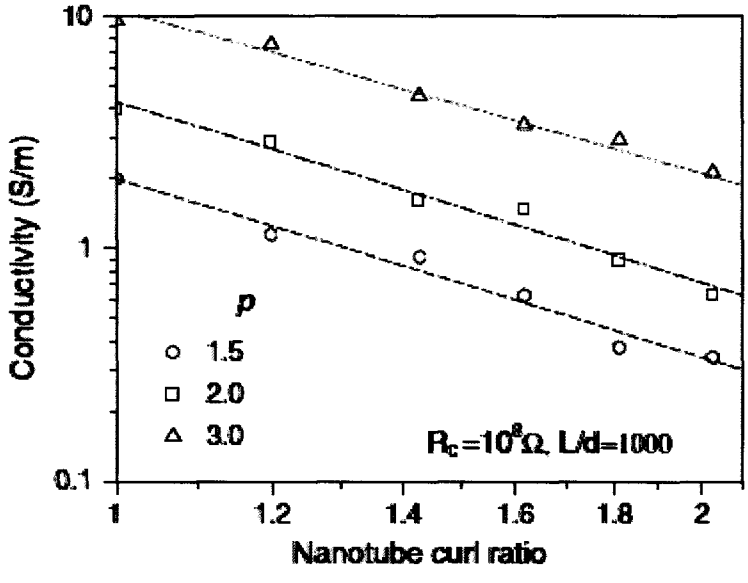

Figure 4.31. Effect of nanotube curl ratio on the conductivity of nanotube composites (adapted from Li *et al*).

The nanotube curl ratio has an inverse power law relation with the conductivity. Hence, by controlling the waviness using alignment we can reduce the number of contact points. This will in turn reduce the contact resistance and enhance the electrical conductivity of the composite. SEM and Raman analysis were used to characterize the alignment of SWNTs in the MDPE composites.

4.4.2.4 Characterization of alignment and network formation of SWNTs in MDPE composites.

Figure 4.32 shows the SEM image of aligned and non aligned bucky paper. It can be seen that the electric field helps in alignment of SWNTs.

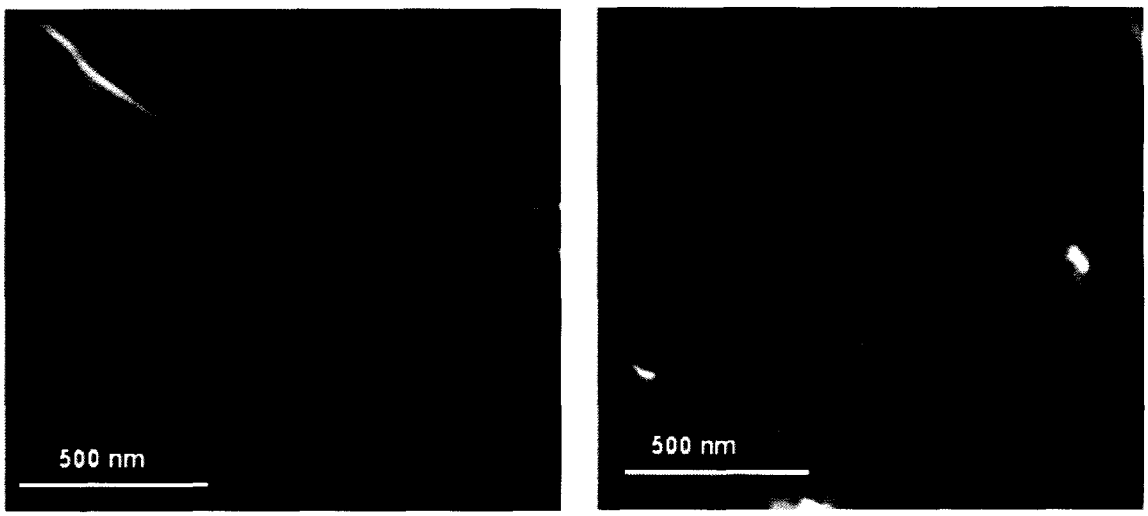

Figure 4.32. Aligned and non aligned bucky paper.

Alignment of SWNTs in 10 wt% SWNTs/MDPE composites (samples subjected to 75 V/cm electric field) is shown in Figure 4.33. A net alignment at the micro level is observed. Nanotube rich regions surrounded by the polyethylene matrix are observed in the figure. A bicontinuous structure with nanotubes close to each other surrounded by polymer was also reported by Du *et al* .[139]

They used an infiltration method to infiltrate epoxy into a nanotube mat. Nitrogen gasification was used to selectively etch away the PMMA from the PMMA-nanotube composites and then infiltrate the epoxy. They found that the electrical properties and the thermal properties of the composite are enhanced by the heterogeneous dispersion of nanotubes in the polymer matrix which is contrary to the widely accepted approaches that well dispersed nanotubes improve the electrical conduction in polymer matrices.

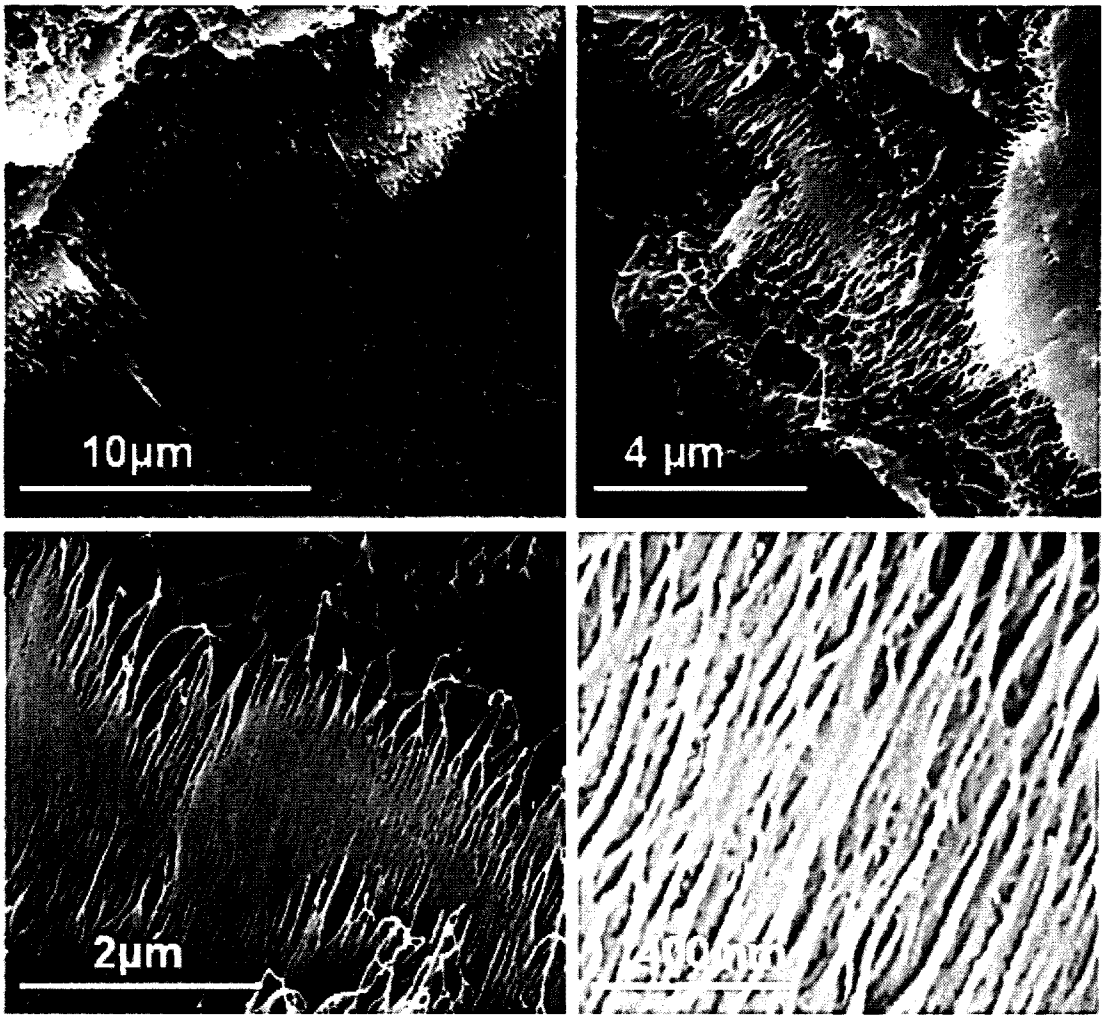

Figure 4.33. Net alignment of nanotubes in PE/SWNT composites showing some waviness and curling.

Alignment with optimal dispersion of nanotubes close together and reduced waviness helps in improving the electrical properties of the composite. Figure 4.34 shows the nanotubes being coated with modest amount of polymer with no over coating on the SWNTs and the SWNTs are in contact with each other.

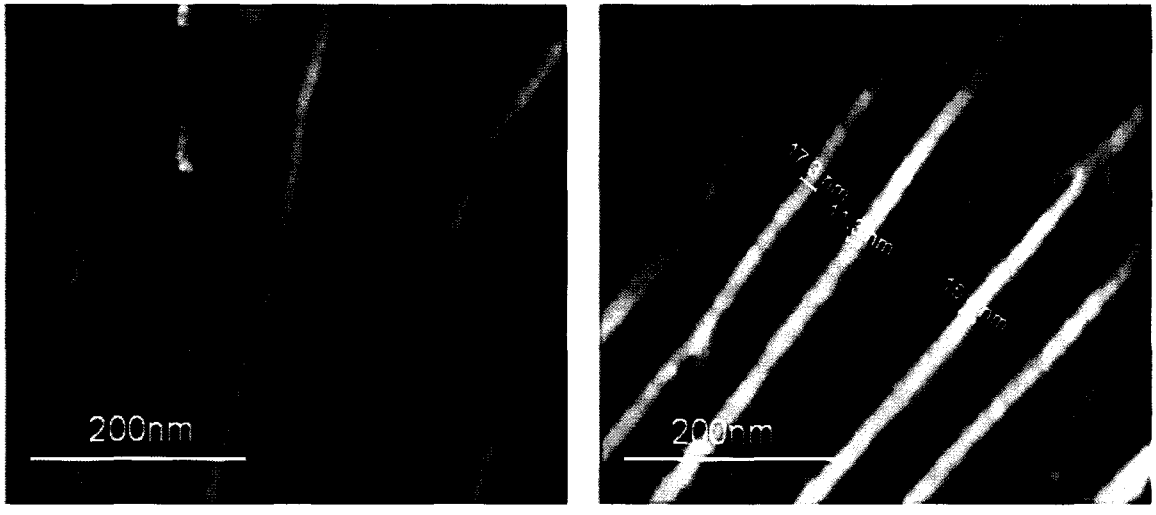

Figure 4.34. Aligned SWNTs coated with polyethylene.

Polarized Raman spectroscopy has been made a useful tool to study the alignment of carbon nanotubes because of their strong anisotropic absorption of polarized radiation. [140, 141] Polarized Raman spectroscopy of isolated single walled carbon nanotubes was studied by Duesberg *et al.* [142] They found that the maximum intensity of all the Raman modes was obtained when the CNTs were aligned parallel to the direction of incident polarized laser beam and attributed this to the depolarization caused by 1D nature of the nanotubes and also the resonance effects. Gommans *et al* [143] processed single walled carbon nanotube fibers using a process similar to melt spinning of polymers. They also found that the Raman polarized intensity was strongly dependent on the SWNT anisotropy. The decrease in intensity when the beam is perpendicular to the aligned direction was explained as a loss of Raman scattering.

Figures 4.35, 4.36 and 4.37 show the Raman spectra of 10 wt% SWNT/MDPE composites obtained at 0° and 90° orientations for the complete wavelength scale and the intensity reductions of the G modes and the RBMS.

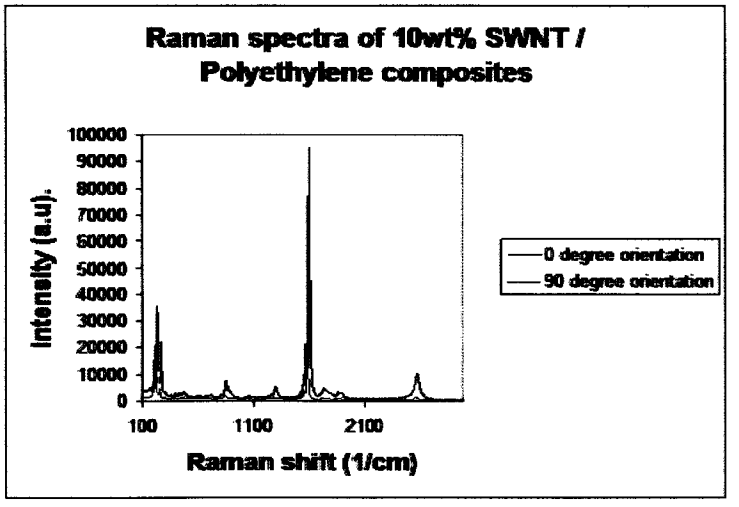

Figure 4.35. Raman spectra of 10wt%/MDPE composites orientated at 0 and 90 degrees showing the reduction in the intensity of all the Raman modes.

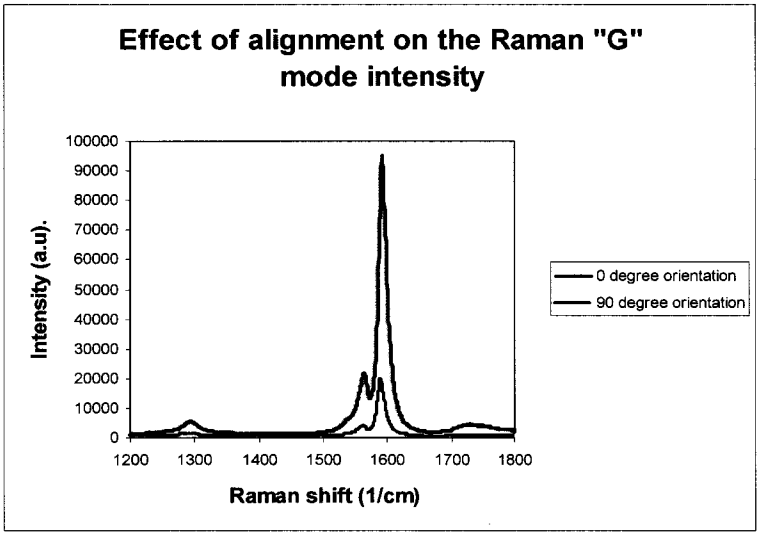

Figure 4.36. Reduction in the tangential "G" mode intensity of the composites aligned parallel and perpendicular to the direction of laser beam by almost a factor of 5.

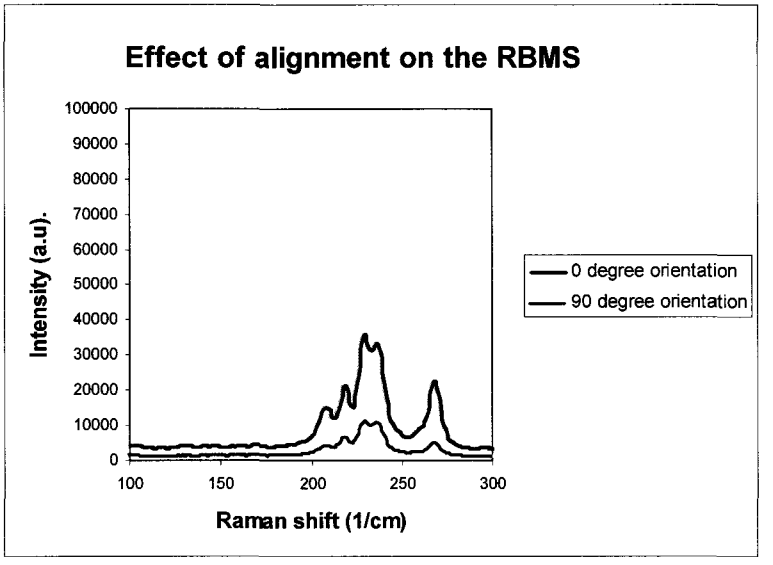

Figure 4.37. Reduction in the intensity of the radial breathing modes for 10 wt% SWNT/MDPE composites in the aligned and perpendicular directions.

The effect of alignment on 10 wt% HiPco-MDPE samples processed is shown in Figure 4.38. An average of 10 scans per sample was obtained and plotted for consistency purposes. It was also observed that the anisotropy in electrical resistivity correlates to the anisotropy in the Raman intensity. The electrical resistivity of the samples shown in Figure 4.35 is 0.00875 Ω.cm in the aligned direction and 0.0374 Ω.cm in the non aligned direction. The calculated resistivity anisotropy ratio is 4.27 and that of the intensities is close to 5. A possible reasoning for this disparity is due to the spot size of Raman laser which is ~ 5 microns and probe spacing which is larger than 5 microns because the probes are spaced much farther apart (0.0625 inches). Therefore we obtain a bulk conductivity measurement and this gives a slightly different ratio as compared to the Raman analysis because the local alignment in some places might be better than the large scale global alignment of SWNT in the composite film.

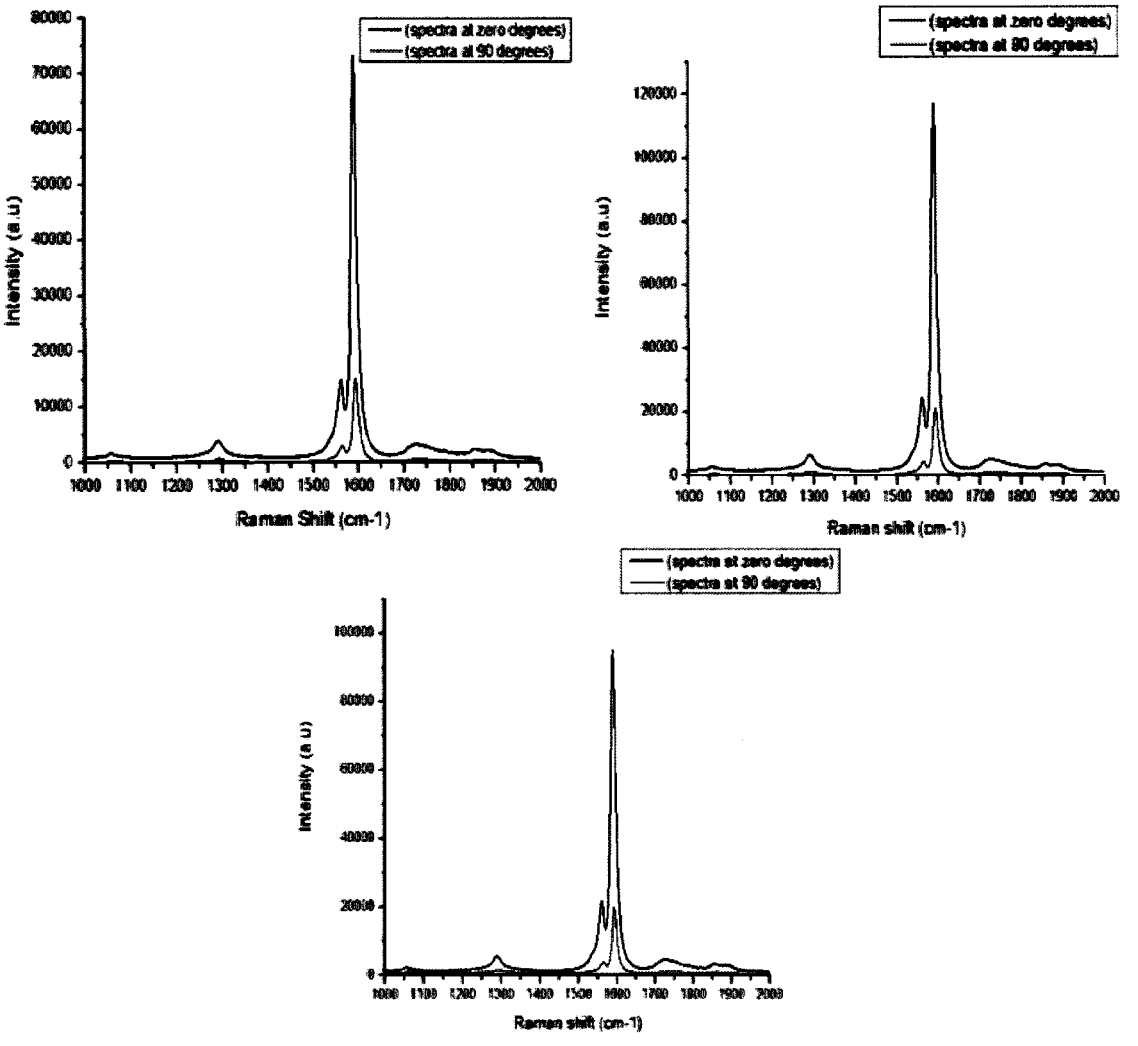

Figure 4.38. Reduction in G peak intensities for the 10 wt% SWNT – HiPco composite films.

Fisher *et al* [144] studied the orientation and anisotropic transport properties in magnetically aligned thin films. Magnetic fields of 7T and 26T were used to study the alignment. To study the effect of anisotropy they modeled the bucky paper as an ensemble of 1D path in the plane of the sample containing an average number of individual CNTs and ropes of fixed length and resistance. They calculated the average number of elements in the path for current flow parallel to the applied magnetic field and found a strong correlation

between the anisotropy in electrical conductivity and Raman peak intensities. Pint *et al* [145] extensively characterized the films they processed using dry contact transfer printing of aligned nanotubes by optical characterization techniques like IR and Raman spectroscopy. They believe that IR absorbance can be distinguished as an effective tool for the characterization of the alignment and can also be used to analyze of the diameter range of the SWNT population. Ratios of anisotropy in electrical conductivity and Raman spectroscopy obtained for our samples are shown in Table 4.4.

Table 4.4. Comparison of anisotropy in resistivity and Raman G modes for 10wt% SWNT-MDPE composites subjected to 75 V/cm DC field.

Sample	G (parallel) / G (perpendicular)	Resistivity (parallel) / Resistivity (perpendicular)
Sample 1	5	4.27
Sample 2	5.2	5.54
Sample 3	5.8	3.23
Sample 4	4.5	2.17

The mode of conduction on these composite films was determined by plotting the natural log of resistivity as a function of the nanotube concentration. Kilbride *et al* [146] and Curran et al [147] state the conduction mechanism in polymer CNT thin films is due to fluctuation induced quantum tunneling mechanism. A correlation between the electrical conductivity and concentration is given by $\ln \sigma_{DC} = p^{-1/3}$ where p is the nanotube concentration. They find that if a linear relationship exists between the conductivity and the concentration, the

dominant mechanism for electron hopping is through tunneling. A plot of the DC conductivity as a function of concentration is shown in Figure 4.39 and a near linear relationship is observed.

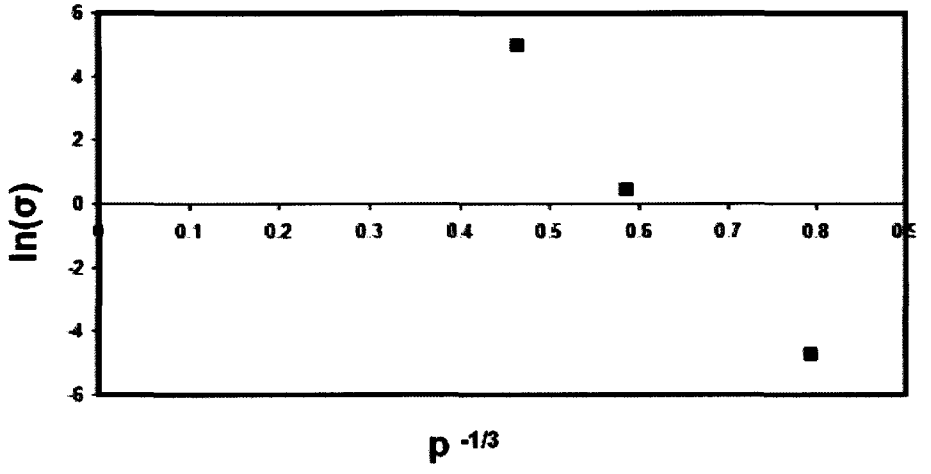

Figure 4.39. Plot of ln (σ) vs. $p^{-1/3}$ for SWNT/MDPE composites.

Since a linear relationship is observed, we believe that the conduction mechanism in the composite film is due to electron hopping through tunneling.

4.5. Conclusions

Different approaches to improve the electrical conductivity of polyethylene/SWNTs systems are shown. In comparison with other systems, where alignment of SWNTs was studied, their alignment in polyethylene by use of an electric field is a challenge due to its high viscosity and non-UV curable characteristics. When the composites were directly subjected to electric field, the high viscosity hindered the nanotube movement and this limited the maximum conductivity that could be achieved. Also, using high currents lead to instant heating of the polymer followed by degradation (shown in DSC data in

Appendix-1). The application of ANOVA on the values obtained from this process with resistance as the response variable showed that individually viscosity, decanting and electric field have a significant effect. While the interactions between these parameters have shown nullifying effect, only the interaction between electric field and the viscosity was also found to have significant effect. The new electric field vacuum spray process incorporated takes advantage of both low concentration and low viscosity demonstrating enhanced alignment. Composite films showed resistivity values two orders of magnitude lower than the values achieved by the previous method at room temperature. Polarized Raman studies and SEM show that there is global alignment in the sample with deviations at the micro/nano level. We believe that this new method will open up doors for more research in improving the properties of commonly engineered plastics since it combats the viscosity issue and helps in achieving a modest alignment in the composite.

CHAPTER 5: Conclusions

The electrical properties of a polymer nanocomposites can be modified and enhanced by optimizing the behavior of the carbon nanotubes in the polymer matrix. Dispersion, surface coverage, alignment, are some of the key parameters that dictate the electrical properties. In this dissertation, fabrication, processing and electrical properties of polymer composites were studied.

A new hybrid high temperature composite using Ni-SWNTs as nanofillers was processed and characterized to improve electrical conductivity. These nanofillers showed improved dispersions, which AFM and DLS analysis confirmed. Coating the nanotubes with nickel also enabled better interface with the carbon fiber and the BMI resin. The effect of exclusively using Ni-SWNTs nanofillers without conductive screens for lightning strike protection of the hybrid composites is demonstrated. Ni-SWNTs composites showed improved resistance to surface area damage compared to their unfilled counterparts. Raman and SEM analysis validate that the simulated lightning strike does not have an adverse effect on the nanofillers and the carbon fibers. Results from the lightning strike tests indicated that the high electrical energy generated during testing is: (1) partially dissipated in vaporizing the nickel whose latent heat of vaporization is lower than the carbon nanotubes and (2) also dissipated through a continuous network of nanotubes, as ICP-MS analysis shows no Ni is present in the region where lightning strike damage occurs. SEM and Raman analysis show no permanent damage to the nanotubes occurred in the lighting strike region. Ni-SWNTs proved to be a promising choice of nanofillers that can be used along with conductive screens for lightning strike protection.

The dispersion and network formation concept was further applied to improving the electrical conductivity of polyethylene composites. The orientation of SWNTs is also a key factor that affects the electrical conductivity of a polymer – SWNT composite. A new method "Electric field Vacuum Spray process" was successfully developed to overcome the process limitations of viscosity and the non UV-curable characteristics of polyethylene for effective alignment of SWNTs under the influence of applied electric field. The electrical resistivity of the polymer thin films reduced to an average of $8.75*10^{-3}$ Ω·cm due to enhanced alignment of SWNTs in the matrix. Polarized Raman spectroscopy and SEM analysis corroborate the alignment of SWNTs in MDPE. The anisotropy in electrical resistivity ($E_{\parallel}$ to $E_{\perp}$) correlates well to the anisotropy in the intensities of the Raman G band in the parallel and perpendicular orientations. This new method opens doors for exciting research due to its simplicity and feasibility.

In summary, the major contributions of this research to the field of polymer nanocomposites are:

- The proof that improved dispersions can be obtained by decanting and decorating the SWNTs with nickel. Coating the SWNTs with nickel aids in disrupting the Van der Waal's attraction and does not damage the sp^2 hybridization thereby retaining their inherent electrical properties.
- Use of a spray process to incorporate the SWNTs in the carbon fiber polymer matrix which improves their dispersion and provides uniform surface coverage on the carbon plies. By using this method, the process limitations such as, increase in viscosity of the polymer matrix due to addition of SWNTs, the amount of

SWNTs that can be used, their distribution in the required area depending on the material properties designed can be overcome.

- ❖ Use of Ni-SWNTs nanofillers independently or in conjunction with conductive mesh for lightning strike protection of polymer composites.
- ❖ Development of a new method to improve the directed network formation, dispersion and alignment of SWNTs in a polyethylene matrix. The simplicity of this method can be used for any polymer – nanotube system. Polyethylene composite films were processed using this method and the average resistivity obtained was ~ 0.009 Ω·cm which is the lowest reported for 10 wt% SWNTs – MDPE system.

FUTURE OUTLOOK

High temperature BMI/CARBON FIBER/Ni-SWNT composites for lightning strike protection

This research has made significant progress towards the development of polymer composites with improved dispersion and directed network formation of SWNTs but their remains much to be done.

Suggestions for future work are:

(1) Achieving higher conductivities by optimizing the alignment and also the concentration of the nanotubes required, since our focus was to use a low amount of nanotubes. For applications like lightning strike, the conductivity of the composites should be in the order of 10^3 S/cm.

(2) Using the Ni-SWNTs in addition to metal mesh that is currently being studied, to understand their effect in withstanding multiple lightning strikes.

(3) Improving the multifunctionality of the composites by enhancing their thermal and mechanical properties along with electrical properties.

Achieving high electrical conductivities in polyethylene – carbon nanotube composite systems

Suggestions for future work are,

(1) Study the effect of nanotube quality, purity and initial conditions on the electrical properties of the composites.

(2) Previous literature has shown that AC fields have a better effect on the alignment than DC fields. Hence use of AC fields needs to be further investigated.

(3) Better interactions between the polymers and SWNTs can be obtained by functionalizing or wrapping them. This can further improve the multifunctionality of the polymer composite.

REFERENCES

1. Ajayan, P.M. & Tour, J.M. Materials Science: Nanotube composites. *Nature* **447**, 1066-1068 (2007).
2. Baughman, R.H. Carbon Nanotubes--the Route Toward Applications. *Science* **297**, 787-792 (2002).
3. Du, F., Fischer, J.E. & Winey, K.I. Coagulation method for preparing single-walled carbon nanotube/poly(methyl methacrylate) composites and their modulus, electrical conductivity, and thermal stability. *J. Polym. Sci. B Polym. Phys.* **41**, 3333-3338 (2003).
4. Committee on High-Performance Structural Fibers for Advanced Polymer Matrix Composites, National Research Council *High-Performance Structural Fibers for Advanced Polymer Matrix Composites*. (The National Academies Press: Washington, D.C., 2005).
5. Hussain, F., Hojjati, M., Okamoto, M. & Gorga, R.E. Review article: Polymer-matrix Nanocomposites, Processing, Manufacturing, and Application: An Overview. *Journal of Composite Materials* **40**, 1511-1575 (2006).
6. Luo, J. & Daniel, I.M. Characterization and modeling of mechanical behavior of polymer/clay nanocomposites. *Composites Science and Technology* **63**, 1607-1616 (2003).
7. Nano report 2004 fin.pdf. at <http://www.nanotec.org.uk/report/Nano%20report%202004%20fin.pdf>
8. Iijima, S. Helical microtubules of graphitic carbon. *Nature* **354**, 56-58 (1991).
9. Dresselhaus, M.S., Dresselhaus, G. & Avouris, P. *Carbon nanotubes: synthesis, structure, properties, and applications*. (Springer: 2001).
10. Nemes, L. A Review of: "Science of Fullerenes and Carbon Nanotubes, Dresselhaus M.S. Dresselhaus, G. Eklund, P.C. Laszlo Nemes, Academic Press, Inc., New York, 1996". *Fullerene Science and Technology* **5**, 627 (1997).
11. Ebbesen, T.W. & Ajayan, P.M. Large-scale synthesis of carbon nanotubes. *Nature* **358**, 220-222 (1992).
12. José-Yacamán, M., Miki-Yoshida, M., Rendón, L. & Santiesteban, J.G. Catalytic growth of carbon microtubules with fullerene structure. *Appl. Phys. Lett.* **62**, 657 (1993).
13. Guo, T., Nikolaev, P., Thess, A., Colbert, D. & Smalley, R. Catalytic growth of single-walled manotubes by laser vaporization. *Chemical Physics Letters* **243**, 49-54 (1995).
14. Spires . T, Brown.M.R Jr SINGLE WALLED CARBON NANOTUBES. at <http://www.botany.utexas.edu/facstaff/facpages/mbrown/ongres/tspires/nano.htm>
15. Thess, A. et al. Crystalline Ropes of Metallic Carbon Nanotubes. *Science* **273**, 483-

487 (1996).

16. Hong, S. & Myung, S. Nanotube Electronics: A flexible approach to mobility. *Nat Nano* **2**, 207-208 (2007).
17. Hone, J., Whitney, M. & Zettl, A. Thermal conductivity of single-walled carbon nanotubes. *Synthetic Metals* **103**, 2498-2499 (1999).
18. Berber, S., Kwon, Y. & Tom□nek, D. Unusually High Thermal Conductivity of Carbon Nanotubes. *Phys. Rev. Lett.* **84**, 4613 (2000).
19. Krishnan, A., Dujardin, E., Ebbesen, T., Yianilos, P. & Treacy, M. Young's modulus of single-walled nanotubes. *Phys. Rev. B* **58**, 14013-14019 (1998).
20. Schewe.F.P, Stein.B Physics News Update Number 279 - Electrical and Mechanical Properties of Individual Carbon Nanotubes. at <http://www.aip.org/enews/physnews/1996/split/pnu279-2.htm>
21. Yu, M., Files, B.S., Arepalli, S. & Ruoff, R.S. Tensile Loading of Ropes of Single Wall Carbon Nanotubes and their Mechanical Properties. *Phys. Rev. Lett.* **84**, 5552 (2000).
22. Walters, D.A. et al. In-plane-aligned membranes of carbon nanotubes. *Chemical Physics Letters* **338**, 14-20 (2001).
23. Song, Y.S. & Youn, J.R. Influence of dispersion states of carbon nanotubes on physical properties of epoxy nanocomposites. *Carbon* **43**, 1378-1385 (2005).
24. Dyke, C.A. & Tour, J.M. Covalent Functionalization of Single-Walled Carbon Nanotubes for Materials Applications. *The Journal of Physical Chemistry A* **108**, 11151-11159 (2004).
25. Mitchell, C.A., Bahr, J.L., Arepalli, S., Tour, J.M. & Krishnamoorti, R. Dispersion of Functionalized Carbon Nanotubes in Polystyrene. *Macromolecules* **35**, 8825-8830 (2002).
26. Duque, J.G. et al. Diameter-Dependent Solubility of Single-Walled Carbon Nanotubes. *ACS Nano* **4**, 3063-3072 (2010).
27. Zhu, J. et al. Improving the Dispersion and Integration of Single-Walled Carbon Nanotubes in Epoxy Composites through Functionalization. *Nano Letters* **3**, 1107-1113 (2003).
28. Sun, Y., Fu, K., Lin, Y. & Huang, W. Functionalized Carbon Nanotubes: Properties and Applications. *Accounts of Chemical Research* **35**, 1096-1104 (2002).
29. Zhu, J. et al. Improving the Dispersion and Integration of Single-Walled Carbon Nanotubes in Epoxy Composites through Functionalization. *Nano Letters* **3**, 1107-1113 (2003).
30. Nish, A., Hwang, J., Doig, J. & Nicholas, R.J. Highly selective dispersion of single-walled carbon nanotubes using aromatic polymers. *Nat Nano* **2**, 640-646 (2007).
31. Calvaresi, M., Dallavalle, M. & Zerbetto, F. Wrapping Nanotubes with Micelles, Hemimicelles, and Cylindrical Micelles. *Small* **5**, 2191-2198 (2009).

32. Tummala, N.R. & Striolo, A. SDS surfactants on carbon nanotubes: aggregate morphology. *ACS Nano* **3**, 595-602 (2009).

33. Cheng, Q., Debnath, S., Gregan, E. & Byrne, H.J. Ultrasound-Assisted SWNTs Dispersion: Effects of Sonication Parameters and Solvent Properties. *The Journal of Physical Chemistry C* **114**, 8821-8827 (2010).

34. Park, C. et al. Dispersion of single wall carbon nanotubes by in situ polymerization under sonication. *Chemical Physics Letters* **364**, 303-308 (2002).

35. Frank, S., Poncharal, P., Wang, Z.L. & Heer, W.A.D. Carbon Nanotube Quantum Resistors. *Science* **280**, 1744-1746 (1998).

36. Shiraishi, M. & Ata, M. Conduction mechanisms in single-walled carbon nanotubes. *Synthetic Metals* **128**, 235-239 (2002).

37. Wei, B.Q., Vajtai, R. & Ajayan, P.M. Reliability and current carrying capacity of carbon nanotubes. *Appl. Phys. Lett.* **79**, 1172 (2001).

38. Fuhrer, M.S. et al. Crossed Nanotube Junctions. *Science* **288**, 494-497 (2000).

39. Buldum, A. & Lu, J.P. Contact resistance between carbon nanotubes. *Phys. Rev. B* **63**, 161403 (2001).

40. Foygel, M., Morris, R.D., Anez, D., French, S. & Sobolev, V.L. Theoretical and computational studies of carbon nanotube composites and suspensions: Electrical and thermal conductivity. *Phys. Rev. B* **71**, 104201 (2005).

41. Holm, R. The Electric Tunnel Effect across Thin Insulator Films in Contacts. *J. Appl. Phys.* **22**, 569 (1951).

42. Ajayan, P.M., Stephan, O., Colliex, C. & Trauth, D. Aligned Carbon Nanotube Arrays Formed by Cutting a Polymer Resin--Nanotube Composite. *Science* **265**, 1212-1214 (1994).

43. Moniruzzaman, M. & Winey, K.I. Polymer Nanocomposites Containing Carbon Nanotubes. *Macromolecules* **39**, 5194-5205 (2006).

44. Bryning, M.B., Islam, M., Kikkawa, J. & Yodh, A. Very Low Conductivity Threshold in Bulk Isotropic Single-Walled Carbon Nanotube-Epoxy Composites. *Advanced Materials* **17**, 1186-1191 (2005).

45. Li, C., Thostenson, E.T. & Chou, T. Dominant role of tunneling resistance in the electrical conductivity of carbon nanotube–based composites. *Appl. Phys. Lett.* **91**, 223114 (2007).

46. Gardiner.G Lightning Strike Protection For Composite Structures: CompositesWorld.com. at <http://www.compositesworld.com/articles/lightning-strike-protection-for-composite-structures>

47. boeinglightni_b.pdf. at <http://seattletimes.nwsource.com/news/business/links/boeinglightni_b.pdf>

48. Fielding, D.J.C. & Gibson, T. Electrical conductivity measurements and lightning Strike results of nano/macro materials enhanced polymeric composites. *Proceedings of SAMPE Fall Technical Conference 2008*, Sept 8-11, 2008, Memphis, TN.

49. Gou, J. et al. Carbon nanofiber paper for lightning strike protection of composite materials. *Composites Part B: Engineering* **41**, 192-198 (2010).

50. Ajayan, P.M. Nanotubes from Carbon. *Chemical Reviews* **99**, 1787-1800 (1999).

51. Treacy, M.M.J., Ebbesen, T.W. & Gibson, J.M. Exceptionally high Young's modulus observed for individual carbon nanotubes. *Nature* **381**, 678-680 (1996).

52. Gou, J. et al. Carbon nanofiber paper for lightning strike protection of composite materials. *Composites Part B: Engineering* **In Press, Corrected Proof**,

53. Research In Review: Paper Promise. at <http://www.rinr.fsu.edu/spring2006/features/paperpromise.html>

54. Kotov, N.A. Materials science: Carbon sheet solutions. *Nature* **442**, 254-255 (2006).

55. AFRL/MLBP Reaches a Milestone With Vapor Grown Carbon Nanofibers. at <http://www.ml.afrl.af.mil/stories/MLB/afrl_ws_05_1651.html>

56. Defense Tech Briefs - Nasa Tech Briefs. at <http://www.defensetechbriefs.com/>

57. Chiang, I.W. et al. Purification and Characterization of Single-Wall Carbon Nanotubes (SWNTs) Obtained from the Gas-Phase Decomposition of CO (HiPco Process). *The Journal of Physical Chemistry B* **105**, 8297-8301 (2001).

58. Bittencourt, C. et al. Decorating carbon nanotubes with nickel nanoparticles. *Chemical Physics Letters* **436**, 368-372 (2007).

59. Ang, L. et al. Electroless Plating of Metals onto Carbon Nanotubes Activated by a Single-Step Activation Method. *Chemistry of Materials* **11**, 2115-2118 (1999).

60. J. D. Kim, E. V. Barrera, C. D. Armeniades Incorporation of carbon nanotubes in epoxy composites. *Proceeding of the 35th International SAMPE Technical Conference*

61. Liu, J. et al. Controlled deposition of individual single-walled carbon nanotubes on chemically functionalized templates. *Chemical Physics Letters* **303**, 125-129 (1999).

62. Ausman, K.D., Piner, R., Lourie, O., Ruoff, R.S. & Korobov, M. Organic Solvent Dispersions of Single-Walled Carbon Nanotubes: Toward Solutions of Pristine Nanotubes. *The Journal of Physical Chemistry B* **104**, 8911-8915 (2000).

63. Giordani, S. et al. Debundling of Single-Walled Nanotubes by Dilution: Observation of Large Populations of Individual Nanotubes in Amide Solvent Dispersions. *The Journal of Physical Chemistry B* **110**, 15708-15718 (2006).

64. Hirsch, A. & Vostrowsky, O. Functionalization of Carbon Nanotubes. *Functional Molecular Nanostructures* 193-237 (2005).at <http://dx.doi.org/10.1007/b98169>

65. Giordani, S. et al. Debundling of Single-Walled Nanotubes by Dilution: Observation of Large Populations of Individual Nanotubes in Amide Solvent Dispersions. *The Journal of Physical Chemistry B* **110**, 15708-15718 (2006).

66. Sano, N. et al. Pressure effects on nanotubes formation using the submerged arc in water method. *Chemical Physics Letters* **378**, 29-34 (2003).

67. Ayala, P. et al. Decorating carbon nanotubes with nanostructured nickel particles via chemical methods. *Chemical Physics Letters* **431**, 104-109 (2006).

68. Zhang, Y., Franklin, N.W., Chen, R.J. & Dai, H. Metal coating on suspended carbon nanotubes and its implication to metal-tube interaction. *Chemical Physics Letters* **331**, 35-41 (2000).

69. Kong, F.Z. et al. Continuous Ni-layer on multiwall carbon nanotubes by an electroless plating method. *Surface and Coatings Technology* **155**, 33-36 (2002).

70. Rostro, B. Novel Fibrillar Carbon Nanotube Heat Transfer Gels with Enhanced Thermal Conductivities. (2005).

71. Maeda, Y. et al. Dispersion of Single-Walled Carbon Nanotube Bundles in Nonaqueous Solution. *The Journal of Physical Chemistry B* **108**, 18395-18397 (2004).

72. Dresselhaus, M., Dresselhaus, G., Saito, R. & Jorio, A. Raman spectroscopy of carbon nanotubes. *Physics Reports* **409**, 47-99 (2005).

73. Rao, A.M. et al. Diameter-Selective Raman Scattering from Vibrational Modes in Carbon Nanotubes. *Science* **275**, 187-191 (1997).

74. Thomsen, C. & Reich, S. Raman Scattering in Carbon Nanotubes. *Light Scattering in Solid IX* 115-234 (2007).at <http://dx.doi.org.ezproxy.rice.edu/10.1007/978-3-540-34436-0_3>

75. Sethi, R. & Barron, A. Characterization of Single-Walled Carbon Nanotubes by Raman Spectroscopy. at <http://cnx.org/content/m22925/latest/>

76. Loos, M.R., Coelho, L.A.F., Pezzin, S.H. & Amico, S.C. Effect of carbon nanotubes addition on the mechanical and thermal properties of epoxy matrices. *Mat. Res.* **11**, (2008).

77. Hubert, P. et al. Synthesis and characterization of carbon nanotube-reinforced epoxy: Correlation between viscosity and elastic modulus. *Composites Science and Technology* **69**, 2274-2280 (2009).

78. Xiao, K. & Zhang, L. Effective separation and alignment of long entangled carbon nanotubes in epoxy. *Journal of Materials Science* **40**, 6513-6516 (2005).

79. Ruckenstein, E. & Hong, L. Conducting rubberlike copolymer-carbon fiber composites. *Journal of Applied Polymer Science* **53**, 923-932 (1994).

80. Maser, W.K. et al. Carbon Nanotube Composite Materials: Opportunities and Processing Issues. *Nanostructured Materials for Advanced Technological Applications* 181-198 (2009).at <http://dx.doi.org.ezproxy.rice.edu/10.1007/978-1-4020-9916-8_18>

81. Park, J., Kim, J. & Yoon, D. Interfacial evaluation and microfailure mechanisms of single carbon fiber/bismaleimide (BMI) composites by tensile and compressive fragmentation tests and acoustic emission. *Composites Science and Technology* **62**, 743-756 (2002).

82. Liu, L., Gu, A., Fang, Z., Tong, L. & Xu, Z. The effects of the variations of carbon

nanotubes on the micro-tribological behavior of carbon nanotubes/bismaleimide nanocomposite. *Composites Part A: Applied Science and Manufacturing* **38**, 1957-1964 (2007).

83. Choudhary, V., Fitzer, E. & Heine, M. Carbon fibre reinforced bismaleimide composites, I. *Angewandte Makromolekulare Chemie* **160**, 17-28 (1988).

84. Heisey, C.L., Wood, P.A., McGrath, J.E. & Wightmany, J.P. Measurement of Adhesion Between Carbon Fibers and Bismaleimide Resins. *The Journal of Adhesion* **53**, 117 (1995).

85. Favre, J. et al. Fiber/Matrix mechanical interaction in carbon fiber/bismaleimide model composites. *Polymer Composites* **17**, 937-947 (1996).

86. Zhang. B, Chen. X, Li. P, Yi. X, Toughness and Hot/Wet Properties of a Novel Modified BMI/Carbon Fiber Composite. *Journal of Materials Science and Technology* **17**, 17-19

87. Cheng, Q. et al. High Mechanical Performance Composite Conductor: Multi-Walled Carbon Nanotube Sheet/Bismaleimide Nanocomposites. *Advanced Functional Materials* **19**, 3219-3225 (2009).

88. Cheng, Q., Wang, B., Zhang, C. & Liang, Z. Functionalized Carbon-Nanotube Sheet/Bismaleimide Nanocomposites: Mechanical and Electrical Performance Beyond Carbon-Fiber Composites. *Small* **6**, 763-767 (2010).

89. Bauhofer, W. & Kovacs, J.Z. A review and analysis of electrical percolation in carbon nanotube polymer composites. *Composites Science and Technology* **69**, 1486-1498 (2009).

90. Dresselhaus, M.S., Jorio, A., Hofmann, M., Dresselhaus, G. & Saito, R. Perspectives on Carbon Nanotubes and Graphene Raman Spectroscopy. *Nano Letters* **0**,

91. Burghard, M. Electronic and vibrational properties of chemically modified single-wall carbon nanotubes. *Surface Science Reports* **58**, 1-109 (2005).

92. Schadler, L.S., Giannaris, S.C. & Ajayan, P.M. Load transfer in carbon nanotube epoxy composites. *Appl. Phys. Lett.* **73**, 3842-3844 (1998).

93. Grosvenor, A.P., Biesinger, M.C., Smart, R.S.C. & McIntyre, N.S. New interpretations of XPS spectra of nickel metal and oxides. (2006).at <http://arrow.unisa.edu.au:8081/1959.8/42233>

94. Kasumov, A.Y., Khodos, I.I., Ajayan, P.M. & Colliex, C. Electrical resistance of a single carbon nanotube. *Europhys. Lett.* **34**, 429-434 (1996).

95. Paul L. McEuen, Michael S. Fuhrer, and Hongkun Park Single-Walled Carbon Nanotube Electronics. *IEEE TRANSACTIONS ON NANOTECHNOLOGY* **1**, 78-87 (2001).

96. Grossiord, N. et al. High-Conductivity Polymer Nanocomposites Obtained by Tailoring the Characteristics of Carbon Nanotube Fillers. *Adv. Funct. Mater.* **18**, 3226-3234 (2008).

97. Li, C., Thostenson, E.T. & Chou, T. Effect of nanotube waviness on the electrical conductivity of carbon nanotube-based composites. *Composites Science and Technology* **68**, 1445-1452 (2008).

98. Buldum, A. & Lu, J.P. Contact resistance between carbon nanotubes. *Phys. Rev. B* **63**, 161403 (2001).

99. Paulson, S., Helser, A. & Nardelli, M. Tunable Resistance of a Carbon Nanotube-Graphite Interface. *Science* **290**, 1742-1744 (2000).

100. Gao, F., Qu, J. & Yao, M. Electronic structure and contact resistance at an open-end carbon nanotube and copper interface. *Appl. Phys. Lett.* **96**, 102108 (2010).

101. Buldum, A. & Lu, J.P. Contact resistance between carbon nanotubes. *cond-mat/0005523* (2000).doi:doi:10.1103/PhysRevB.63.161403

102. Wakaya, F., Katayama, K. & Gamo, K. Contact resistance of multiwall carbon nanotubes. *Microelectronic Engineering* **67-68**, 853-857 (2003).

103. Foygel, M., Morris, R.D., Anez, D., French, S. & Sobolev, V.L. Theoretical and computational studies of carbon nanotube composites and suspensions: Electrical and thermal conductivity. *Phys. Rev. B* **71**, 104201 (2005).

104. Ramasubramaniam, R., Chen, J. & Liu, H. Homogeneous carbon nanotube/polymer composites for electrical applications. *Appl. Phys. Lett.* **83**, 2928-2930 (2003).

105. Skákalová, V., Dettlaff-Weglikowska, U. & Roth, S. Electrical and mechanical properties of nanocomposites of single wall carbon nanotubes with PMMA. *Synthetic Metals* **152**, 349-352 (2005).

106. Kovacs, J.Z. et al. On the influence of nanotube properties, processing conditions and shear forces on the electrical conductivity of carbon nanotube epoxy composites. *Nanotechnology* **20**, 155703 (2009).

107. Grossiord, N. et al. On the influence of the processing conditions on the performance of electrically conductive carbon nanotube/polymer nanocomposites. *Polymer* **49**, 2866-2872 (2008).

108. Kamat, P.V. et al. Self-Assembled Linear Bundles of Single Wall Carbon Nanotubes and Their Alignment and Deposition as a Film in a dc Field. *Journal of the American Chemical Society* **126**, 10757-10762 (2004).

109. Martin, C. et al. Electric field-induced aligned multi-wall carbon nanotube networks in epoxy composites. *Polymer* **46**, 877-886 (2005).

110. Zhu, Y. et al. Alignment of multiwalled carbon nanotubes in bulk epoxy composites via electric field. *J. Appl. Phys.* **105**, 054319 (2009).

111. Ma, C. et al. Alignment and dispersion of functionalized carbon nanotubes in polymer composites induced by an electric field. *Carbon* **46**, 706-710 (2008).

112. Du, F., Fischer, J.E. & Winey, K.I. Effect of nanotube alignment on percolation conductivity in carbon nanotube/polymer composites. *Phys. Rev. B* **72**, 121404 (2005).

113. Park, C. et al. Aligned single-wall carbon nanotube polymer composites using an

electric field. *Journal of Polymer Science Part B: Polymer Physics* **44**, 1751-1762 (2006).

114. Walters, D.A. et al. In-plane-aligned membranes of carbon nanotubes. *Chemical Physics Letters* **338**, 14-20 (2001).

115. Choi, E.S. et al. Enhancement of thermal and electrical properties of carbon nanotube polymer composites by magnetic field processing. *J. Appl. Phys.* **94**, 6034 (2003).

116. Raravikar, N.R. et al. Synthesis and Characterization of Thickness-Aligned Carbon Nanotube–Polymer Composite Films. *Chemistry of Materials* **17**, 974-983 (2005).

117. Feng W.[1] et al. Well-aligned polyaniline/carbon-nanotube composite films grown by in-situ aniline polymerization. *Carbon* **41**, 1551-1557 (2003).

118. Haggenmueller, R., Guthy, C., Lukes, J.R., Fischer, J.E. & Winey, K.I. Single Wall Carbon Nanotube/Polyethylene Nanocomposites: Thermal and Electrical Conductivity. *Macromolecules* **40**, 2417-2421 (2007).

119. Kyrylyuk, A.V. & van der Schoot, P. Continuum percolation of carbon nanotubes in polymeric and colloidal media. *Proceedings of the National Academy of Sciences* **105**, 8221-8226 (2008).

120. White, S., DiDonna, B., Mu, M., Lubensky, T. & Winey, K. Simulations and electrical conductivity of percolated networks of finite rods with various degrees of axial alignment. *Phys. Rev. B* **79**, (2009).

121. Haggenmueller, R., Fischer, J.E. & Winey, K.I. Single Wall Carbon Nanotube/Polyethylene Nanocomposites: Nucleating and Templating Polyethylene Crystallites. *Macromolecules* **39**, 2964-2971 (2006).

122. Hennrich, F. et al. The Mechanism of Cavitation-Induced Scission of Single-Walled Carbon Nanotubes. *The Journal of Physical Chemistry B* **111**, 1932-1937 (2007).

123. Cheng, Q., Debnath, S., Gregan, E. & Byrne, H.J. Ultrasound-Assisted SWNTs Dispersion: Effects of Sonication Parameters and Solvent Properties. *The Journal of Physical Chemistry C* **0**,

124. Badaire, S., Poulin, P., Maugey, M. & Zakri, C. In situ measurements of nanotube dimensions in suspensions by depolarized dynamic light scattering. *Langmuir* **20**, 10367-10370 (2004).

125. Lucas, A. et al. Kinetics of Nanotube and Microfiber Scission under Sonication. *The Journal of Physical Chemistry C* **113**, 20599-20605 (2009).

126. Narkis, M., Ram, A. & Stein, Z. Effect of crosslinking on carbon black/polyethylene switching materials. *Journal of Applied Polymer Science* **25**, 1515-1518 (1980).

127. Bin, Y., Kitanaka, M., Zhu, D. & Matsuo, M. Development of Highly Oriented Polyethylene Filled with Aligned Carbon Nanotubes by Gelation/Crystallization from Solutions. *Macromolecules* **36**, 6213-6219 (2003).

128. Senthil Kumar, M. et al. DC electric field assisted alignment of carbon nanotubes on metal electrodes. *Solid-State Electronics* **47**, 2075-2080 (2003).

129. Imholt, T.J. et al. Nanotubes in Microwave Fields: Light Emission, Intense Heat, Outgassing, and Reconstruction. *Chemistry of Materials* **15**, 3969-3970 (2003).

130. Wang, C.Y., Chen, T., Chang, S., Cheng, S. & Chin, T. Strong Carbon-Nanotube-Polymer Bonding by Microwave Irradiation. *Advanced Functional Materials* **17**, 1979-1983 (2007).

131. Du, F. et al. Nanotube Networks in Polymer Nanocomposites: Rheology and Electrical Conductivity. *Macromolecules* **37**, 9048-9055 (2004).

132. Song, Y.S. & Youn, J.R. Influence of dispersion states of carbon nanotubes on physical properties of epoxy nanocomposites. *Carbon* **43**, 1378-1385 (2005).

133. Curran, S.A. et al. Dynamic electrical properties of polymer-carbon nanotube composites: Enhancement through covalent bonding. *Journal of Materials Research* **21**, 1071-1077 (2006).

134. Development of a dispersion process for carbon nanotubes in an epoxy matrix and the resulting electrical properties. at <http://cat.inist.fr/?aModele=afficheN&cpsidt=1843488>

135. Free Energy Change of Mixing. at <http://web.mst.edu/~wlf/Solution/freenergy.html?free+energy+mixing>

136. Bergin, S.D. et al. Towards Solutions of Single-Walled Carbon Nanotubes in Common Solvents. *Advanced Materials* **20**, 1876-1881 (2008).

137. Pulikkathara, M.X., Kuznetsov, O.V., Peralta, I.R.G., Wei, X. & Khabashesku, V.N. Medium density polyethylene composites with functionalized carbon nanotubes. *Nanotechnology* **20**, 195602 (2009).

138. Li, C., Thostenson, E.T. & Chou, T. Effect of nanotube waviness on the electrical conductivity of carbon nanotube-based composites. *Composites Science and Technology* **68**, 1445-1452 (2008).

139. Du, F., Guthy, C., Kashiwagi, T., Fischer, J.E. & Winey, K.I. An infiltration method for preparing single-wall nanotube/epoxy composites with improved thermal conductivity. *Journal of Polymer Science Part B: Polymer Physics* **44**, 1513-1519 (2006).

140. Murakami, Y., Chiashi, S., Einarsson, E. & Maruyama, S. Polarization dependence of resonant Raman scattering from vertically aligned single-walled carbon nanotube films. *Phys. Rev. B* **71**, 085403 (2005).

141. Fagan, J.A. et al. Dielectric Response of Aligned Semiconducting Single-Wall Nanotubes. *Phys. Rev. Lett.* **98**, 147402 (2007).

142. Duesberg, G.S., Loa, I., Burghard, M., Syassen, K. & Roth, S. Polarized Raman Spectroscopy on Isolated Single-Wall Carbon Nanotubes. *Phys. Rev. Lett.* **85**, 5436 (2000).

143. Gommans, H.H. et al. Fibers of aligned single-walled carbon nanotubes: Polarized Raman spectroscopy. *J. Appl. Phys.* **88**, 2509 (2000).

144. Fischer, J.E. et al. Magnetically aligned single wall carbon nanotube films:

Preferred orientation and anisotropic transport properties. *J. Appl. Phys.* **93**, 2157 (2003).

145. Pint, C.L. et al. Dry Contact Transfer Printing of Aligned Carbon Nanotube Patterns and Characterization of Their Optical Properties for Diameter Distribution and Alignment. *ACS Nano* **4**, 1131-1145 (2010).
146. Kilbride, B.E. et al. Experimental observation of scaling laws for alternating current and direct current conductivity in polymer-carbon nanotube composite thin films. *J. Appl. Phys.* **92**, 4024 (2002).
147. Curran, S.A. et al. Electrical transport measurements of highly conductive carbon nanotube/poly(bisphenol A carbonate) composite. *J. Appl. Phys.* **105**, 073711 (2009).

APPENDIX-1

SEM analysis of the CG and HiPco SWNTs is shown in Figures 1 and 2. It can be seen that the disentanglement of HiPco SWNTs is better than the CG counterparts.

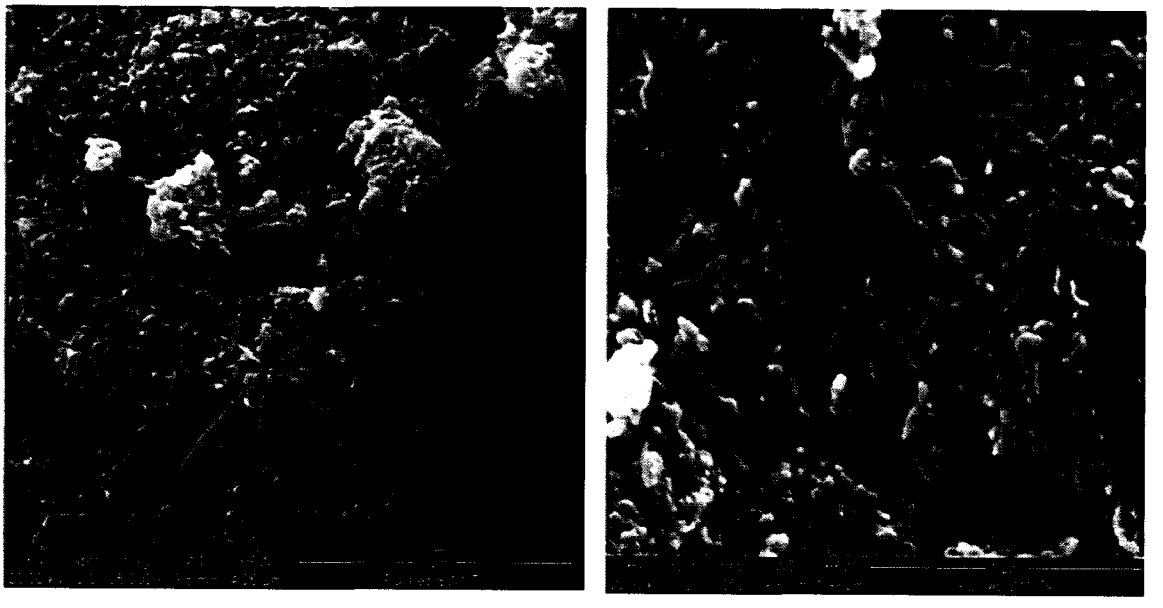

Figure A1.1. SEM images of CG-SWNTs showing heavy agglomerations.

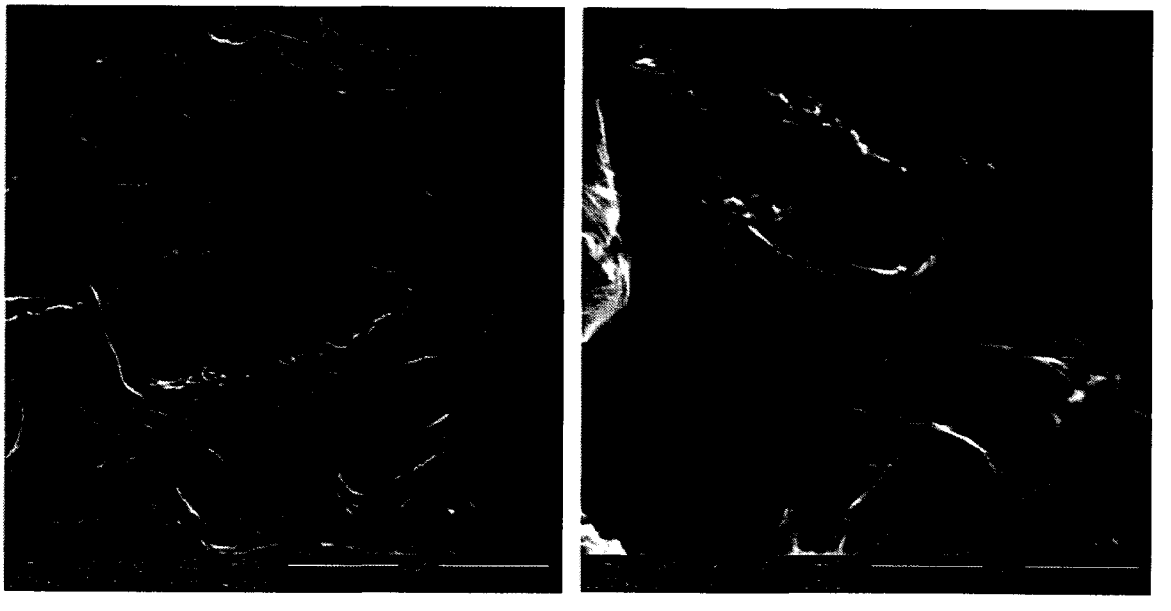

Figure A1.2. SEM images of purified HiPco SWNTs.

Raman spectra of CG and purified HiPco SWNTs are shown in Figures 3 and 4. The D peak of the CG-SWNTs is higher than the D peak of the purified HiPco indicating that HiPco has fewer defects than the CG-SWNTs.

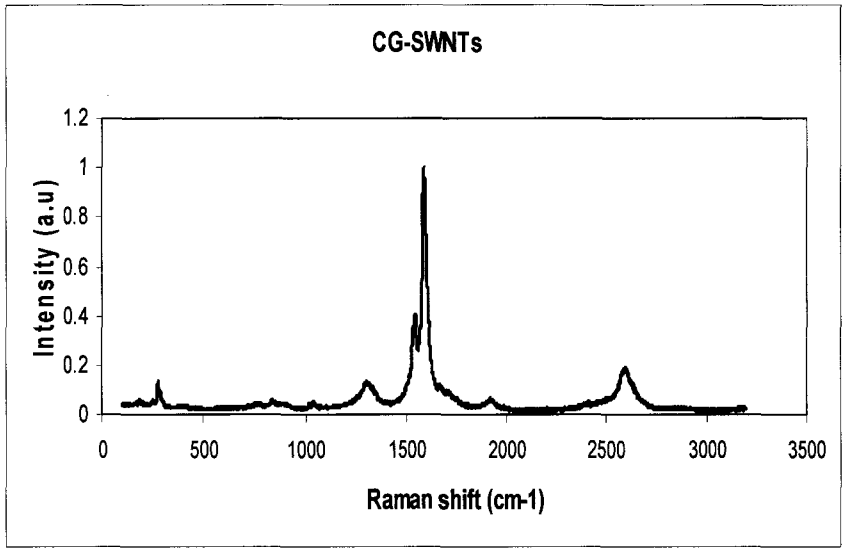

Figure A1.3. Raman spectrum of CG-SWNTs.

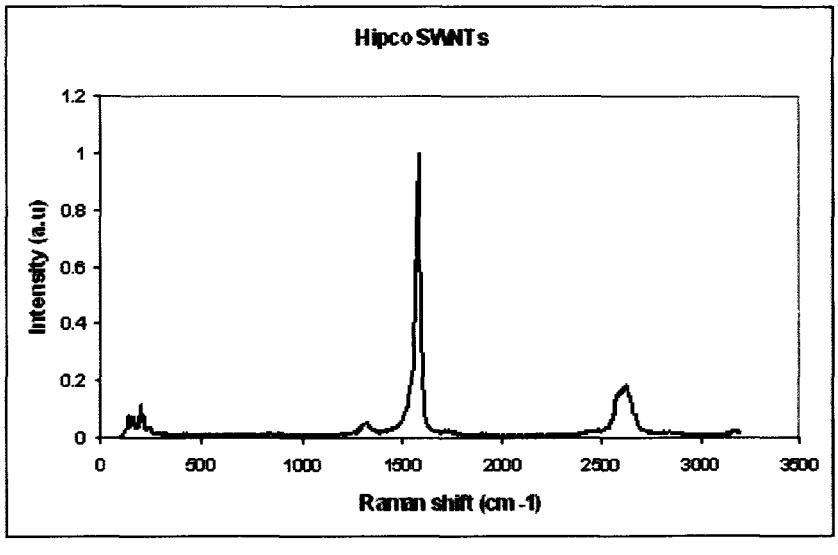

Figure A1.4. Raman spectrum of purified HiPco-SWNTs.

Differential scanning thermograms of neat MDPE, 10 wt% - MDPE composites processed by hot coagulation method, composites subjected to electric field and samples processed by electric field vacuum spray process is shown Figures 5, 6, 7 and. 8 respectively.

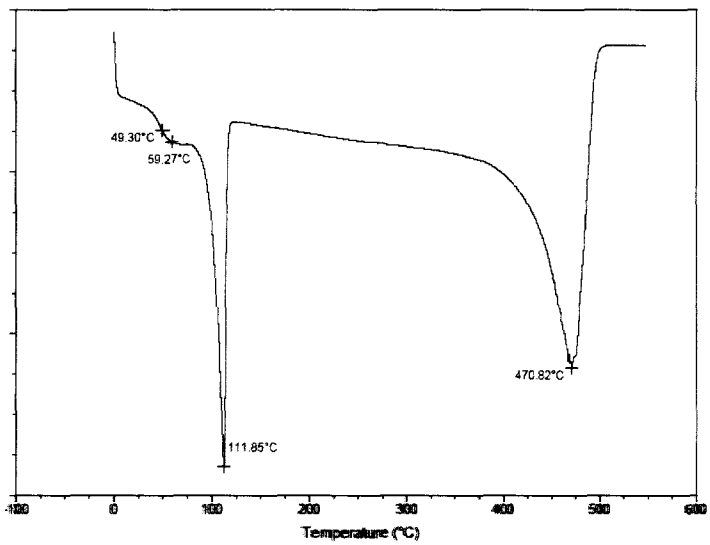

Figure A1.5. DSC thermogram of neat MDPE.

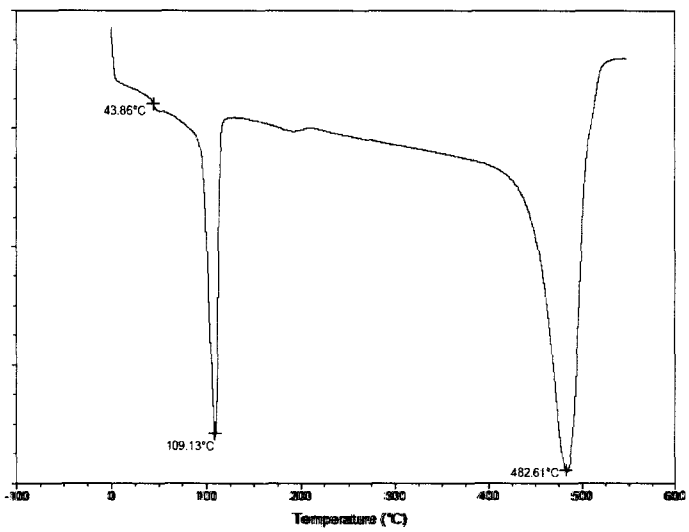

Figure A1.6. DSC thermogram 10 wt%-MDPE composites processed by hot coagulation method.

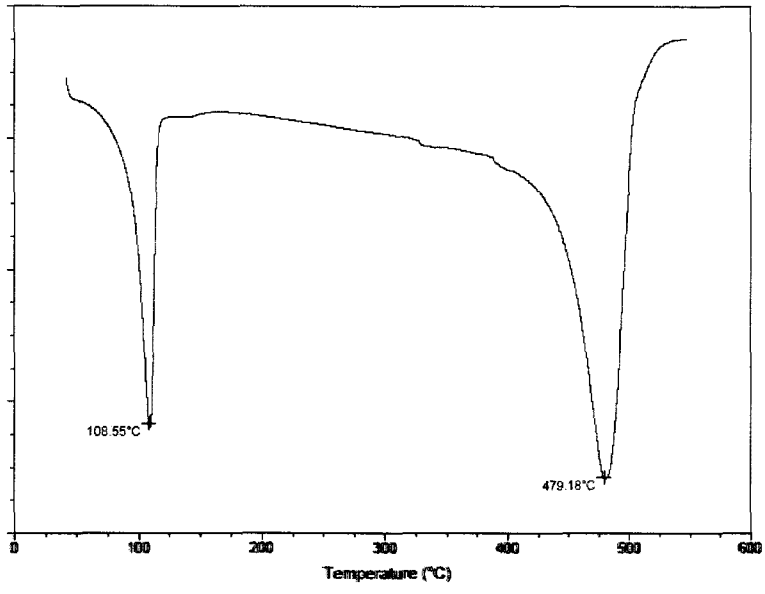

Figure A1.7. DSC thermogram of composites processed by hot coagulation method subjected to low DC field.

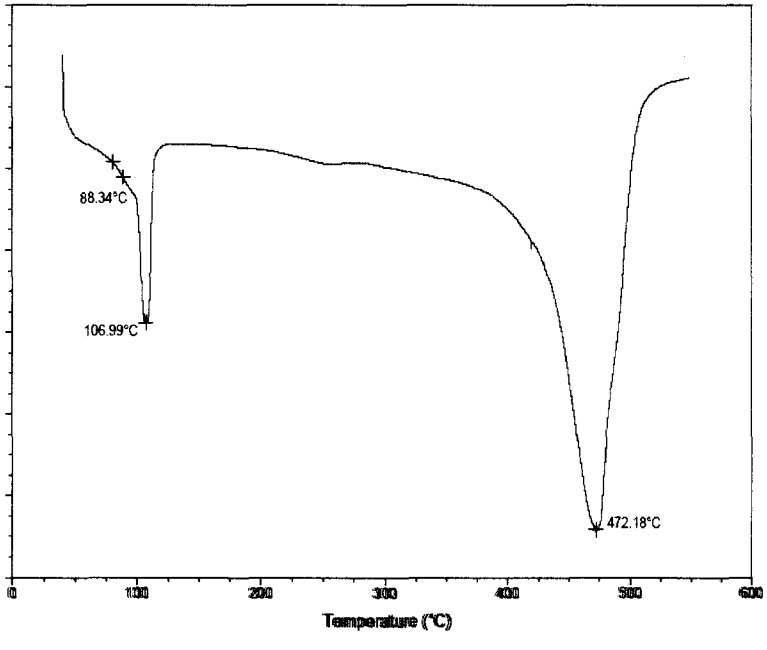

Figure A1.8.DSC thermogram of composites processed by electric field vacuum spray process.

The samples subjected to high currents were analyzed using DSC by Mike Searfass at Nanoridge Inc. Integration of the decomposition endotherms of the starting material and the material subjected to high currents showed that the thermal and E-field treatments decomposed 60% of the polymer. The DSC thermogram of the analysis is shown in Figure 9.

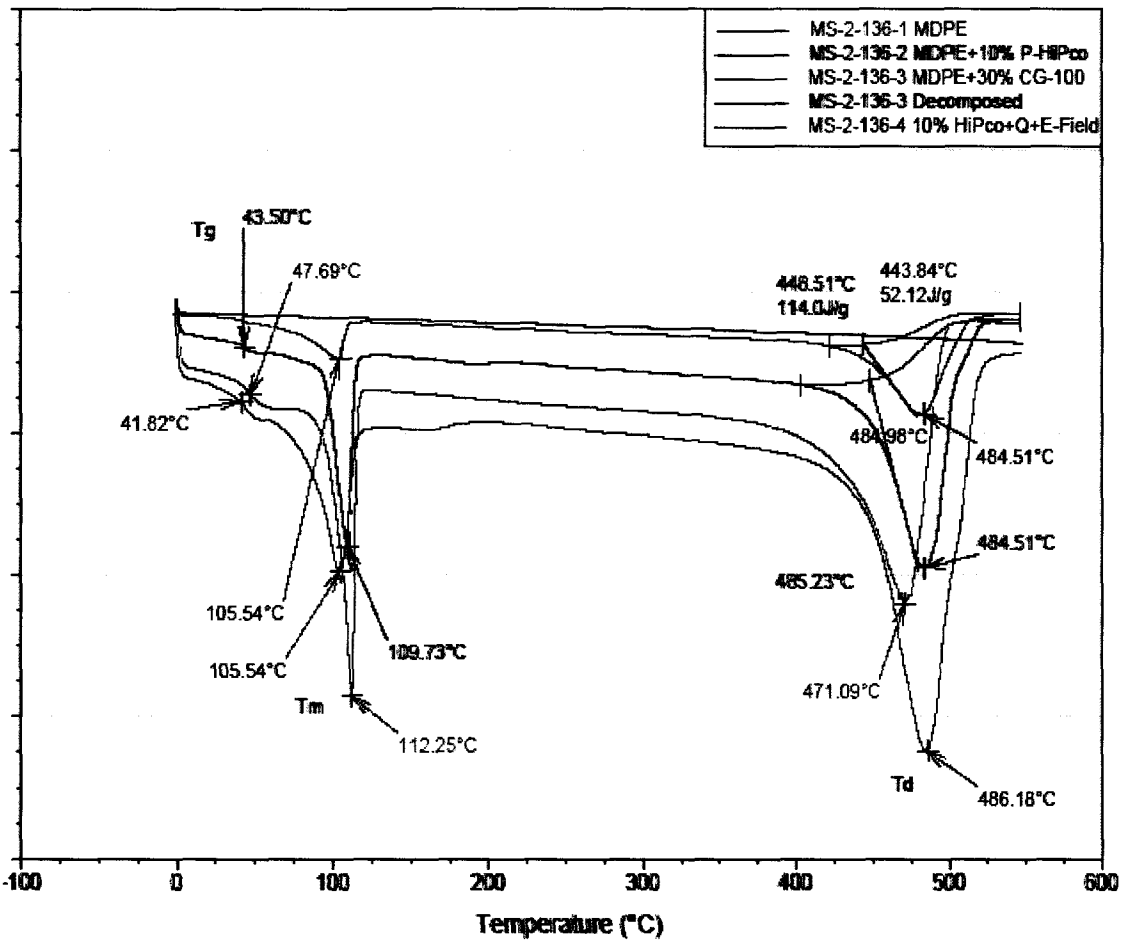

Figure A1.9. DSC thermograms of the various samples processed using the hot coagulation method subjected to electrical and current conditioning.

Tukey's studentized test was used to analyze the effect of electric field, viscosity and decanting on the resistance of the final composites. This test was performed for resistance

values obtained at 145 deg C. Tukey's test is a multiple comparison test used with ANOVA (analysis of variance) to find which means are significantly different from each other. We have 5 independent readings for each level with a total of 60 readings. The null hypothesis states that there is no significant difference in means of the response when the levels of factor are varied. All tests are performed at 95% confidence intervals (alpha = 0.05). For p-values less than alpha we reject the null hypothesis. Figure 10 shows the results obtained for the ANOVA analysis. From the p-values it can be observed that all the factors affect the response significantly. Also the interaction effect between electric field and viscosity significantly affects the resistance.

Source	DF	Type I SS	Mean Square	F Value	Pr > F
Decanting	1	125.13704	125.13704	31.22	<.0001
Efield	1	19861.66204	19861.66204	4955.30	<.0001
Viscosity	2	10601.09175	5300.54587	1322.44	<.0001
Decanting*Efield	1	3.57704	3.57704	0.89	0.3495
Efield*Viscosity	2	2472.87508	1236.43754	308.48	<.0001
Decanting*Viscosity	2	12.04608	6.02304	1.50	0.2328
Decant*Efield*Viscos	2	15.51608	7.75804	1.94	0.1554

Figure A1.10. Effect of the variables on the electrical resistivity of the composite (if P_r the probability is less than F, the variable has an effect).

Figure 11 shows the parameter interaction plot for resistance. If the plot with level chosen for the parameter is parallel the interaction between the parameters do no have a significant effect on the electrical resistance. On the contrary, if the plots are not parallel

the interactions between the parameters have a significant effect on the electrical resistance.

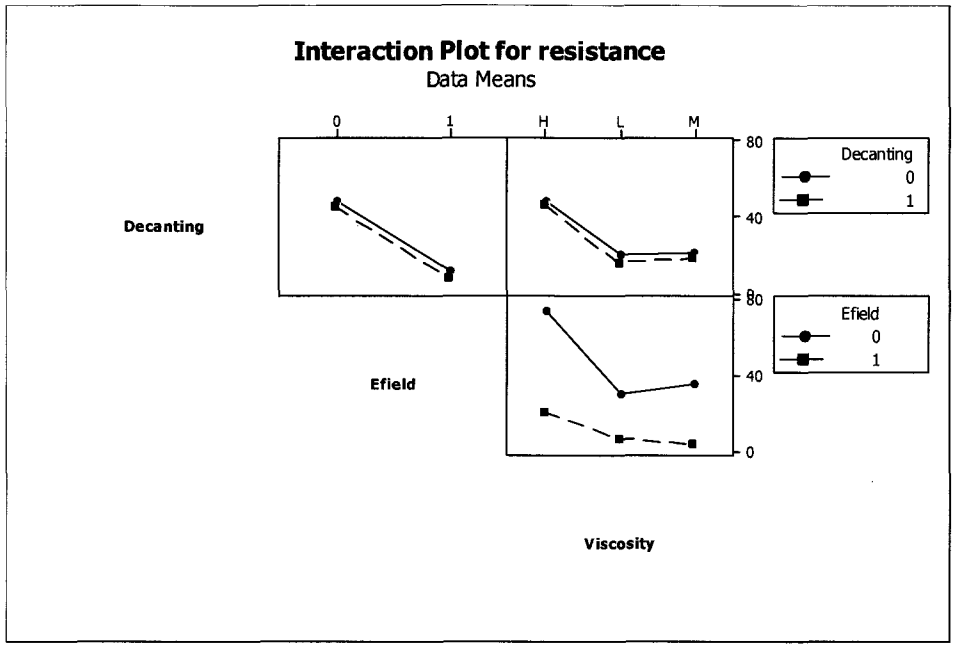

Figure A1.11. Effect of interaction between the parameters on the electrical resistance.